2015

Mathematical modelling in nanotechnology using calculus of variations

Nawa Awad H Alshammari
University of Wollongong

Mathematical Modelling in Nanotechnology Using Calculus of Variations

Nawa Awad H Alshammari

A thesis presented for the degree of

Doctor of Philosophy

School of Mathematics and Applied Statistics

University of Wollongong

Australia

2015

Declaration

I, Nawa Awad H Alshammari, declare that this thesis, submitted in partial fulfilment of the requirements for the award of Doctor of Philosophy, in the School of Mathematics and Applied Statistics, University of Wollongong, is wholly my own work unless otherwise referenced or acknowledged. This document has not been submitted for qualifications at any other academic institution.

Nawa Awad H Alshammari

2015

Abstract

The purpose of this thesis is to use the classical technique known as calculus of variations to investigate three problems in nanotechnology.

Curvature-dependent energies are used in modelling biological molecules including the shape of red blood cells and protein backbone structures. In this thesis, we investigate another application of such energies to model nanoantennas. Targeting mid-infrared rays, nanoantennas (which are defined as tiny gold squares or spirals set in specially treated forms of polyethylene) can convert energy into electricity giving rise to theoretical efficiency which is much higher than current solar cell technology. Since shape and size are critical to the performance of nanoantennas, here we investigate a certain type of nanoantenna which is a spherical helix or another similar curve that winds around a sphere. Using the Euler-Lagrange equations for extremal curves, we find classes of energies which permit curves on the sphere as extremizers.

The second problem is the joining between carbon nanostructures by using calculus of variations. Carbon nanostructures have received a lot of attention for their use in nanoscale devices. Joining carbon nanostructures has been shown to enhance the property of the combined structures. In this thesis we model the join of carbon nanocones with fullerenes, two nanocones, plane sheet of graphene with nanocones, fullerene with plane sheet of graphene and nanocone with two parallel sheets of graphene. We illustrate that a perfect join configuration of absolute minimum energy is possible in some circumstances. In general, we study two models, which are based on the curvature of the join profile. Model I refers to the positive curvature only and Model II refers to the positive and negative curvatures. In addition, we consider three cases of joining nanocones with exactly half a sphere, more than half a sphere and less than half a sphere. In joining two nanocones, we investigate the joining between two symmetric carbon nanocones,

two different angles nanocones and two different angles nanocones for five possible angles of the first nanocone. These combined structures may be useful for the design of scanning tunnelling microscopy and other nanoscale devices.

Finally, this thesis compares two different energies used in modelling of the joining between different carbon nanostructures. The first energy depends on the axial curvature only. As carbon nanotubes deform according to perfect elasticity, the elastic energy is used to determine the join region which contains a finite number of discrete bonds. Secondly, we consider the Willmore energy that depends on the axial and rotational curvature. As a result we use a piece of catenoid to join carbon nanostructures as it is an absolute minimizer of the Willmore energy. In particular, we investigate using the two energies for joining carbon nanocones with carbon nanotubes, two carbon nanocones and two fullerenes. We conclude that both of these energies can be used for these two cases of joining as they are similar in the joining profile.

The major contribution of this thesis is the use of applied mathematical modelling to determine optimal configurations of nanostructures. Three problems are investigated, based on geometry of space curves on a sphere, geometry of joining to combine different nanostructures and comparison of different energies for the same joining scenario.

Dedication

To the spirit of my father.

To my mother, my husband, my sons, my brothers and my sisters.

Acknowledgments

I thank Almighty God for giving me the courage and the determination, as well as guidance in conducting this research study, despite all difficulties. Pursuing a PhD is a both painful and enjoyable experience, and I would not have been able to complete this journey without the aid and support of countless people. I acknowledge that this thesis would not have been possible without the scholarship of the ministry of higher education in Saudi Arabia.

I must first express my special appreciation and thanks to my supervisors A/Prof James McCoy and A/Prof Natalie Thamwattana, both of you have been a tremendous mentor for me. I would like to thank you both for your grateful support, encouragement and assistance during my PhD journey. Also a special thanks for Assistant Prof. Duangkamon Baowan for her assistance specially in Maple codes.

My sincere thanks also goes to Mrs. Lisa Pyle for her generous support and advice.

Words cannot express how grateful I am to my father Awad and my mother Nashmiyah who inspired me beginning when I was seven years old, to pursue a doctorate; your prayer for me was what sustained me thus far.

I am very greatly indebted to my devoted husband Mohammed. His love and support without any complaint or regret has enabled me to complete my PhD. I owe my every achievement to him.

I am very thankful for my father in-law and my mother in-law for their prayer, love, encouragement and support.

I am grateful for my princes Talal and Salman. Before you entered my life, I used to wonder what I might accomplish; now, I want only to be the best Mammy I can be.

A special thanks to my sisters and my brothers for all of the sacrifices that you have made on

my behalf.

Finally, I thank all those who have assisted, encouraged and supported me during this journey.

Contents

List of Figures

Chapter 1

Introduction

1.1 Background

Nanotechnology is one of the most active research areas within the scientific community today. Nanotechnology is a multidisciplinary research field combining various disciplines, including physics, chemistry, biology and engineering. Importantly, mathematical modelling can provide insight into the behaviours of nanostructured materials under different conditions and enhance our understanding through new applications within this arena. This thesis comprises three topics, namely:

- Modelling curves on a sphere with an application to spherical nanoantennas,
- Modelling the joining of carbon nanostructures,
- Comparing different energies for modelling the joining of different nanostructures.

1.1.1 Modelling curves on the sphere

1.1.1.1 Antennas

An antenna is usually defined as a metallic device (as a rod or wire) for radiating or receiving radio waves [9]. Research into antennas began with James Clerk Maxwell in 1873 when he combined the theories of electricity and magnetism into a set of equations which are commonly known as Maxwell's equations. The Germany physicist Heinrich Rudolph Hertz developed the first wireless electromagnetic system in 1886 [9]. During the Second World War researchers worked to develop radar technology to see targets from hundreds of miles away, even at night. This research resulted in the rapid development of high-frequency radar antennas [51]. More

recently the principle aim of the research on antennas is how to create them for broadband application with small sizes for communication systems [51].

There are many applications for antennas. It is an important element of the performance of many systems such as communications, radar, radio astronomy, navigation and instrumentation [94].

Measuring the performance of an antenna depends on many important properties, the study in [8] has defined these properties as below.

1. Radiation pattern: The radiation pattern of an antenna can be defined as a mathematical function or graphical representation of the radiation properties which include power flux density, radiation intensity, field strength and polarization.

2. Directivity: The directivity of an antenna can be defined as the ratio of the radiation intensity in a given direction from the antenna to the radiation intensity averaged over all directions, and it is desirable to express directivity in decibels (dB). Thus the radiation intensity is the power radiated from an antenna per unit solid angle.

3. Gain: The gain is an important measure that describes the performance of an antenna. It is closely related to the directivity and it takes into account the efficiency of the antenna and its directional capabilities. Thus the gain of an antenna might be defined as that the ratio of the intensity, in a given direction, to the radiation intensity that would be obtained if the power accepted by the antenna were radiated isotropically.

4. Efficiency: The total antenna efficiency is used to take into account losses at input terminals and within the structure of the antenna.

5. Bandwidth: Bandwidth of an antenna is the range of frequencies within which the performance of the antenna, with respect to some characteristics, conforms to a specified standard.

6. Polarization: It is the polarization of the wave transmitted (radiated) by the antenna.

7. Input impedance: Input impedance of an antenna is defined as the impedance presented by an antenna at its terminals or the ratio of the voltage to current at a pair of terminals or the ratio of the appropriate components of the electric to magnetic fields at a point.

The study in [51] determined some types of antennas such as wire type antennas which include dipoles, monopoles, helices, Yagi-Uda and log-periodic antennas.

1.1.1.2 Helical antenna

A helical antenna is one type of antenna, that started with the invention of the cylindrical helical antenna by Kraus [55]. Other shapes of this special type of antenna with different properties were proposed by many researchers. In particular, a study by Virginia Polytechnic in [92] was the first to present the spherical helix antenna and described its properties. In [21] the spherical helix antenna was studied with circular polarization over a broad beam. This study indicated that the spherical helix is a wire antenna in a helix shape that is wound over a spherical surface; it is fed coaxially with the inner conductor of the coaxial cable becoming the helix and the outer conductor forming the conducting ground plane. As a result of this study, the researchers concluded that the spherical helix antenna has valuable applications in communication systems with low channel capacity. Further research into this type of antenna was proposed in [22]. The researchers studied the radiation characteristics of a spherical helical antenna and showed that spherical helical antennas have different properties from cylindrical helical antennas. Specifically, the spherical helix antenna has a narrower frequency range and exhibits circular polarization over a major portion of the main beam. This leads to usage of this type of antenna in mobile radio communications system.

Subsequently research into the input impedance and the gain of spherical helix antenna in [52] showed that increasing the number of turns of the spherical helix antenna gives rise to adverse effects on the input impedance and the antenna gain. This study compared the input impedances of a 5-turn, 7-turn and 3-turn of the spherical helix antenna. It also showed that increasing the number of turns gives rise to varying impedance with frequency. This means that it is unlikely to obtain a constant impedance region and hence the useful bandwidth of the antenna is reduced.

Thus, an increase in the number of turns of the helix does not favour the impedance bandwidth for a spherical helical antenna [52]. Moreover the antenna gains for a 3-turn and a 7-turn antennas have been compared to conclude that a relatively stable gain (within 1 dB) can be obtained for the 3-turn antenna from $C/\gamma = 1.1$ to $C/\gamma = 1.3$ where C is the circumference of the sphere and γ is the wavelength. On the other hand, the gain of the 7-turn antenna changes more rapidly with frequency. The maximum gain of the 3-turn antenna is 11.1 dB measured at $C/\gamma = 1.28$ and that of the 7-turn antenna is only 9.9dB at $C/\gamma = 1.18$. The generally smaller gain of the 7-turn antenna is due to its deeper mismatched impedance when compared with that of the 3-turn antenna [52].

In 2005 the study by Ding et al. [36] presented a new spherical helical antenna. This study explained the structure, radiation characteristics and input impedance of the spherical helical antenna. These researchers indicated that there are two radiation modes of the spherical helical antenna which are axial mode which has complex impedance, and axial-null mode which has stabilizes impedance.

In [104] a novel low-profile spherical helical antenna was proposed comprising of two wires winded centrosymmetrically on the part surface of the sphere where the spaces between the helices becoming broader from the top to the bottom. In particular they calculated the radiation properties, the directivity and an axial ratio (ratio of maximum to minimum power contained in the field components of the polarization ellipse [25]) of this antenna. This study concluded that this antenna has a directivity of more than 6 dB and an axial ratio of smaller than 3 dB over $2:1$ bandwidth and the radiation patterns have broad beam and 20 dB front-to-back ratio. These properties show that this antenna is useful in microwave measurements and satellite communication systems [104].

Many helical structures have been found in nature, for example circular, cylindrical, conical, spherical and elliptical helices. The research in [42] has shown that the main property of the spherical helix is the circular polarization over a very broad beam width which gives the spherical helix importance in communications systems. Another advantage of the spherical helix rather

than the cylindrical helix is the small electrical size which is useful in situations where size and weight limitations require to be intensely observed [42], [28].

Increasing demand of electricity is leading to extensive pressure on renewable energy sources. Scientists encounter enormous challenges to achieve methods that assist in producing large amount of energy and power. One answer to this problem is the use of solar cell technology, which is the most common converting sunlight into electricity. However, solar cells have a limitation; their theoretical limit is only 30% conversion of the sunlight which is a small amount compared to the huge amount of the sunlight available [86].

The abundance of energy from the sun gives rise to increasing research in this field. As a result, researchers have created a new device for converting energy from the sun into electricity called the nanoantenna. This device targets mid-infrared wavelength, where conventional photovoltaic solar cells are inefficient and where there is plenty of solar energy [54].

In this thesis, modelling curves on a sphere with an application to nanoantenna is presented. Using calculus of variations, the thesis aims to find the energy density functions that give spherical helices as solutions for Euler-Lagrange equations.

1.1.2 Modelling the joining of carbon nanostructures

Many experimental and theoretical studies have investigated the nature of materials at the nanoscale. Nanomaterials have size ranging between 1 to 100 nm in one or more dimensions [87] [48]. Based on their special thermal, mechanical, electronic and biological properties which are not found in conventional materials [91], [26], [27] [34], nanomaterials have been studied for varied applications in physics, chemistry, biology, engineering and computer science [77]. Carbon nanostructures are examples of these nanomaterials, and they can be classified based on their structures such as graphene, carbon nanotubes, fullerenes and carbon nanocones [10] [11] [103].

Nanostructure materials are of interest to many research fields due to their physical, chemical and electronic properties [10] [38] [79]. Owing to their unique properties, carbon nanostructures have received much attention for the development of many nanoscale devices. Many

researchers have explored the dynamics of carbon nanostructures such as graphene, carbon nanotubes, fullerene and carbon nanocones due to their extraordinary properties which distinguish them in nanoscale devices development [17]. Fullerenes are important elements of the carbon family in nanoscale. They have a similar structure to graphene, which is formed by linking hexagonal rings, but fullerenes contain pentagonal rings that are required to close the spherical shell [10]. On the other hand, there are many different types of fullerenes such as $C_{10}, C_{20}, C_{30}, C_{50}, C_{60}, C_{70}, C_{119}, C_{120}, C_{195}$, and C_{260} [84]. Fullerenes have many interesting chemical and physical properties, which have been exploited to develop biological and medical applications, including drug delivery, osteoporosis therapy and x-ray contrast agents to reduce toxicity [38, 32, 80, 19].

Carbon nanotubes have attracted scientists attention since their discovery due to their unique

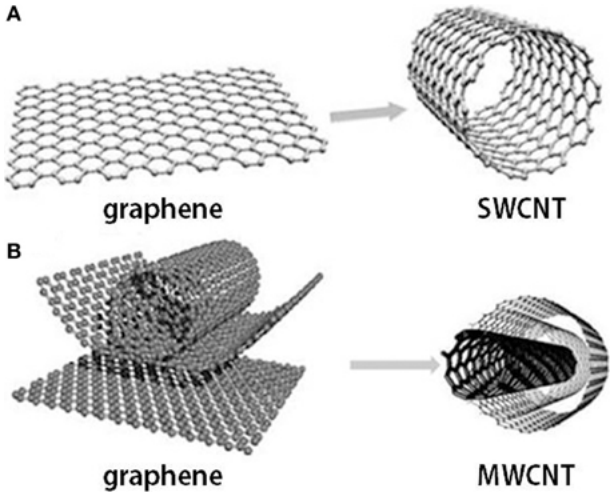

Figure 1.1: Single and multi walled carbon nanotubes [76].

properties and potential applications [43]. The first observation of the tubular carbon structures was in 1991 by Iijima [53]. Carbon nanotubes are effectively long, thin cylinders of graphite that made up of layers of carbon atoms arranged in a hexagonal lattice. Two years after the discovery of carbon nanotubes, scientists have proved that two different shapes of carbon nanotubes are found in their fabrication, including single walled and multi-walled carbon nanotubes [53], as shown in Figure 1.1. Experimentally, there are many ways to synthesize carbon nanotubes. The commonly used methods are; arc discharge, laser ablation, chemical vapor deposition [79], the sol-gel and gas phase metal catalyst [53]. Wide ranges of applications of carbon nanotubes

include nanoelectronic devices, atomic probe, gas storage devices, actuators, high power electrochemical capacitors, nanothermometers and Fe-filled nanotubes as magnetic storage devices [53] [66] [43] [89].

Structurally, single-walled carbon nanotubes can be viewed as a single graphene layer rolled up into a seamless cylinder, one atom thick, with a small number of carbon atoms around the circumference and a great length along the cylindrical axis. Let $\mathbf{C}$ be the chiral vector indicating the direction of the rolling as in Figure 1.2, $\mathbf{C}$ can be written as

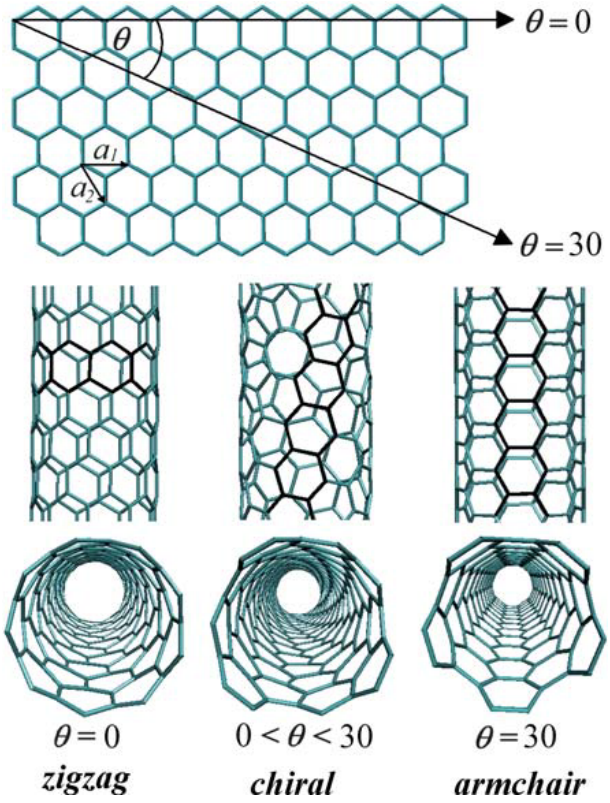

Figure 1.2: The roll-up vector as linear combinations of base vectors a_1 and a_2, single- and multi-walled carbon nanotubes structures [40].

$$\mathbf{C} = n\mathbf{a_1} + m\mathbf{a_2},$$

where (n, m) are a pair of indices that denote the number of unit vectors $n\mathbf{a_1}$ and $m\mathbf{a_2}$. A single walled carbon nanotube of different atomic structure depends on various choices of n and m as in Figure 1.2. If $(m = 0)$ the nanotube is called zigzag nanotube which corresponds to $\theta = 0°$. If $(n = m)$ the nanotube is called armchair nanotube which corresponds to $\theta = 30°$ and the chiral nanotube is all other carbon nanotubes corresponds to $0 < \theta < 30°$. The diameter d can

be calculated from

$$d = |\mathbf{C}|/\pi = a\sqrt{(}n_2 + nm + m_2),$$

where $a = 2.49$ Å is the lattice constant of the graphene sheet [66].

Multi-walled carbon nanotubes can be considered as concentric cylindrical graphitic tubes which are more complex structures than single-walled carbon nanotubes. Moreover, the single-walled carbon nanotubes that extract from multi-walled carbon nanotubes may have quite different structures for example, length and chirality. Although multi-walled carbon nanotubes are easier to produce in significant quantities than single-walled carbon nanotubes, their structures are less well understood than single-walled carbon nanotubes because of their complexity and variety [73].

While fullerenes and carbon nanotubes are widely studied, little attention has been paid to carbon nanocones. Carbon nanocones might be defined as curved graphene sheet with the addition of pentagons at the cone tips [93]. They are found on the caps of nanotubes as free-standing structures that are generated in a carbon arc [5]. Accordingly, only a small amount of carbon nanocones is produced [10, 11, 30]. Nevertheless carbon nanocones have potential applications to be used as tips in atomic force microscopes and scanning tunneling microscopes. They also have useful applications in deformation problems [16] [17] [97]. Moreover, carbon nanocones might be possible candidates for hydrogen storage and field emission tips [93]. Further, theoretical studies suggest that the oscillation of nanocones inside carbon nanotubes can create gigahertz frequency which can be used as ultra-sensitive nanoantenna and ultra-fast signalling devices [11] [3]. Carbon nanocones also have good mechanical, electrical and thermal properties [101]. In particular, they are useful for high resolution and high intensity applications because of their small size [98]. Other researchers have found other useful applications of carbon nanocones in different areas, for example in engineering applications [61], cold electron and field emitters [101], adsorbent [65], mechanical sensors [50] and they can be useful as high sensitive resonators [98].

Graphene, as one of carbon allotropes, and its composites has attracted considerable attention

due to its exceptional physical and chemical properties such as excellent electron mobility, theoretically large surface area of ~ 2600 m^2/g, high thermal conductivity of ~ 5000 W $m^{-1}K^{-1}$ and optical transparency [39] [18] [70] [83] [7] [59]. As a result of these properties, graphene has promising applications in different aspects for example, in biosensors, nanoelectronics, intercalation materials, drug delivery, catalysis, super capacitors, polymer composites [99], energy storage, sensing, electrocatalysis [39].

The joining of carbon nanostructures can lead to more interesting structures and properties. In this thesis, determination of join regions between carbon nanostructures is investigated. For this purpose, calculus of variations is applied to determine the shape of the join region between many different nanostructures.

1.1.3 Comparison of different energies for joining carbon nanostructures

Joining carbon nanostructures produces new nanostructures with better properties. In this case, we consider two different energies to join carbon nanostructures. Firstly, using the elastic energy which depends on the axial curvature only. The second energy is the Willmore energy which also depends on the axial and rotational curvatures. Taking these two energies into account, we investigate the difference of some carbon nanostructures joining profiles.

This comparison is important because the first energy is only based on the axial bond of the curve. However, the second energy is based on both the axial and the rotational curvature. After that, we identify if the rotational curvature makes any change into the joining structures. The first energy has the advantage of solving the resulting equations quite easily. However, for the second energy, when both of the curvatures are involved, the energy can be used for cell membrane and other structures.

In this thesis, comparison between these two different energies for joining of carbon nanocones and carbon nanotubes, two symmetric carbon nanocones, large and narrow carbon nanocone and two fullerenes is studied. This thesis shows the appropriate energy for these different scenarios of joining.

1.2 Structure of the thesis

The remaining four chapters of this thesis are arranged as follows. Chapter 2 has two main aims: first, to identify and review the research literature pertaining to modelling curves on a sphere with an application to spherical nanoantennas and second, to adopt the approach of the classical calculus of variations to model helices on sphere then concluding with the discussion of the results. Chapter 3 also contains two major purposes; firstly, to review and show the literature concerning the modelling of joining of carbon nanostructures. The second part of this chapter is to adopt calculus of variations and determine new joining profiles for different carbon nanostructures. Chapter 4 is divided into two parts. The first part is to review the literature of comparing different energies for modelling the joining of different carbon nanostructures, and the second part is to compare of different energies for same joining scenario of carbon nanostructures. Chapter 5 contains some concluding remarks and discussion of this thesis. Finally, Maple codes are given, with appendices and bibliography included.

Chapter 2

Modelling curves on a sphere with an application to nanoantennas

2.1 Introduction

Helical structures in nature have received considerable interest from engineers and scientists in recent years. There are many shapes of helices in nature such as circular, cylindrical, conical, spherical and elliptical. Studies such as [15] indicate the existence of helical structures in microscopic systems, such as biomolecules, bacterial fibers, nanosprings, protein chains and DNA. In addition to biological systems, helical structures are useful as antennas for many systems including communications, radar, radio astronomy, navigation and instrumentation [94]. Helical antennas are of particular interest in communication systems because they can produce circular polarization [21]. Polarization might be called wave polarization which defines as an expression

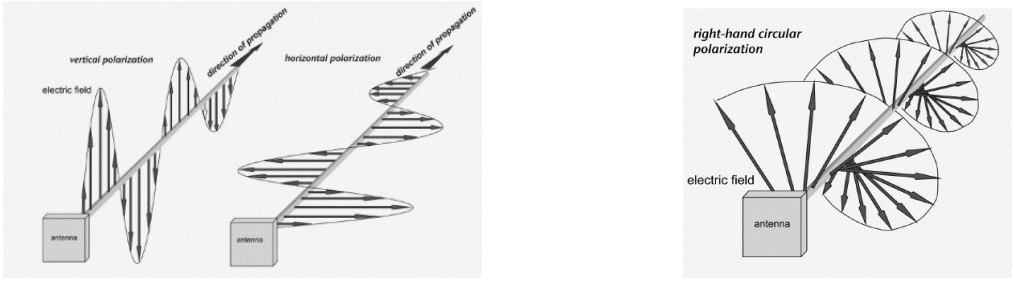

(a) Linear polarization. (b) Circular polarization.

Figure 2.1: Linear and circular polarization [37].

of the orientation of the lines of electric flux in an electromagnetic field. In particular, there are two different types of antenna's polarization as indicated in Figure 2.1 [37]. First is linear polarization in which the electric field is oriented in a single direction (vertical or horizontal) as shown in Figure 2.1a. Second is circular polarization, where the plane of polarization rotates in

a corkscrew pattern making one complete revolution for every wavelength. It radiates energy in horizontal, vertical planes and every plane in between. If the rotation is clockwise then it is called right-hand circular, and if it is counterclockwise then it called left-hand circular as shown in Figure 2.1b [74]. Using circular polarization for antennas removes the need to continuously align the two antennas, maximizing received power and also avoiding the need of complex tracking system [105]. This chapter reviews the significant background and configurations of spherical helix and nanoantennas, and includes mathematical models for curves on the sphere.

2.1.1 Spherical helix

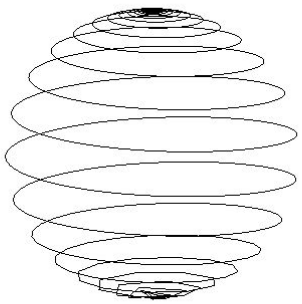

Figure 2.2: Spherical helix.

A mathematical general helix is a curve in space such that there is a fixed vector $\mathbf{V}$ in the direction of the axis of the helix, which makes a fixed angle with the tangent vector at each point on the curve. As shown in Figure 2.2, spherical helix is a variation of the conventional helix which holds the spacing S between turns constant and varies the diameter D and pitch angle α. Spherical helix might be determined by the number of turns N and the radius r. By using spherical coordinates (r, θ, ϕ), the geometry of spherical helix can be described such that each turn sweeps 2π radius in ϕ coordinate with total of $2\pi N$ radius for the entire spherical helix of N turns. As ϕ varies from 0 to $2\pi N$ we have

$$r = a,$$

$$\theta = \cos^{-1}(\frac{\phi}{N\pi} - 1),$$

$$0 \leq \phi \leq 2\pi N.$$

Furthermore, spherical coordinates (r, θ, ϕ) are used to derive the expression describing the spherical helix. Specifically, the coordinates of the spherical helix are defined as

$$X = r\cos\theta\cos\phi,$$

$$Y = r\sin\theta\sin\phi,$$

$$Z = r\cos\theta.$$

The studies in [28] and [92] have explained the radiation characteristics of the spherical helix. In particular the performance of this type of helix is independent of the number of turns. However, with a very small number of turns the helix loses its spherical shape and with a very large number of turns it becomes a spherical cavity. Moreover spherical helix includes two different modes of radiation in the overall axial regime; axial and axial-null modes. The axial mode is analogous to the axial mode of the standard helix with a single main lobe along the axis of the helix and it operates in a circumference range of approximately 0.75λ to 2.0λ, where the axial-null mode operates in a normalized circumference range of about 2λ to 2.8λ where λ denotes the wavelength [28].

2.1.2 Nanoantenna

The history of the nanoantenna dates back to Robert L. Bailey in 1972 who proposed the first electromagnetic wave converter [75]. In 1984 Alvin M. Marks used sub-micron-sized antenna in a device to create electricity [2]. In 1996 Guang H. Lin was the first researcher to show the absorption of resonant light by fabrication of a nanostructure [44].

The most important feature for nanoantennas is the high theoretical efficiency which is 85% compared to 25% of the solar cell. Also, nanoantennas receive higher frequencies and shorter wavelengths. On the other hand, there is a restriction in using nanoantenna due to the production process by electron beam (e-beam lithography). This process is slow and expensive because

parallel processing is not possible with e-beam lithography. Also, operation frequency is one of the main limitations of nanoantennas. However metal-insulator-metal tunneling diodes show promising features for use in nanoantennas [1].

The study in [57] defines nanoantennas as tiny gold squares or spirals set in specially treated form of polyethylene. This study showed that materials can change properties at high-frequency wavelengths. Furthermore, computer modelling of nanoantennas concluded that these nanoantennas can harvest up to 92% of the energy at infrared wavelength. The potential application of these nanoantennas can be used as skins that can power everything including hybrid cars and mobile technology with higher efficiency than solar cells. The ability of nanoantennas to absorb infrared radiation lead to their usage in cooling devices. Nanoantennas can collect infrared rays and re-emit the energy at harmless wavelengths, as a result, they may be used to cool down buildings and computers without power sources like air conditioners and fans.

In this chapter, modelling curves on a sphere with an application to nanoantennas is investigated by assuming that the energy density depends on the geometry of the curve which is controlled by the curvature κ and the torsion τ of the curve. Note that up to rigid motions a smooth curve in space is completely determined by its curvature and torsion functions. Supporting our assumption above, here we use calculus of variations approach through Euler-Lagrange equations which are derived in [85].

In [85] calculus of variations is used to investigate the protein structure when the energy functional is dependent on the curvature, torsion and their derivatives. Certain forms of energy are considered, which depending on the curvature and the torsion, results in Euler-Lagrange constraints. In particular, conical helix is studied in detail and in [67] energies that give rise to helices as solutions of the Euler-Lagrange equations are investigated. As a result, the classes of energy for which all circular helices are solutions are found. More recently, the study in [68] used the same procedure to investigate when the cylindrical helices are solutions to the Euler-Lagrange equations. From these studies, this chapter focuses on other types of curves which are curves on the sphere, which may be useful to model the structures of nanoantennas. Since

shape and size are critical to the performance of nanoantennas, here we investigate a particular type of nanoantenna which is a spherical helix and revolutionary curves on a sphere. Spherical helix antennas are not well studied compared to cylindrical helix antennas, but they have some useful properties including circular polarisation over a wide beamwidth, leading to potential applications in communication systems [22], [36]. Moreover, spherical helix nanoantennas have been shown to exhibit similar properties to that of cylindrical helix antenna with high efficiency for higher frequencies.

Thinking of a spherical antenna as a rod wound around a sphere, by minimizing the energy of the rod we may determine energies which give rise to stable helical structures. In this chapter, the thin rod is assumed as a curve in three-dimensional space. As such we can adopt the calculus of variations, applied to space curves, to determine energy density functions. In section 2.2 we adopt the approach of the classical calculus of variations to model helices on a sphere. Mathematical results are presented together with a discussion of the outcome in section 2.3. Finally, the conclusion of the chapter is given in section 2.4.

2.2 Model and mathematical background

2.2.1 Geometry of space curves

If C is a curve in three-dimensional Euclidean space $\mathbb{R}^3$, the position vector of points on C may be written as

$$\mathbf{r}(t) = (x(t), y(t), z(t)) .$$

A tangent vector to C at $\mathbf{r}(t)$ is

$$\frac{d}{dt}\mathbf{r}\,(t) = \left(\frac{d}{dt}x(t), \frac{d}{dt}y(t), \frac{d}{dt}z(t)\right).$$

The curve C is *regular* if $\frac{d}{dt}\mathbf{r}\,(t) \neq 0$. Provided $\mathbf{r}$ is smooth enough, the curvature κ and the torsion τ of C are given respectively by

$$\kappa(t) = \frac{|\dot{\mathbf{r}} \times \ddot{\mathbf{r}}|}{|\dot{\mathbf{r}}|^3}, \tag{2.1}$$

and

$$\tau(t) = \frac{\det(\dot{\mathbf{r}}, \ddot{\mathbf{r}}, \dddot{\mathbf{r}})}{|\dot{\mathbf{r}} \times \ddot{\mathbf{r}}|^2}, \tag{2.2}$$

where the dot denotes derivative with respect to t. Let $\{\mathbf{T}(t), \mathbf{N}(t), \mathbf{B}(t)\}$ denote a moving orthonormal frame along C, where $\mathbf{T}$ is the unit tangent vector, $\mathbf{N}$ is normal vector and $\mathbf{B}$ is the binormal vector at position $\mathbf{r}(t)$, if s denotes the arc length of C and the parametrization is of unit speed $|\dot{\mathbf{r}}(s)| = 1$. The usual three dimensional Frênet formulae relating derivatives of the moving frame vectors are [85]:

$$\begin{aligned} \dot{\mathbf{T}}(s) &= \kappa(s)\mathbf{N}(s), \\ \dot{\mathbf{N}}(s) &= -\kappa(s)\mathbf{T} + \tau(s)\mathbf{B}(s), \\ \dot{\mathbf{B}}(s) &= -\tau(s)\mathbf{N}(s), \end{aligned} \tag{2.3}$$

above and from now on we will use the dot to donate derivative with respect to arc length.

2.2.2 Mathematical helix

In general, a curve is a mathematical helix if and only if the ratio of the torsion to the curvature is constant,

$$\frac{\tau}{\kappa} = constant. \tag{2.4}$$

2.2.3 Curves on sphere

Theorem 1 *A smooth regular space curve $\mathbf{r} : I \longrightarrow \mathbb{R}^3$ is contained in a sphere of radius R, if and only if [69]*

$$\frac{1}{\kappa^2} + \left(\frac{\dot{\kappa}}{\kappa^2\tau}\right)^2 = R^2, \tag{2.5}$$

where $\kappa \neq 0$ and $\tau \neq 0$. To prove this, we follow [62] as below.

Proof: For convenience we may assume the unit sphere is centred at the origin, then take $y_0 = 0$. If a curve given by $\mathbf{r}(s)$ lies on this sphere then

$$\mathbf{r}(s) \cdot \mathbf{r}(s) = R^2.$$

By differentiating this we obtain:

$$2\mathbf{r} \cdot \dot{\mathbf{r}} = 0,$$

or

$$\mathbf{r} \cdot \mathbf{T} = 0,$$

then by differentiating this again:

$$\mathbf{r} \cdot \dot{\mathbf{T}} + \dot{\mathbf{r}} \cdot \mathbf{T} = 0,$$

or

$$\kappa \mathbf{r} \cdot \mathbf{N} + 1 = 0,$$

noting that $\kappa \neq 0$ and

$$\mathbf{r} \cdot \mathbf{N} = \frac{-1}{\kappa},$$

then by differentiating this again we get:

$$\dot{\mathbf{r}} \cdot \mathbf{N} + \mathbf{r} \cdot \dot{\mathbf{N}} = \frac{\dot{\kappa}}{\kappa^2},$$

or

$$\mathbf{r} \cdot (\kappa \mathbf{T} + \tau \mathbf{B}) = \frac{\dot{\kappa}}{\kappa^2}.$$

Also, by using $\mathbf{r} \cdot \mathbf{T} = 0$, where $\tau \neq 0$, we get

$$\mathbf{r} \cdot \mathbf{B} = \dot{\kappa}/\kappa^2\tau,$$

so the components of $\mathbf{r}$, with respect to $\mathbf{T}, \mathbf{N}, \mathbf{B}$ are $0, -1/\kappa, \dot{\kappa}/\kappa^2\tau$, so we obtain that

$$\mathbf{r} = \frac{-1}{\kappa}\mathbf{N} + \frac{\dot{\kappa}}{\kappa^2\tau}\mathbf{B},$$

and hence

$$\mathbf{r} \cdot \mathbf{r} = \left(\frac{-1}{\kappa}\mathbf{N} + \frac{\dot{\kappa}}{\kappa^2\tau}\mathbf{B}\right) \cdot \left(\frac{-1}{\kappa}\mathbf{N} + \frac{\dot{\kappa}}{\kappa^2\tau}\mathbf{B}\right) = \left(\frac{1}{\kappa}\right)^2 + \left(\frac{\dot{\kappa}}{\kappa^2\tau}\right)^2 = R^2.$$

□

2.2.4 Mathematical helices on a sphere

Solving equation (2.5), curve on the sphere of radius 1 with $\tau = c\kappa$ satisfies

$$\begin{aligned}
&\frac{1}{\kappa^2} + [\frac{\dot{\kappa}}{\kappa^2 (c\kappa)}]^2 = 1, \\
&\frac{1}{\kappa^2} + \frac{\dot{\kappa}}{c^2\kappa^6} = 1, \\
&\frac{\kappa^2 \left(c^2\kappa^4 + \dot{\kappa}^2\right)}{c^2\kappa^8} = 1, \\
&\frac{c^2\kappa^4 + \dot{\kappa}^2}{c^2\kappa^6} = 1, \\
&\frac{\dot{\kappa}}{\kappa^2\sqrt{\kappa^2 - 1}} = c,
\end{aligned}$$

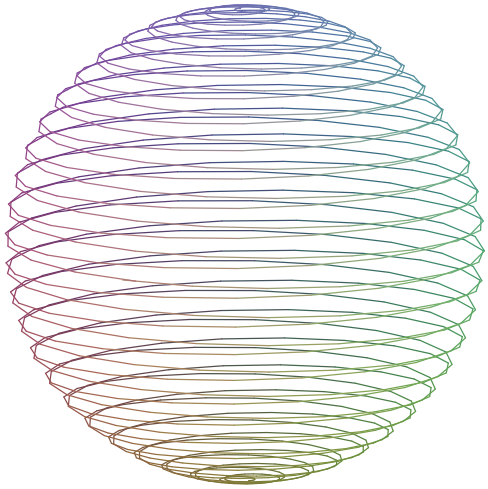

Figure 2.3: Mathematical helix.

Where c is a constant. By integrating bottom sides we obtain the curvature

$$\kappa(s) = \frac{1}{\sqrt{1 - c^2 s^2}}, \tag{2.6}$$

and since $\tau = c\kappa$ we have

$$\tau(s) = \frac{c}{\sqrt{1 - c^2 s^2}}. \tag{2.7}$$

As shown in [69], for parameter $c \neq 0$, another curve on a sphere can be prescribed by the position vector

$$\begin{aligned} \mathbf{r}(t) \quad = \quad & \left(\cos t \cos\left(\frac{\sqrt{1+c^2}}{c} t\right) + \frac{c}{\sqrt{1+c^2}} \sin t \sin\left(\frac{\sqrt{1+c^2}}{c} t\right), \right. \\ & \left. - \cos t \sin\left(\frac{\sqrt{1+c^2}}{c} t\right) + \frac{c}{\sqrt{1+c^2}} \sin t \cos\left(\frac{\sqrt{1+c^2}}{c} t\right), \frac{\sin t}{\sqrt{1+c^2}} \right), \end{aligned}$$

which may also be written in arc length parametrization as

$$\begin{aligned} \mathbf{r}(s) = \Bigg(& \sqrt{1 - c^2 s^2} \cos\left(\frac{\sqrt{1+c^2}\arcsin(cs)}{c}\right) + \frac{c^2 s}{\sqrt{1+c^2}} \sin\left(\frac{\sqrt{1+c^2}\arcsin(cs)}{c}\right), \\ & - \sqrt{1 - c^2 s^2} \sin\left(\frac{\sqrt{1+c^2}\arcsin(cs)}{c}\right) + \frac{c^2 s}{\sqrt{1+c^2}} \cos\left(\frac{\sqrt{1+c^2}\arcsin(cs)}{c}\right), \\ & \frac{cs}{\sqrt{1+c^2}} \Bigg). \end{aligned} \tag{2.8}$$

In this case, the ratio of the torsion to the curvature is

$$\frac{c}{\sqrt{1 - c^2 s^2}} \sqrt{1 - c^2 s^2} = c,$$

which means that it is a mathematical helix and for

$$\frac{1}{\kappa^2}+\left(\frac{\dot{\kappa}}{\kappa^2\tau}\right)^2=1,$$

$$1-c^2s^2+\left[\frac{c^2s}{(1-c^2s^2)^{\frac{3}{2}}\,\frac{c}{(1-c^2s^2)^{\frac{3}{2}}}}\right]^2=1,$$

which means that it is a curve on the sphere, so it is clear to see that this curve is mathematical helix on the sphere as shown in Figure 2.3.

2.2.5 Revolutionary curve on a sphere

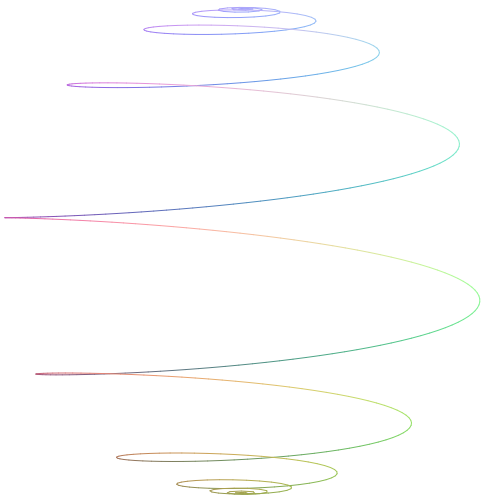

Figure 2.4: Revolutionary curve on a sphere.

Here we describe a curve that is not a mathematical helix on the unit sphere, but there is an axis about which the curve makes an entire rotation. It has position vector

$$\hat{\mathbf{r}}(s)=(\sin\theta\cos\phi,\sin\theta\sin\phi,\cos\theta)\,, \tag{2.9}$$

where, for a parameter $\gamma\neq 0$,

$$\theta=\frac{s}{\sqrt{1+\gamma^2}},\quad \phi=\gamma\log\left(\tan\frac{\theta}{2}\right). \tag{2.10}$$

We note that the projection of $\hat{\mathbf{r}}$ in the xy plane makes a complete revolution around the origin. So this curve does wind all the way around the z-axis and it is parameterized by arc length. To find the curvature, firstly we find

$$|\dot{\mathbf{r}}\times\ddot{\mathbf{r}}|=\left(1+\gamma^2\right)\sqrt{\frac{\beta^6\left\{-\gamma^2-1+[\cos\theta\,(s)]^2\right\}}{s^6\left\{-1+[\cos\theta\,(s)]^2\right\}}},$$

and

$$|\dot{\mathbf{r}}|^3 = \beta^2 \left(1+\gamma^2\right)^{3/2} \sqrt{\frac{\beta^2}{s^2}} s^{-2},$$

and by substituting this into (2.1) we get

$$\kappa = \frac{1}{\sqrt{(1+\gamma^2)}} \sqrt{1 + \frac{\gamma^2}{\sin^2(\theta)}}, \tag{2.11}$$

and to find the torsion, first we find

$$\det(\dot{\mathbf{r}}, \ddot{\mathbf{r}}, \dddot{\mathbf{r}}) = \frac{\beta^6 \gamma \left(1 + 2\,\gamma^2 + \gamma^4\right)}{s^6 \left(-1 + \left[\cos\left(\theta\left(s\right)\right)\right]^2\right)},$$

and

$$|\dot{\mathbf{r}} \times \ddot{\mathbf{r}}|^2 = \frac{\beta^6 \left(-1 + \left[\cos\theta\left(s\right)\right]^2 - 3\,\gamma^2 + 2\,\gamma^2 \left[\cos\theta\left(s\right)\right]^2 - 3\,\gamma^4 + \gamma^4 \left[\cos\theta\left(s\right)\right]^2 - \gamma^6\right)}{t^6 \left(-1 + \left[\cos\theta\left(s\right)\right]^2\right)},$$

and by substituting this into (2.2) we get:

$$\tau = -\frac{\gamma}{\gamma^2 + \sin^2(\theta)}, \tag{2.12}$$

in this case $\frac{\tau}{\kappa} \neq$ constant which means that it is not mathematical helix, however, from the expression for $\mathbf{r}(s)$ the curve is on the sphere. So we conclude that this curve is a curve on the sphere but it is not a mathematical helix as shown in Figure 2.4.

2.2.6 Calculus of variations

Generally, the objective of calculus of variations is to find a function $y(x)$ which will minimize or maximize some integral or energy like

$$I[y] = \int_a^b f(x, y, y')dx,$$

with conditions $y(a) = A$, $y(b) = B$ for constants A and B. The integrand f is a suitably smooth function of x, y and $y'(x)$. By assuming that $u(x)$ is a suitably smooth function which minimizes I let:

$$y(x) = u(x) + \varepsilon v(x),$$

when ε is a parameter and v is a smooth function defined on $[a,b]$ with compact support which means v and all its derivatives go to zero at the endpoints of the interval a and b. Now we define J as:

$$I[y+\varepsilon v] = J(\varepsilon) = \int_a^b f(x, u(x)+\varepsilon v(x), u'(x)+\varepsilon v'(x))dx.$$

Since $u(x)$ is a minimizer of I (this is true for suitable smooth f), it should be that $J'(0) = 0$ where dot denotes the derivative with respect to ε. We calculate

$$\begin{aligned} J'(\varepsilon) = \int_a^b \Big[& \frac{\partial f}{\partial y}(x, u(x)+\varepsilon v(x), u'(x)+\varepsilon v'(x))v(x) \\ & + \frac{\partial f}{\partial y'}(x, u(x)+\varepsilon v(x), u'(x)+\varepsilon v'(x))v'(x)\Big]dx, \end{aligned}$$

therefore

$$J'(0) = \int_a^b \left[\frac{\partial f}{\partial y}(x, u(x), u'(x))v(x) + \frac{\partial f}{\partial y'}(x, u(x), u'(x))v'(x)\right] dx,$$

which is called the first variation of I. When we integrate by parts for the second term of this equation and use v has compact support (so there is no boundary term from integration by parts), we get:

$$0 = J'(0) = \int_a^b \left[\frac{\partial f}{\partial y}(x, u(x), u'(x)) - \frac{d}{dx}\frac{\partial f}{\partial y'}(x, u(x), u'(x))\right] v(x)dx.$$

So from the fundamental lemma of the calculus of variations we must have

$$\frac{\partial f}{\partial y}\left(x, u(x), u'(x)\right) - \frac{d}{dx}\frac{\partial f}{\partial y'}\left(x, u(x), u'(x)\right) = 0.$$

This is the Euler-Lagrange equation for u; critical functions in the energy functional I as shown in [68].

2.2.6.1 Normal variations of space curve

In this subsection, we review the idea in [68] to find extremal curves in three-dimensional Euclidean space by using calculus of variations. Assume that C is a curve in three-dimensional space, represented by the position vector $\mathbf{r}(s)$ for $s \in [a,b]$ which minimizes some energy

$$I[\mathbf{r}] = \int_c f(\kappa, \tau)dl.$$

The energy is a line integral along the curve C which has arc length element dl and energy density $f(\kappa, \tau)$ which depends on curvature and torsion of the curve C. To obtain Euler-Lagrange equations for minimizing $I[\mathbf{r}]$, first we observe that we parameterize the line integral as

$$I[\mathbf{r}] = \int_a^b f(\kappa(s), \tau(s))|\dot{\mathbf{r}}(s)|ds,$$

where the arc length element is $dl = |\dot{\mathbf{r}}(s)|ds$. Assuming $\mathbf{r}(s)$ is a suitably smooth curve minimizing $I[f]$. Define a varied curve

$$\tilde{\mathbf{r}}(s) = r(s) + \varepsilon_1\psi_1(s)\mathbf{N}(s) + \varepsilon_2\psi_2(s)\mathbf{B}(s),$$

where $\mathbf{r}$ has a Frênet frame $\{\mathbf{T}(s), \mathbf{N}(s), \mathbf{B}(s)\}$, ψ_1, ψ_2 are real-valued functions and $\varepsilon_1, \varepsilon_2$ are parameters. This is called a normal variation of the curve given by $\mathbf{r}(s)$. If the curve C with position vector $\mathbf{r}(s)$ is a minimizer, the function $J(\varepsilon_1, \varepsilon_2) = I[\tilde{\mathbf{r}}]$ has a critical point at $\varepsilon_1 = \varepsilon_2 = 0$ which means

$$\frac{\partial}{\partial\varepsilon_1}J(\varepsilon_1, \varepsilon_2)|_{\varepsilon=0} = 0, \tag{2.13}$$

and

$$\frac{\partial}{\partial\varepsilon_2}J(\varepsilon_1, \varepsilon_2)|_{\varepsilon=0} = 0. \tag{2.14}$$

These equations give the two Euler-Lagrange equations which should be satisfied by the curvature and torsion of critical curve.

2.2.6.2 Euler-Lagrange equations

If the energy density has the form $f(\kappa, \tau, \dot{\kappa}, \dot{\tau})$, which depends upon the curvature and torsion functions and their first derivatives, the Euler-Lagrange equations corresponding equations (2.13) and equation (2.14) are

$$\begin{aligned}
&\frac{d^2}{ds^2}\left[\frac{\partial f}{\partial\kappa} - \frac{d}{ds}(\frac{\partial f}{\partial\dot{\kappa}})\right] + \frac{2\tau}{\kappa}\frac{d^2}{ds^2}\left[\frac{\partial f}{\partial\tau} - \frac{d}{ds}(\frac{\partial f}{\partial\dot{\tau}})\right] \\
&+ (\frac{\dot{\tau}}{\kappa} - \frac{2\dot{\kappa}\tau}{\kappa^2})\frac{d}{ds}\left[\frac{\partial f}{\partial\tau} - \frac{d}{ds}(\frac{\partial f}{\partial\dot{\tau}})\right] + (\kappa^2 - \tau^2)\left[\frac{\partial f}{\partial\kappa} - \frac{d}{ds}(\frac{\partial f}{\partial\dot{\kappa}})\right] \\
&+ 2\kappa\tau\left[\frac{\partial f}{\partial\tau} - \frac{d}{ds}(\frac{\partial f}{\partial\dot{\tau}})\right] + \kappa\left[\dot{\kappa}\frac{\partial f}{\partial\dot{\kappa}} + \dot{\tau}\frac{\partial f}{\partial\dot{\tau}} - f\right] = 0,
\end{aligned} \tag{2.15}$$

and

$$
\begin{aligned}
&-\frac{1}{\kappa}\frac{d^3}{ds^3}\left[\frac{\partial f}{\partial \tau}-\frac{d}{ds}(\frac{\partial f}{\partial \dot{\tau}})\right]+\frac{2\dot{\kappa}}{\kappa^2}\frac{d^2}{ds^2}\left[\frac{\partial f}{\partial \tau}-\frac{d}{ds}(\frac{\partial f}{\partial \dot{\tau}})\right]\\
&+2\tau\frac{d}{ds}\left[\frac{\partial f}{\partial \kappa}-\frac{d}{ds}(\frac{\partial f}{\partial \dot{\kappa}})\right]+(\frac{\tau^2}{\kappa}+\frac{\ddot{\kappa}}{\kappa^2}-\frac{2\dot{\kappa}^2}{\kappa^3}-\kappa)\frac{d}{ds}\left[\frac{\partial f}{\partial \tau}-\frac{d}{ds}(\frac{\partial f}{\partial \dot{\tau}})\right]\\
&\dot{\tau}\left[\frac{\partial f}{\partial \kappa}-\frac{d}{ds}(\frac{\partial f}{\partial \dot{\kappa}})\right]-\dot{\kappa}\left[\frac{\partial f}{\partial \tau}-\frac{d}{ds}(\frac{\partial f}{\partial \dot{\tau}})\right]=0. \qquad (2.16)
\end{aligned}
$$

The calculations to obtain these equations are shown in detail in Appendix A.

2.3 Mathematical results

To find the energy density f for which curves on a sphere solve the Euler-Lagrange equations, we consider three special cases: firstly, the energy density depends on the curvature only $f = f(\kappa)$, secondly, when the energy density depends on the curvature and its first derivative $f = f(\kappa, \dot{\kappa})$ and finally, when the energy density depends on the curvature and the torsion of the curve $f = f(\kappa, \tau)$.

2.3.1 Energy densities of the form $f = f(\kappa)$

In this case the energy density depends only on the curvature of the curve. The Euler-Lagrange equations (2.15) and (2.16) reduce to

$$\frac{d^2}{ds^2}f' + (\kappa^2 - \tau^2)f' - \kappa f = 0, \qquad (2.17)$$

and

$$\dot{\tau}f' + 2\tau\frac{d}{ds}f' = 0, \qquad (2.18)$$

where we write $f' = df/d\kappa$.

The study in [67] found all mathematical helix solutions of equations (2.17) and (2.18). Note that (2.18) may be integrated to give

$$\tau = \frac{C_1}{(f')^2}, \qquad (2.19)$$

for some constant C_1. For genuine space curves, this constant should not be equal to zero.

2.3.1.1 Mathematical spherical helix

Mathematical helices satisfy (2.4) and this leads from (2.19) to energy densities of the form $f(\kappa) = \pm 2\sqrt{\frac{C_1}{c}}\kappa^{\frac{1}{2}} + C_2$, where c comes from the relation (2.4) and C_2 is the constant of the integration. It was then shown in [67] that for (2.17) to be satisfied, the mathematical helices must lie on a catenary cylinder, so they do not lie on a sphere.

2.3.1.2 Revolutionary curves on a sphere

Here we would like to see if revolutionary curves on a sphere of the form (2.9), with curvature and torsion given by (2.11) and (2.12) respectively, are solutions of (2.17) and (2.18) for any energy density function $f(\kappa)$. First note that using (2.11) and (2.12) we may write τ as a function of κ as

$$\tau = \frac{1}{\gamma\kappa^2(1+\gamma^2)} - \frac{1}{\gamma}. \tag{2.20}$$

In view of (2.18) we must therefore have

$$f' = \sqrt{-C_1\gamma\,(1+\gamma^2)}\,\frac{\kappa}{\sqrt{(1+\gamma^2)\,\kappa^2 - 1}}, \tag{2.21}$$

as we seek real valued solutions we must require

$$\begin{aligned} &(1+\gamma^2)\kappa^2 - 1 > 0, \\ &\kappa^2 > \frac{1}{1+\gamma^2}. \end{aligned} \tag{2.22}$$

We comment that the larger the parameter γ, the less restrictive this condition. Also the larger γ gives more winds in view of definition of angle ϕ in equation (2.10). By integration, the energy density must have the form

$$f(\kappa) = \sqrt{\frac{-C_1\gamma}{1+\gamma^2}}\sqrt{(1+\gamma^2)\,\kappa^2 - 1} + C_2. \tag{2.23}$$

The condition (2.22) implies $f(\kappa) > C_2$, and the larger γ the closer the energy may approach the regular arc length. On the other hand, for fixed γ provided we look only for curves on the sphere with curvature satisfying (2.22), the energy density f in (2.23) satisfies the requirement. From (2.21) we compute

$$\frac{d}{ds}f' = -\frac{\sqrt{-C_1\gamma\,(1+\gamma^2)}}{[(1+\gamma^2)\,\kappa^2 - 1]^{\frac{3}{2}}}\dot{\kappa},$$

and

$$\frac{d^2}{ds^2}f' = -\frac{\sqrt{-C_1\gamma\left(1+\gamma^2\right)}}{\left[\left(1+\gamma^2\right)\kappa^2-1\right]^{\frac{5}{2}}}\left\{\left[\left(1+\gamma^2\right)\kappa^2-1\right]\ddot{\kappa}-3\left(1+\gamma^2\right)\kappa\dot{\kappa}^2\right\} \tag{2.24}$$

Moreover, by differentiating (2.11) we have

$$\dot{\kappa} = -\frac{\gamma^2}{\left(1+\gamma^2\right)^{\frac{3}{2}}}\frac{\cos\theta}{\sin^3\theta}\frac{1}{\kappa}, \tag{2.25}$$

and

$$\ddot{\kappa} = \frac{\gamma^2}{\left(1+\gamma^2\right)^2}\frac{\sin^2\theta+3\cos^2\theta}{\sin^4\theta}\frac{1}{\kappa} - \frac{\gamma^4}{\left(1+\gamma^2\right)^3}\frac{\cos^2\theta}{\sin^6\theta}\frac{1}{\kappa^3}, \tag{2.26}$$

Using the formulas for

$$\sin^2\theta = \frac{\gamma^2}{\left[\left(1+\gamma^2\right)\kappa^2-1\right]},$$

and

$$\cos^2\theta = 1-\frac{\gamma^2}{\left[\left(1+\gamma^2\right)\kappa^2-1\right]},$$

equation (2.25) becomes

$$\dot{\kappa}^2 = \frac{\left(\kappa^2-1\right)\left\{\left[\kappa^2\left(1+\gamma^2\right)\right]-1\right\}^2}{\kappa^2\left(1+\gamma^2\right)^2\gamma^2}, \tag{2.27}$$

and (2.26) becomes

$$\begin{aligned}\ddot{\kappa} = &\left[\frac{\gamma^2}{\left(1+\gamma^2\right)\kappa^2-1}+3\frac{\left(1+\gamma^2\right)\left(\kappa^2-1\right)}{\left(1+\gamma^2\right)\kappa^2-1}\right]\left[\left(1+\gamma^2\right)\kappa^2-1\right]^2\gamma^{-2}\left(1+\gamma^2\right)^{-2}\kappa^{-1}\\ &-\frac{\left(\kappa^2-1\right)\left[\left(1+\gamma^2\right)\kappa^2-1\right]^2}{\gamma^2\left(1+\gamma^2\right)^2\kappa^3}.\end{aligned} \tag{2.28}$$

Substituting theses two equations into (2.24), we have

$$\begin{aligned}\frac{d^2}{ds^2}f' = \frac{-\sqrt{-C_1\gamma(1+\gamma^2)}}{[(1+\gamma^2)\kappa^2-1]^{\frac{5}{2}}}\Bigg\{&[(1+\gamma^2)\kappa^2-1]\Bigg(\frac{\left[\frac{\gamma^2}{(1+\gamma^2)\kappa^2-1}+\frac{3(1+\gamma^2)(\kappa^2-1)}{(1+\gamma^2)\kappa^2-1}\right][(1+\gamma^2)\kappa^2-1]^2}{\gamma^2(1+\gamma^2)^2\kappa}\\ &-\frac{(\kappa^2-1)[(1+\gamma^2)\kappa^2-1]^2}{\gamma^2[1+\gamma^2]^2\kappa^3}\Bigg)-\frac{3(\kappa^2-1)[(1+\gamma^2)\kappa^2-1]^2}{(1+\gamma^2)\kappa\gamma^2}\Bigg\}.\end{aligned} \tag{2.29}$$

By substituting equations (2.20), (2.21), (2.23) and (2.29) into (2.17) we obtain that $-\kappa C_2 = 0$. Therefore, if $C_2 = 0$ then the curve does have an energy density $f(\kappa)$ of the form of the equation

(2.23).

We comment that using (2.5) in (2.18) it is possible to transform (2.17) and (2.18) into a very complicated single fourth order ordinary differential equation for κ. Solving this would give the curvature function $\kappa(s)$ for a space curve on the curve which was an extremal curve of the energy whose density could be recovered via (2.18).

2.3.1.3 Another case of $f = f(\kappa)$

From equations (2.5), (2.17) and (2.19), if we substitute equation (2.19) into equation (2.5) with $R = 1$ we obtain

$$\begin{aligned}
&\frac{1}{\kappa^2} + \left\{ \frac{\dot{\kappa}}{\kappa^2 \left[\frac{C_1}{(f')^2} \right]} \right\}^2 = 1, \\
&\frac{1}{\kappa^2} + \left[\frac{\dot{\kappa}^2 (f')^4}{\kappa^4 C_1^2} \right] = 1 \\
&(f')^4 = \frac{C_1^2 \kappa^2 \left(\kappa^2 - 1 \right)}{\dot{\kappa}^2}.
\end{aligned} \tag{2.30}$$

If we differentiate $(f')^4$ twice we obtain

$$\begin{aligned}
&\frac{d}{ds}(f')^4 = 4(f')^3 \frac{d}{ds} f', \\
&\frac{d^2}{ds^2}(f')^4 = 4(f')^3 \frac{d^2}{ds^2} f' + \frac{3}{4(f')^4} \left(\frac{d}{ds}(f')^4 \right)^2,
\end{aligned} \tag{2.31}$$

substituting these derivatives into equation (2.17) gives

$$\frac{d^2}{ds^2}(f')^4 - \frac{3}{4(f')^4} \left(\frac{d}{ds}(f')^4 \right)^2 + 4 \left(\kappa^2 - \frac{C_1^2}{(f')^4} \right) (f')^4 - 4\kappa (f')^3 f = 0,$$

which can be written as

$$f = \frac{1}{4\kappa (f')^3} \left[\frac{d^2}{ds^2}(f')^4 - \frac{3}{4(f')^4} \left(\frac{d}{ds}(f')^4 \right)^2 + 4\kappa^2 (f')^4 - 4C_1^2 \right], \tag{2.32}$$

then differentiate this with respect to s and write it into the form

$$\begin{aligned}
\dot{\kappa}(f')^4 = \frac{1}{4\kappa} \frac{d^3}{ds^3}(f')^4 - \frac{\dot{\kappa}}{4\kappa^2} \frac{d^2}{ds^2}(f')^4 - \frac{9}{16\kappa (f')^4} \frac{d}{ds}(f')^4 \frac{d^2}{ds^2}(f')^4 + \frac{3\dot{\kappa}}{16\kappa^2 (f')^4} \left(\frac{d}{ds}(f')^4 \right)^2 \\
+ \frac{3C_1^2}{4\kappa (f')^4} \frac{d}{ds}(f')^4 + \frac{21}{64\kappa (f')^8} \left(\frac{d}{ds}(f')^4 \right)^3 + \frac{1}{4} \kappa \frac{d}{ds}(f')^4 + \dot{\kappa}(f')^4 + \frac{\dot{\kappa} C_1^2}{\kappa^2},
\end{aligned}$$

which can be written as

$$\frac{1}{4\kappa}\frac{d^3}{ds^3}(f')^4-\frac{1}{4\kappa}\left(\frac{\dot\kappa}{\kappa}+\frac{9}{4(f')^4}\frac{d}{ds}(f')^4\right)\frac{d^2}{ds^2}(f')^4+\frac{3}{4\kappa(f')^4}\left(\frac{\dot\kappa}{4\kappa}+\frac{7}{16(f')^4}\frac{d}{ds}(f')^4\right)\left(\frac{d}{ds}(f')^4\right)^2 + \frac{1}{4}\left(\frac{3C_1^2}{\kappa(f')^4}+\kappa\right)\frac{d}{ds}(f')^4+\frac{\dot\kappa C_1^2}{\kappa^2}=0,$$

multiply this by 4κ gives

$$\frac{d^3}{ds^3}(f')^4-\left(\frac{\dot\kappa}{\kappa}+\frac{9}{4(f')^4}\frac{d}{ds}(f')^4\right)\frac{d^2}{ds^2}(f')^4+\frac{3}{(f')^4}\left(\frac{\dot\kappa}{4\kappa}+\frac{7}{16(f')^4}\frac{d}{ds}(f')^4\right)\left(\frac{d}{ds}(f')^4\right)^2 + \kappa\left(\frac{3C_1^2}{\kappa(f')^4}+\kappa\right)\frac{d}{ds}(f')^4+\frac{4\dot\kappa C_1^2}{\kappa}=0. \quad (2.33)$$

Now by computing the first, second and third derivatives of equation (2.30) one obtains

$$\frac{d}{ds}(f')^4=2C_1^2\left(\frac{\kappa}{\dot\kappa}(2\kappa^2-1)-\kappa^2(\kappa^2-1)\frac{\ddot\kappa}{\dot\kappa^3}\right), \quad (2.34)$$

$$\frac{d^2}{ds^2}(f')^4=2C_1^2\left(\frac{-3\ddot\kappa\kappa}{\dot\kappa^2}(2\kappa^2-1)+\frac{3\ddot\kappa^2\kappa^2}{\dot\kappa^4}(\kappa^2-1)+(6\kappa^2-1)-\frac{\dddot\kappa\kappa^2}{\dot\kappa^3}(\kappa^2-1)\right), \quad (2.35)$$

and

$$\frac{d^3}{ds^3}(f')^4=2C_1^2\left\{\frac{12\ddot\kappa^2\kappa}{\dot\kappa^3}(2\kappa^2-1)-\frac{12\ddot\kappa^3\kappa^2}{\dot\kappa^5}(\kappa^2-1)-\frac{3\ddot\kappa}{\dot\kappa}(6\kappa^2-1)+\frac{9\dddot\kappa\ddot\kappa\kappa^2}{\dot\kappa^4}(\kappa^2-1) - \frac{5\dddot\kappa\kappa}{\dot\kappa^2}(2\kappa^2-1)+12\kappa\dot\kappa-\frac{\ddddot\kappa\kappa^2}{\dot\kappa^3}(\kappa^2-1)\right\}. \quad (2.36)$$

Substituting equations (2.30), (2.34), (2.35) and (2.36) into equation (2.33) gives

$$\frac{C_1^2}{2\kappa\dot\kappa^5(\kappa^2-1)^2}\Bigg\{4\dddot\kappa\ddot\kappa\dot\kappa^2\kappa^3\left[3\kappa^2(\kappa^2-1)+(1-\kappa^6)\right]+2\dddot\kappa\Big[-9\ddot\kappa\dot\kappa\kappa^3\Big(3\kappa^2(\kappa^2-1)+(1-\kappa^6)\Big) + \dot\kappa^3\kappa^2\Big(\kappa^2(2-\kappa^2)-1\Big)\Big]+15\ddot\kappa^3\kappa^3\left[3\kappa^2(\kappa^2-1)+(1-\kappa^6)\right]-3\ddot\kappa^2\dot\kappa^2\kappa^2\left[\kappa^2(2-\kappa^2)-1\right] + \ddot\kappa\left[4\dot\kappa^2\kappa^5\Big(3\kappa^2(\kappa^2-1)+(1-\kappa^6)\Big)+9\dot\kappa^4\kappa\big(\kappa^2(3-2\kappa^2)-1\big)\right]+3\dot\kappa^6\left[2\kappa^2(8\kappa^2-7)+5\right] + 4\dot\kappa^4\kappa^4\left[2\kappa^2(2+\kappa^4)-(5\kappa^4+1)\right]\Bigg\}=0. \quad (2.37)$$

As there is no explicit s in equation (2.37), we can reduce the order by 1. By writing

$$\dot\kappa=p(s), \quad (2.38)$$

now we find its derivatives as below

$$\ddot\kappa=\frac{dp}{d\kappa}p, \quad (2.39)$$

$$\dddot{\kappa} = \frac{d^2p}{d\kappa^2}p^2 + \left(\frac{dp}{d\kappa}\right)^2 p, \tag{2.40}$$

and

$$\ddddot{\kappa} = \frac{d^3p}{d\kappa^3}p^3 + 4p^2\left(\frac{d^2p}{d\kappa^2}\right)\left(\frac{dp}{d\kappa}\right) + \left(\frac{dp}{d\kappa}\right)^3 p. \tag{2.41}$$

If we substitute equations (2.38)-(2.41) into equation (2.37) we obtain the following equation

$$\left[4\kappa^3p^2\frac{d^3p}{d\kappa^3} - 2p\kappa^3\frac{d^2p}{d\kappa^2}\frac{dp}{d\kappa} + \kappa^3\left(\frac{dp}{d\kappa}\right)^3 + 4\kappa^5\frac{dp}{d\kappa}\right][3\kappa^2(\kappa^2-1) + (1-\kappa^6)]$$
$$+ [2\kappa^2p^2\frac{d^2p}{d\kappa^2} - \kappa^2p\left(\frac{dp}{d\kappa}\right)^2][\kappa^2(2-\kappa^2) - 1] + 9\kappa p^2\frac{dp}{d\kappa}[\kappa^2(3-2\kappa^2) - 1] + 3p^3[2\kappa^2(8\kappa^2-7) + 5]$$
$$+ 4\kappa^4p[2\kappa^2(2+\kappa^4) - (5\kappa^4+1)] = 0. \tag{2.42}$$

If we write the following terms in the form below

$$3\kappa^2(\kappa^2-1) + (1-\kappa^6) = -(\kappa^2-1)^3$$

$$\kappa^2(2-\kappa^2) - 1 = -(\kappa^2-1)^2$$

$$\kappa^2(3-2\kappa^2) - 1 = -(2\kappa^2-1)(\kappa^2-1)$$

$$2\kappa^2(2+\kappa^4) - (5\kappa^4+1) = (\kappa^2-1)^2(2\kappa^2-1),$$

equation (2.42) becomes

$$-\left[4\kappa^3p^2\frac{d^3p}{d\kappa^3} - 2p\kappa^3\frac{d^2p}{d\kappa^2}\frac{dp}{d\kappa} + \kappa^3\left(\frac{dp}{d\kappa}\right)^3 + 4\kappa^5\frac{dp}{d\kappa}\right](\kappa^2-1)^3$$
$$- [2\kappa^2p^2\frac{d^2p}{d\kappa^2} - \kappa^2p\left(\frac{dp}{d\kappa}\right)^2](\kappa^2-1)^2 - 9\kappa p^2\frac{dp}{d\kappa}[(2\kappa^2-1)(\kappa^2-1)] + 3p^3[2\kappa^2(8\kappa^2-7) + 5]$$
$$+ 4\kappa^4p(\kappa^2-1)^2(2\kappa^2-1) = 0, \tag{2.43}$$

which is the third order nonlinear ODE. If we rewrite equation (2.43) as a system of three first order ODEs for three dependent variables p, q and r where $q = \frac{dp}{d\kappa}$, $r = \frac{dq}{d\kappa} = \frac{d^2p}{d\kappa^2}$ and $\frac{dr}{d\kappa} = \frac{d^3p}{d\kappa^3}$, equation (2.43) becomes

$$\left[-4\kappa^3p^2\frac{dr}{d\kappa} + 2p\kappa^3rq - \kappa^3q^3 - 4\kappa^5q\right](\kappa^2-1)^3$$
$$- [2\kappa^2p^2r - \kappa^2pq^2][(\kappa^2-1)^2] - 9\kappa p^2q[(2\kappa^2-1)(\kappa^2-1)] + 3p^3[2\kappa^2(8\kappa^2-7) + 5]$$
$$+ 4\kappa^4p[(\kappa^2-1)^2(2\kappa^2-1)] = 0. \tag{2.44}$$

Using numerical integration; we applied Runge-Kutta fourth order method to solve equation (2.44) under initial condition of $(p(2), q(2), r(2)) = (2, 2, 2)$, the range of κ from 2 to 3 with step size $h = 0.001$. We plot the curve that shows the relation between κ and $1/p$ as shown in Figure 2.5. From the values of p as a function of κ we may reconstruct s as a function of κ as follows.

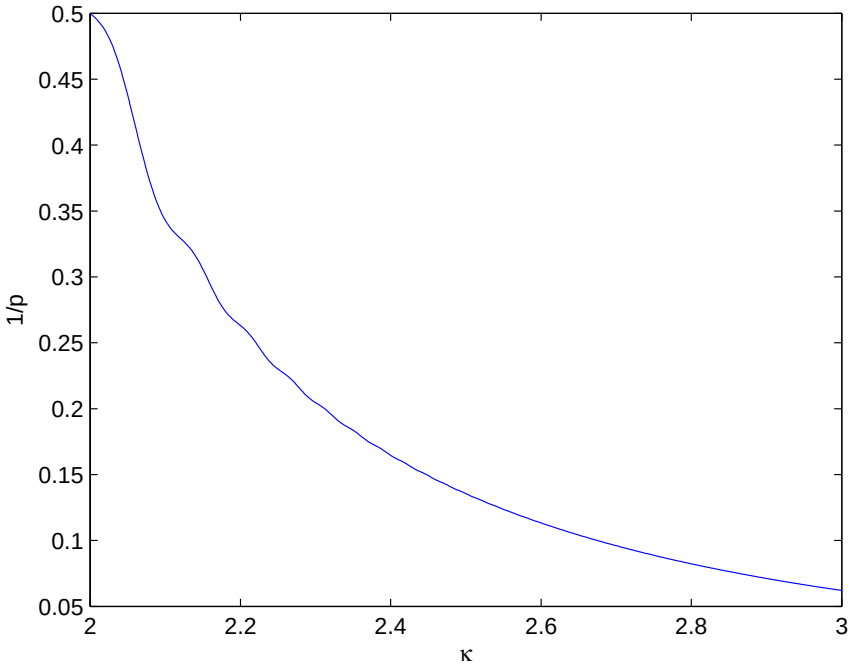

Figure 2.5: The relation curve between κ and $\frac{1}{p}$.

We have $p = \frac{d\kappa}{ds}$, so $\frac{1}{p} = \frac{ds}{d\kappa}$, then if we integrate this with respect to κ we obtain

$$\int_{\kappa_0}^{\kappa} \frac{1}{p} d\kappa = \int \frac{ds}{d\kappa} d\kappa, \tag{2.45}$$

which gives

$$\int_{\kappa_0}^{\kappa} \frac{1}{p} d\kappa = s(\kappa) - s(\kappa_0). \tag{2.46}$$

The left hand side of equation (2.46) corresponds to find the area under the curve in Figure 2.5 that shows the relation between κ and $\frac{1}{p}$, where $\kappa_0 = 2$ and $s(\kappa_0) = 0$. We approximate the area under the curve in Figure 2.5 by using trapezoidal rule with step size $h = 0.001$ and obtain Figure 2.6.

In view of the shape of the curve in Figure 2.6, we use least squares curve fitting with two potential functional forms of s. First if s is a power function $s(\kappa) = a\kappa^b + c$, when $c > 0$ we

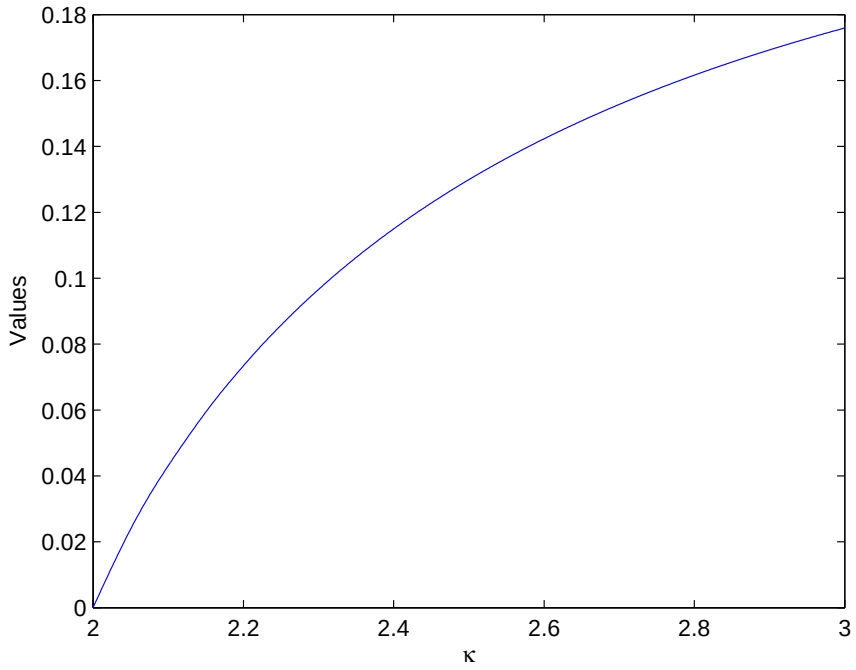

Figure 2.6: The relation curve between κ and the area under the curve by using trapezoidal rule.

obtain the curve in Figure 2.7 by least squares curve fitting where the values of the parameters are $a = -3.802, b = -4.182$ and $c = 0.213$. Then we may write

$$\kappa(s) = \left(\frac{s-c}{a}\right)^{\frac{1}{b}}, \tag{2.47}$$

therefore

$$\dot{\kappa}(s) = \frac{\left(\frac{s-c}{a}\right)^{\frac{1}{b}}}{b(s-c)}, \tag{2.48}$$

to find the torsion in terms of κ, $\dot{\kappa}$ can be written in terms of κ so from equation (2.47) we have $ak^b = s - c$. Substituting this into equation (2.48) gives

$$\dot{\kappa} = \frac{\kappa}{ab\kappa^b}. \tag{2.49}$$

From equation (2.5) we can write

$$\tau = \pm\frac{\dot{\kappa}}{\kappa\sqrt{\kappa^2 - 1}}, \tag{2.50}$$

where we assume

$$\kappa^2 > 1, \tag{2.51}$$

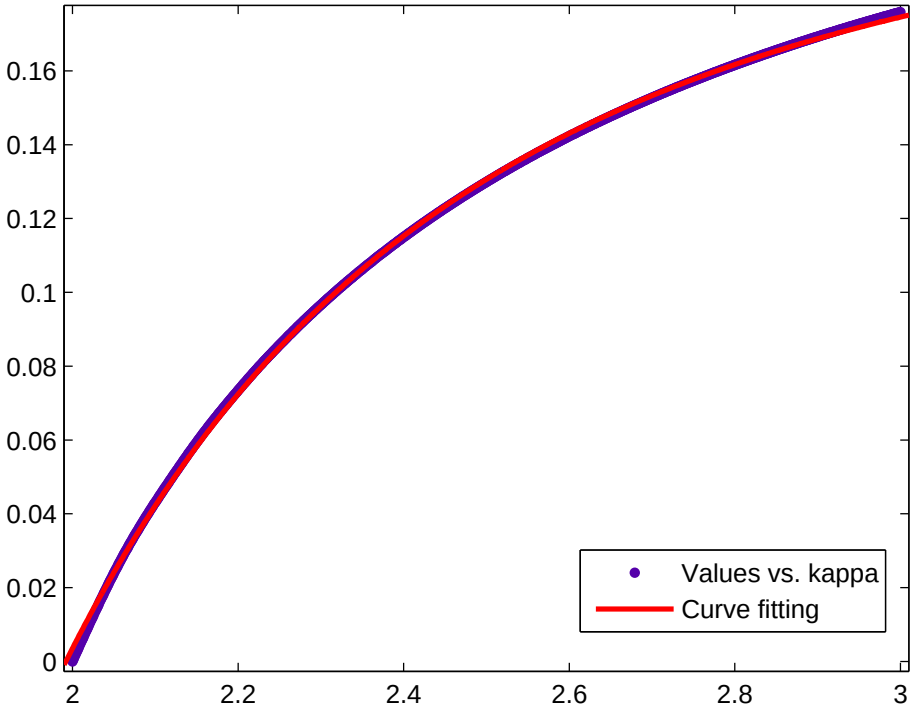

Figure 2.7: Least squares curve fitting when s is a power function and Figure 2.6.

so that τ is real valued (in theorem 1 we consider curves on the sphere whose curvature and torsion are necessarily real valued). By substituting equations (2.47) and (2.49) into (2.50) gives

$$\tau(\kappa) = \pm \frac{1}{ab\kappa^b\sqrt{\kappa^2 - 1}}. \tag{2.52}$$

Now from equations (2.19) and (2.52) we have

$$f(\kappa) = \pm C_1 ab \int \kappa^b \sqrt{\kappa^2 - 1} d\kappa. \tag{2.53}$$

In view of (2.51), $f(\kappa) > 0$, but f may be arbitrarily small if κ approaches to 1, in view of (2.5) this means the energy is small where the curve is close to a great circle. When we restrict to curves with $\kappa^2 > 1$ then (2.53) gives a valid energy density function. Secondly, if s is an exponential function in the form

$$s(\kappa) = -Ae^{bk} + c, \tag{2.54}$$

where $A > 0$ we obtain Figure 2.8 with parameters $A = 14.32, b = -2.159$ and $c = 0.1958$. As a result of equation (2.54)

$$\kappa(s) = \frac{1}{b} \ln\left(\frac{-s + c}{A}\right), \tag{2.55}$$

and

$$\dot{\kappa}(s) = -\frac{1}{(-s+c)b}. \tag{2.56}$$

To find the torsion in terms of κ, we rewrite $\dot{\kappa}$ in terms of κ, thus, from equation (2.55) we can write $Ae^{\kappa b} = -s + c$, which by substituting this into equation (2.56) we obtain

$$\dot{\kappa} = -\frac{1}{Abe^{\kappa b}}. \tag{2.57}$$

By substituting equations (2.55) and (2.57) into (2.5) gives

$$\tau(\kappa) = \pm\frac{-1}{Ae^{b\kappa}\kappa b(\kappa^2-1)^{\frac{1}{2}}}, \tag{2.58}$$

where we assume that $\kappa^2 > 1$ so that τ is real valued. Now from equations (2.19) and (2.58) we have

$$f(\kappa) = \pm(-C_1 Ab)\int e^{b\kappa}\kappa(\kappa^2-1)^{\frac{1}{2}}d\kappa. \tag{2.59}$$

As $\kappa^2 > 1$, $f(\kappa) > 0$, but f may be arbitrarily small if κ approaches to 1 and based on (2.5)

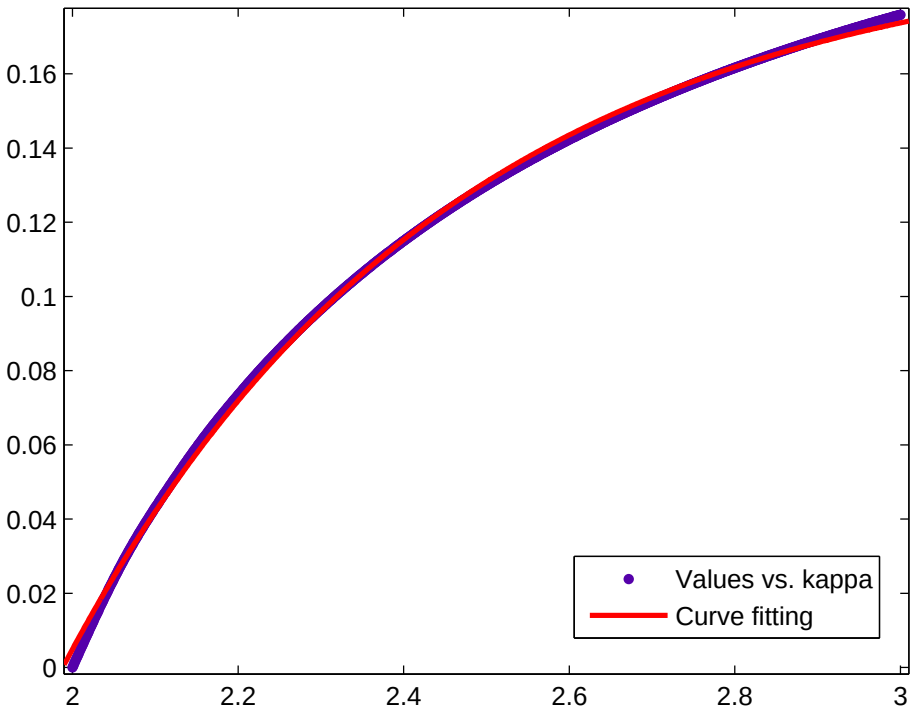

Figure 2.8: Least squares curve fitting when s is an exponential function and Figure 2.6

this means that the energy is small where the curve is close to a great circle. When we restrict

to curves with $\kappa^2 > 1$ then (2.59) gives a valid energy density function.

In summary, we have equation (2.37) that is a fourth order ODE. Firstly we reduce the order of this equation and rewrite it as a system of three first order ODEs. Then we solve this system numerically to find $s(\kappa)$, and apply curve fitting (we obtain two different functions) to find $\kappa(s)$ which can be used in the relation of the curve on the sphere (2.5) to find $\tau(\kappa)$. After that, we substitute $\tau(\kappa)$ into equation (2.19) to find the energy density. As a results, two energy densities are found based on the approximated solutions for equation (2.37) and curves on the sphere are approximate extrema of these energies. The code of this section is provided in Appendix B.

2.3.2 Energy densities of the form $f = f(\kappa, \dot{\kappa})$

In this case the energy densities depend on the curvature and its first derivative, so Euler-Lagrange equations (2.15) and (2.16) reduce to

$$\frac{d^2}{ds^2}\left[\frac{\partial f}{\partial \kappa} - \frac{d}{ds}(\frac{\partial f}{\partial \dot{\kappa}})\right] + (\kappa^2 - \tau^2)\left[\frac{\partial f}{\partial \kappa} - \frac{d}{ds}(\frac{\partial f}{\partial \dot{\kappa}})\right] + \kappa\left[\dot{\kappa}\frac{\partial f}{\partial \dot{\kappa}} - f\right] = 0, \tag{2.60}$$

and

$$2\tau\frac{d}{ds}\left[\frac{\partial f}{\partial \kappa} - \frac{d}{ds}(\frac{\partial f}{\partial \dot{\kappa}})\right] + \dot{\tau}\left[\frac{\partial f}{\partial \kappa} - \frac{d}{ds}(\frac{\partial f}{\partial \dot{\kappa}})\right] = 0. \tag{2.61}$$

Integration of equation (2.61) gives

$$\tau = \frac{C_1}{\left[\frac{\partial f}{\partial \kappa} - \frac{d}{ds}(\frac{\partial f}{\partial \dot{\kappa}})\right]^2} \tag{2.62}$$

Notice that for non-planar curves we must have $C_1 \neq 0$. Here, we use a procedure similar to that of [67] to find a class of extremal curves. Substitution of (2.62) into (2.60) leaves

$$\frac{d^2}{ds^2}\sqrt{\frac{C_1}{\tau}} + (\kappa^2 - \tau^2)\sqrt{\frac{C_1}{\tau}} \pm \kappa\left(\dot{\kappa}\frac{\partial f}{\partial \dot{\kappa}} - f\right) = 0. \tag{2.63}$$

Because f depends on κ and $\dot{\kappa}$ we wish to express all the other terms in (2.63) in terms of these 'independent variables' so we can solve (2.63) as a first order partial differential equation for f. A simple transformation allows us in this case to actually convert (2.63) into an ordinary differential equation.

2.3.2.1 Mathematical spherical helix

In this case we have $\tau = c\kappa$ and substitute this into (2.63) and differentiate, we have

$$\frac{d^2}{ds^2}\sqrt{\frac{C_1}{c\kappa}} + (\kappa^2 - \tau^2)\sqrt{\frac{C_1}{c\kappa}} \pm \kappa\left(\dot{\kappa}\frac{\partial f}{\partial \dot{\kappa}} - f\right) = 0. \tag{2.64}$$

By finding the second derivative of κ in terms of κ and $\dot{\kappa}$ using (2.6) and (2.7), where $\dot{\kappa} = c^2 s\kappa^3$ then $s = \frac{\dot{\kappa}}{c^2\kappa^3}$, we have

$$\ddot{\kappa} = c^2\kappa^3 + 3c^2\kappa^2\dot{\kappa}s$$
$$\ddot{\kappa} = c^2\kappa^3 + 3c^2\kappa^2\dot{\kappa}\left(\frac{\dot{\kappa}}{c^2\kappa^3}\right),$$

so we write $\ddot{\kappa}$ as

$$\ddot{\kappa} = c^2\kappa^3 + \frac{3\dot{\kappa}^2}{\kappa}. \tag{2.65}$$

Now to calculate $\frac{d^2}{ds^2}\sqrt{\frac{C_1}{c\kappa}}$, first we find

$$\frac{d}{ds}\sqrt{\frac{C_1}{c\kappa}} = \frac{1}{2}(\frac{C_1}{c\kappa})^{-}\frac{1}{2}\frac{d}{ds}(\frac{C_1}{c\kappa}) = \frac{1}{2}\frac{-C_1\dot{\kappa}}{\sqrt{\frac{C_1}{c\kappa}}c\kappa^2},$$

therefore

$$\frac{d^2}{ds^2}\sqrt{\frac{C_1}{c\kappa}} = \frac{d}{ds}\left(\frac{1}{2}\frac{-C_1\dot{\kappa}}{\sqrt{\frac{C_1}{c\kappa}}c\kappa^2}\right) = -\frac{1}{4}\frac{C_1(-3\dot{\kappa}^2 + 2\ddot{\kappa}\kappa)}{\sqrt{\frac{C_1}{c\kappa}}c\kappa^3},$$

using equation (2.65) we obtain

$$\frac{d^2}{ds^2}\sqrt{\frac{C_1}{c\kappa}} = \frac{-\frac{1}{4}C_1(3\dot{\kappa}^2 + 2c^2\kappa^4)}{\sqrt{\frac{C_1}{c\kappa}}c\kappa^3}.$$

Since $(\kappa^2 - \tau^2) = (1 - c^2)\kappa^2$, equation (2.64) becomes

$$-\frac{1}{4}\frac{C_1(3\dot{\kappa}^2 + 2c^2\kappa^4)}{\sqrt{\frac{C_1}{c\kappa}}c\kappa^3} + (1 - c^2)\kappa^2\sqrt{\frac{C_1}{c\kappa}} \pm \kappa\left(\dot{\kappa}\frac{\partial f}{\partial \dot{\kappa}} - f\right) = 0, \tag{2.66}$$

which is

$$-\frac{2}{4}\frac{C_1c^2\kappa^4}{\kappa^3\sqrt{\frac{C_1}{c\kappa}}c} - \frac{3}{4}\frac{C_1\dot{\kappa}^2}{\kappa^3\sqrt{\frac{C_1}{c\kappa}}c} + (1 - c^2)\kappa^2\sqrt{\frac{C_1}{c\kappa}} \pm \kappa\left(\dot{\kappa}\frac{\partial f}{\partial \dot{\kappa}} - f\right) = 0,$$

which can be simplified to give

$$a_1\kappa^{\frac{3}{2}} + a_2\dot{\kappa}^2\kappa^{\frac{-5}{2}} \pm \kappa\left(\dot{\kappa}\frac{\partial f}{\partial \dot{\kappa}} - f\right) = 0, \tag{2.67}$$

where

$$a_1 = \sqrt{\frac{C_1}{c}}\left(1 - \frac{3}{2}c^2\right), \tag{2.68}$$

and

$$a_2 = -\frac{3}{4}\sqrt{\frac{C_1}{c}}. \tag{2.69}$$

Dividing (2.67) by $\kappa^{\frac{-5}{2}}$, gives

$$a_1\kappa^4 + a_2\dot{\kappa}^2 \pm \kappa^{\frac{7}{2}}\left(\dot{\kappa}\frac{\partial f}{\partial \dot{\kappa}} - f\right) = 0.$$

Now, we try to find function $g(\kappa, \dot{\kappa})$ such that $\frac{\partial g}{\partial \dot{\kappa}} = \dot{\kappa}\frac{\partial f}{\partial \dot{\kappa}} - f$,

$$\frac{\partial}{\partial \dot{\kappa}}(\frac{f}{\dot{\kappa}}) = \frac{1}{\dot{\kappa}^2}(\dot{\kappa}\frac{\partial f}{\partial \dot{\kappa}} - f),$$

noting that

$$\dot{\kappa}^2\frac{\partial}{\partial \dot{\kappa}}(\frac{f}{\dot{\kappa}}) = \dot{\kappa}\frac{\partial f}{\partial \dot{\kappa}} - f, \tag{2.70}$$

by substituting (2.70) into (2.67) gives

$$a_1\kappa^4 + a_2\dot{\kappa}^2 \pm \kappa^{\frac{7}{2}}\left(\dot{\kappa}^2\frac{\partial}{\partial \dot{\kappa}}(\frac{f}{\dot{\kappa}})\right) = 0.$$

Writing $g(\kappa, \dot{\kappa}) = \frac{f(\kappa,\dot{\kappa})}{\dot{\kappa}}$, this equation becomes

$$a_1\kappa^4 + a_2\dot{\kappa}^2 \pm \kappa^{\frac{7}{2}}\dot{\kappa}^2\frac{\partial g}{\partial \dot{\kappa}} = 0,$$

which we may now integrate to find

$$g(\kappa, \dot{\kappa}) = \pm a_1\kappa^{\frac{1}{2}}\frac{1}{\dot{\kappa}} \mp a_2\kappa^{\frac{-7}{2}}\dot{\kappa} + g_1(\kappa),$$

where g_1 is an arbitrary function of κ. As a result, we have a class of energy densities which gives rise to extremal curves that are mathematical helices on the sphere, namely

$$f(\kappa, \dot{\kappa}) = \pm a_1\kappa^{\frac{1}{2}} \pm a_2\kappa^{\frac{-7}{2}}\dot{\kappa}^2 + \dot{\kappa}g_1(\kappa), \tag{2.71}$$

where the nonzero constants a_1 and a_2 are given by (2.68) and (2.69). In particular, the constants C_1 and c can be chosen such that each of the terms in the energy density is positive. In the

special case $c^2 = \frac{3}{2}$, we have $a_1 = 0$ with a corresponding simpler class of energy densities. In summary, energy densities of this form give rise to extremal curves which are mathematical helices on the sphere.

In this case, we consider that

1. From

$$\kappa = \frac{1}{\sqrt{1 - c^2 s^2}}$$

we have

$$\dot{\kappa} = \frac{sc^2}{(1 - c^2 s^2)^{\frac{3}{2}}} \tag{2.72}$$

and

$$s = \pm \frac{1}{c} \sqrt{1 - \frac{1}{\kappa^2}} \tag{2.73}$$

by substituting (2.73) into (2.72) we get an expression for $\dot{\kappa}$ in terms of κ

$$\dot{\kappa} = \pm \kappa^2 c \sqrt{\kappa^2 - 1}. \tag{2.74}$$

Now if we use (2.74) in (2.66) for the first term, we obtain the equation of form

$$g_1(\kappa) - \frac{\partial g}{\partial \dot{\kappa}} = 0,$$

where g_1 has precise form from (2.66) by using (2.74)

$$-\frac{C_1^{\frac{1}{2}} c^2 \kappa^{\frac{1}{2}}}{4} \left(3(\kappa^2 - 1) + 2\right) + (1 - c^2)\kappa \sqrt{\frac{C_1}{c\kappa}},$$

$$g_1(\kappa) = \frac{\partial g}{\partial \dot{\kappa}}.$$

Thus, we have

$$g = \dot{\kappa} g_1(\kappa) + g_2(\kappa),$$

for an arbitrary function $g_2(\kappa)$. In terms of f we have

$$\frac{1}{\dot{\kappa}} f(\kappa, \dot{\kappa}) = \dot{\kappa} g_1(\kappa) + g_2(\kappa),$$

$$f(\kappa, \dot{\kappa}) = \dot{\kappa}^2 g_1(\kappa) + \dot{\kappa} g_2(\kappa), \tag{2.75}$$

Using $\tau = c\kappa$ for mathematical helices and relation (2.5) for curves on the sphere, we see that (2.75) and (2.71) are equivalent.

2. If we solve κ in terms of $\dot{\kappa}$ from (2.74) we have

$$\kappa = \pm\sqrt{\frac{\dot{\kappa}}{c\sqrt{\kappa^2-1}}}. \tag{2.76}$$

By substituting (2.76) into (2.66), we may obtain new ordinary differential equations which can be solved to determine g and f. The resulting equations are more complicated than the previous ordinary differential equations which we solved explicitly. Let us give another procedure for producing more ordinary differential equations, again, in our setting the resulting equations are quite complicated however we feel the technique is of interest given that the coupled nonlinear ordinary differential equations we are working with are difficult to analyze.

3. From (2.74) we have $\dot{\kappa}^2 = c^2\kappa^4(\kappa^2-1)$ which can be written as

$$c^2\kappa^6 - c^2\kappa^4 - \dot{\kappa}^2 = 0.$$

If we assume $\kappa^2 = y$ we obtain

$$y^3 - y^2 - \frac{\dot{\kappa}^2}{c^2} = 0.$$

As a cubic in y, this equation has at least one real solution. In fact, based on the Cardano's formula [82], this equation has exactly one real solution (and two complex conjugate solutions). The real solution is given by

$$y = \kappa^2 = \left(\left[\frac{1}{27} - \frac{\dot{\kappa}^2}{2c^2}\right] + \frac{\dot{\kappa}}{c}\left[-\frac{1}{27} - \frac{\dot{\kappa}^2}{4c^2}\right]^{\frac{1}{2}}\right)^{\frac{1}{3}} + \left(\left[\frac{1}{27} - \frac{\dot{\kappa}^2}{2c^2}\right] - \frac{\dot{\kappa}}{c}\left[-\frac{1}{27} - \frac{\dot{\kappa}^2}{4c^2}\right]^{\frac{1}{2}}\right)^{\frac{1}{3}}.$$

That is

$$\left(\frac{1}{27} - \frac{\dot{\kappa}^2}{2c^2}\right) \pm \frac{\dot{\kappa}}{c}\left(-\frac{1}{27} - \frac{\dot{\kappa}^2}{4c^2}\right)^{\frac{1}{2}} = A \pm Bi,$$

and calculating the third root of each in polar form using de Moivre's theorem. The sum of these roots is then

$$y = \kappa^2 = r^{\frac{1}{3}}\cos\left(\frac{1}{3}\tan^{-1}\frac{B}{A}\right),$$

which is real and positive where $r = \sqrt{A^2+B^2}$. By writing κ in terms of $\dot{\kappa}$ and substituting into (2.66), we can obtain a different ordinary differential equation which can be solved to obtain another class of energy functionals.

2.3.2.2 Revolutionary curves on sphere

Here, we know that not all spherical curves are mathematical helices [45], some are simply curves on the sphere. Here we study another type of curves on the sphere that are revolutionary curves which are not mathematical helix, given by (2.9). We note that the projection of $\hat{\mathbf{r}}$ in the $xy-$plane makes a complete revolution around the origin. The curvature and the torsion of these curves are given in (2.11) and (2.12) respectively. The first term of equation (2.63) is

$$\frac{d^2}{ds^2}\sqrt{\frac{C_1}{\tau}} = -\frac{\sqrt{C_1}}{4}\tau^{-\frac{5}{2}}(2\tau\ddot{\tau} - 3\dot{\tau}^2),$$

and equation (2.63) becomes

$$-\frac{\sqrt{C_1}}{4}\tau^{-\frac{5}{2}}(2\tau\ddot{\tau} - 3\dot{\tau}^2) + (\kappa^2 - \tau^2)\sqrt{C_1}\tau^{\frac{-1}{2}} \pm \kappa\left(\dot{\kappa}\frac{\partial f}{\partial \dot{\kappa}} - f\right) = 0. \tag{2.77}$$

Equation (2.77) may be written as

$$2\tau\ddot{\tau} - 3\dot{\tau}^2 - 4\tau^2(\kappa^2 - \tau^2) \mp \frac{4\kappa}{\sqrt{C_1}}\tau^{\frac{5}{2}}\dot{\kappa}^2\frac{\partial g}{\partial \dot{\kappa}} = 0, \tag{2.78}$$

where again

$$g(\kappa, \dot{\kappa}) = \frac{f(\kappa, \dot{\kappa})}{\dot{\kappa}}.$$

Using (2.20) where we write τ as a function of κ, we have

$$\dot{\tau} = \frac{-2\dot{\kappa}}{\gamma(1+\gamma^2)\kappa^3},\ \ddot{\tau} = -\frac{2}{\gamma(1+\gamma^2)}\left(\frac{-3\dot{\kappa}^2}{\kappa^4} + \frac{\ddot{\kappa}}{\kappa^3}\right). \tag{2.79}$$

Combining (2.5) and (2.20) gives rise to

$$\dot{\kappa}^2 = \frac{1}{\gamma^2}\left[\frac{1}{(1+\gamma^2)^2} - \frac{1}{\kappa^2(1+\gamma^2)^2} - \frac{2\kappa^2}{(1+\gamma^2)} + \frac{2}{(1+\gamma^2)} + \kappa^4 - \kappa^2\right], \tag{2.80}$$

which can be differentiated with respect to s to obtain

$$\ddot{\kappa} = \frac{1}{\gamma^2}\left[\frac{1}{\kappa^3(1+\gamma^2)^2} - \frac{2\kappa}{(1+\gamma^2)} + 2\kappa^3 - \kappa\right]. \tag{2.81}$$

Next, we substitute (2.20) and (2.79) into (2.78) and on using (2.80) and (2.81) we find

$$-\frac{4}{\gamma^2(1+\gamma^2)^3\kappa^4}\left[3\kappa^2(1+\gamma^2) - 3\kappa^4(1+\gamma^2)^2 + \kappa^6(1+3\gamma^2+3\gamma^4+\gamma^6) - 1\right]$$
$$\mp \frac{4\kappa}{\sqrt{C_1}}\left[\frac{1-(1+\gamma^2)\kappa^2}{\gamma(1+\gamma^2)\kappa^2}\right]^{\frac{5}{2}}\dot{\kappa}^2\frac{\partial g}{\partial \dot{\kappa}} = 0.$$

Dividing by $\frac{4\kappa}{\sqrt{C_1}}\left[\frac{1-(1+\gamma^2)\kappa^2}{\gamma(1+\gamma^2)\kappa^2}\right]^{\frac{5}{2}}$, we see that equation (2.77) can be written on the form

$$g_1(\kappa) + \dot{\kappa}^2 \frac{\partial g}{\partial \dot{\kappa}} = 0, \tag{2.82}$$

where

$$g_1(\kappa) = \pm \frac{-\sqrt{C_1}}{\kappa^5 (1+\gamma^2)^3 \gamma^2 \left[\frac{1-(1+\gamma^2)\kappa^2}{\gamma(1+\gamma^2)\kappa^2}\right]^{\frac{5}{2}}} \left(\gamma^2\kappa^2 + \kappa^2 - 1\right)^3. \tag{2.83}$$

Solving (2.82), we have

$$g(\kappa, \dot{\kappa}) = \frac{g_1(\kappa)}{\dot{\kappa}} + g_2(\kappa),$$

where $g_2(\kappa)$ is an arbitrary function of κ. Since $f(\kappa, \dot{\kappa}) = \dot{\kappa} g(\kappa, \dot{\kappa})$, we finally obtain

$$f(\kappa, \dot{\kappa}) = g_1(\kappa) + \dot{\kappa} g_2(\kappa), \tag{2.84}$$

where $g_2(\kappa)$ is arbitrary but $g_1(\kappa)$ is given previously by (2.83). Using (2.80) to substitute $\dot{\kappa}^2$ in terms of κ, we may obtain a different ordinary differential equation. However, integration with respect to $\dot{\kappa}$ introduces an arbitrary function of κ; by rearrangement we can see that this does not yield any other different solutions.

Some comments regarding (2.71) and (2.84) are in order. We observe that both the energy densities (2.71) and (2.84) include a term of the form $\dot{\kappa} g(\kappa)$ for an arbitrary function $g(\kappa)$. This term arises as the arbitrary function of integration of the ordinary differential equation whose independent variable is $\dot{\kappa}$. The two classes of energy density (2.71) and (2.84) are, however, fundamentally different, because their other terms are different, comprising functions of κ, and perhaps $\dot{\kappa}$, which are prescribed via the Euler-Lagrange equations. It is important to note however that variations of these energy densities are also possible because using the individual parametrization of the helices involved, there is more than one way to write $\ddot{\kappa}$ and τ in terms of κ and $\dot{\kappa}$. We have chosen as far as possible to write $\ddot{\kappa}$ and τ in terms of κ and minimize the $\dot{\kappa}$ dependence, the latter leading to more complicated ordinary differential equations to solve. Nevertheless, this would present an avenue for uncovering further energy densities with the given curves as extremal curves.

Now, noting that for revolutionary curves on a sphere, from (2.5) we have

$$\dot{\kappa}^2 = (\kappa^2 - 1)\kappa^2\tau^2,$$

and from (2.80) we can write

$$(1+\gamma^2)^2\kappa^6 - (3+\gamma^2)(1+\gamma^2)\kappa^4 + [(2\gamma^2+3) - \gamma^2(1+\gamma^2)^2\dot{\kappa}^2]\kappa^2 - 1 = 0.$$

If we assume $\kappa^2 = y$ we can write this equation as

$$(1+\gamma^2)^2 y^3 - (3+\gamma^2)(1+\gamma^2)y^2 + [(2\gamma^2+3) - \gamma^2(1+\gamma^2)^2\dot{\kappa}^2]y - 1 = 0,$$

which is a cubic equation, so we use Cardano's formula to solve it for y,

$$y = \kappa^2 = \left[a + (b-c)^{\frac{1}{2}}\right]^{\frac{1}{3}} + \left[a - (b-c)^{\frac{1}{2}}\right]^{\frac{1}{3}},$$

where

$$a = \frac{1}{54}\frac{\gamma^2\Big(-81 - 9\gamma^2 + 2\gamma^3\Big) + 9\dot{\kappa}^2\gamma^2\Big(4\gamma^2 + \gamma^4 + 3\Big) - 54}{(1+\gamma^2)^3},$$

$$b = \frac{1}{2916}\frac{\Big[\gamma^2\Big(-81 - 9\gamma^2 + 2\gamma^3\Big) + 9\dot{\kappa}^2\gamma^2\Big(4\gamma^2 + \gamma^4 + 3\Big) - 54\Big]^2}{(1+\gamma^2)^6},$$

and

$$c = \frac{1}{729}\frac{\gamma^6\Big[\gamma^2 - 3 + 3\dot{\kappa}^2(1+\gamma^2)\Big]^3}{(1+\gamma^2)^6}.$$

Again, we can substitute this expression of y into (2.63) to find a new ordinary differential equation which may be solved to obtain more energies for which the curves of the form (2.9) are extrema.

2.3.2.3 Case of $f = f(\kappa, \dot{\kappa})$

In [85] the transformations $h = p - \dot{P}$ and $k = q - \dot{Q}$ where $p = \frac{\partial f}{\partial \kappa}$, $q = \frac{\partial f}{\partial \tau}$, $P = \frac{\partial f}{\partial \dot{\kappa}}$ and $Q = \frac{\partial f}{\partial \dot{\tau}}$ are introduced. Here we use dots to denote differentiation with respect to the arc length s. Based on these transformations, equations (2.15) and (2.16) reduce to

$$w = \kappa h + \tau k + \dot{\kappa} P + \dot{\tau} Q - f. \tag{2.85}$$

If $w = 0$ then there is a solution for Euler-Lagrange equations and the energy density can be written as

$$f(\kappa, \tau, \dot{\kappa}, \dot{\tau}) = \kappa\left[\frac{\partial f}{\partial \kappa} - \frac{d}{ds}\left(\frac{\partial f}{\partial \dot{\kappa}}\right)\right] + \tau\left[\frac{\partial f}{\partial \tau} - \frac{d}{ds}\left(\frac{\partial f}{\partial \dot{\tau}}\right)\right] + \dot{\kappa}\frac{\partial f}{\partial \dot{\kappa}} + \dot{\tau}\frac{\partial f}{\partial \dot{\tau}}. \tag{2.86}$$

Based on this conclusion in [85], here if we consider the energy density depending on κ and $\dot{\kappa}$, here $\tau = 0$, then $k = 0$ then equation (2.86) becomes

$$f(\kappa, \dot{\kappa}) = \kappa \left[\frac{\partial f}{\partial \kappa} - \frac{d}{ds} \left(\frac{\partial f}{\partial \dot{\kappa}} \right) \right] + \dot{\kappa} \frac{\partial f}{\partial \dot{\kappa}}. \tag{2.87}$$

Thus, if $f(\kappa, \dot{\kappa})$ is a homogeneous function of degree one, namely

$$\frac{\partial f}{\partial \kappa} \kappa + \frac{\partial f}{\partial \dot{\kappa}} \dot{\kappa} = f, \tag{2.88}$$

based on this equation (2.87) becomes

$$\frac{d}{ds} \left(\frac{\partial f}{\partial \dot{\kappa}} \right) = 0, \tag{2.89}$$

which gives

$$f = c\dot{\kappa} + g(\kappa), \tag{2.90}$$

for some function $g(\kappa)$. Using equation (2.88) we have

$$\frac{dg}{d\kappa} \kappa + c\dot{\kappa} = c\dot{\kappa} + g(\kappa),$$

so g must satisfy $\frac{dg}{d\kappa} \kappa = g$ and by solving this equation by gives $g(\kappa) = \tilde{c}\kappa$ where $\tilde{c}$ is a constant. Thus we obtain the energy density of the form

$$f(\kappa, \dot{\kappa}) = \tilde{c}\kappa + c\dot{\kappa}. \tag{2.91}$$

2.3.2.4 Another case of $f = f(\kappa, \dot{\kappa})$

From equation (2.5) we have

$$\tau = \pm \frac{\dot{\kappa}}{\kappa \sqrt{R^2 \kappa^2 - 1}}, \tag{2.92}$$

and from equation (2.62), equation (2.92) becomes

$$\frac{\partial f}{\partial \kappa} - \frac{d}{ds} \frac{\partial f}{\partial \dot{\kappa}} = \sqrt{\frac{C_1 \kappa}{\dot{\kappa}}} \sqrt[4]{R^2 \kappa^2 - 1}. \tag{2.93}$$

Using equation (2.93) and (2.87) from the last case, we obtain that

$$f - \dot{\kappa} \frac{\partial f}{\partial \dot{\kappa}} = \left[C_1^{\frac{1}{2}} \kappa^{\frac{3}{2}} \left(R^2 \kappa^2 - 1 \right)^{\frac{1}{4}} \dot{\kappa}^{-\frac{1}{2}} \right],$$

which is the first order partial differential equation for $f(\kappa, \dot{\kappa})$. If we look for solutions of the form

$$f(\kappa, \dot{\kappa}) = h(\kappa)g(\dot{\kappa}), \tag{2.94}$$

then we require

$$hg - \dot{\kappa}hg' = C_1^{\frac{1}{2}}\kappa^{\frac{3}{2}}\left(R^2\kappa^2 - 1\right)^{\frac{1}{4}}\dot{\kappa}^{-\frac{1}{2}},$$

so we conclude that

$$h(\kappa) = C_1^{\frac{1}{2}}\kappa^{\frac{3}{2}}\left(R^2\kappa^2 - 1\right)^{\frac{1}{4}}. \tag{2.95}$$

Now to determine function g we have, $g - yg' = y^{-\frac{1}{2}}$, where $y = \dot{\kappa}$, so

$$g' - \frac{1}{y}g = y^{-\frac{3}{2}},$$

which can be written as

$$Ig' - \dot{I}g = \frac{d}{dy}(Ig),$$

$$I = -\ln y,$$

$$\frac{d}{dy}[-\ln yg] = y^{-\frac{3}{2}},$$

that gives

$$g = \frac{2}{y^{\frac{1}{2}}\ln y} - \frac{c}{\ln y}, \tag{2.96}$$

where c is the integration constant. As a result, substituting equations (2.95) and (2.96) into equation (3.4.4) gives

$$f(\kappa, \dot{\kappa}) = C_1^{\frac{1}{2}}\kappa^{\frac{3}{2}}\left(R^2\kappa^2 - 1\right)^{\frac{1}{4}}\left[\frac{2}{\dot{\kappa}^{\frac{1}{2}}\ln\dot{\kappa}} - \frac{c}{\ln\dot{\kappa}}\right]. \tag{2.97}$$

Then from equations (2.62) and (2.87) we obtain

$$\frac{\partial f}{\partial \kappa} - \frac{d}{ds}\frac{\partial f}{\partial \dot{\kappa}} = \frac{1}{\kappa}\left[f - \dot{\kappa}\frac{\partial f}{\partial \dot{\kappa}}\right]. \tag{2.98}$$

To determine the right hand side of this equation, first we differentiate equation (2.97) for $\dot{\kappa}$,

$$\frac{\partial f}{\partial \dot{\kappa}} = \sqrt{C_1}\kappa^{\frac{3}{2}}(R^2\kappa^2 - 1)^{\frac{1}{4}}\left[\frac{-1}{\dot{\kappa}^{\frac{3}{2}}(\ln\dot{\kappa})} - \frac{2}{\dot{\kappa}^{\frac{3}{2}}(\ln\dot{\kappa})^2} + \frac{c}{(\ln\dot{\kappa})^2\dot{\kappa}}\right],$$

then we substitute this into the right hand side of equation (2.98),

$$\frac{-\left[-3(\ln\dot{\kappa})+\dot{\kappa}^{\frac{1}{2}}(\ln\dot{\kappa})c-2+c\dot{\kappa}^{\frac{1}{2}}\right]C_1^{\frac{1}{2}}\kappa^{\frac{1}{2}}(R^2\kappa^2-1)^{\frac{1}{4}}}{\dot{\kappa}^{\frac{1}{2}}(\ln\dot{\kappa})^2}. \tag{2.99}$$

Next we substitute this into equation (2.62),

$$\tau=\frac{\dot{\kappa}(\ln\dot{\kappa})^4}{\kappa\sqrt{R^2\kappa^2-1}\left[-3(\ln\dot{\kappa})+\dot{\kappa}^{\frac{1}{2}}(\ln\dot{\kappa})c-2+c\dot{\kappa}^{\frac{1}{2}}\right]^2},$$

then substituting this into equation (2.5) gives

$$\frac{1}{\kappa^2}+\frac{(R^2\kappa^2-1)\left(-3(\ln\dot{\kappa})+\dot{\kappa}^{\frac{1}{2}}(\ln\dot{\kappa})c-2+c\dot{\kappa}^{\frac{1}{2}}\right)^4}{\kappa^2(\ln\dot{\kappa})^8}=R^2.$$

By writing $\dot{\kappa}=p$ we obtain

$$\left[-3(\ln p)+p^{\frac{1}{2}}(\ln p)c-2+cp^{\frac{1}{2}}\right]^4=(\ln p)^8,$$

and taking 1/4 power of both sides gives

$$-3(\ln p)+p^{\frac{1}{2}}(\ln p)c-2+cp^{\frac{1}{2}}=(\ln p)^2.$$

If we want $\dot{\kappa}=p$ to be 1 a solution, then $c=2$ and

$$\kappa=s+d. \tag{2.100}$$

Substituting equation (2.100) into equation (2.5) we have

$$\tau=\frac{1}{\sqrt{R^2(s+d)^2-1}(s+d)}.$$

As a result we obtain the curve of this case as shown in Figure 2.9.

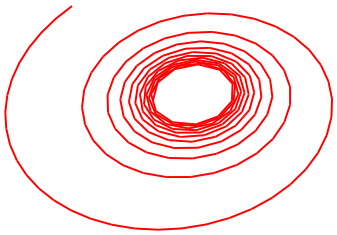

Figure 2.9: The curve based on its curvature and torsion given by $d = 2$ and $R = 1$.

2.3.3 Energy densities of the form $f = f(\tau)$

In the case that the energy densities depend on the curvature and the torsion of the curve. Then Euler-Lagrange equations (2.15) and (2.16) reduce to

$$\frac{d^2}{ds^2}\frac{\partial f}{\partial \kappa} + \frac{2\tau}{\kappa}\frac{d^2}{ds^2}\frac{\partial f}{\partial \tau} + \left(\frac{\dot{\tau}}{\kappa} - \frac{2\dot{\kappa}\tau}{\kappa^2}\right)\frac{d}{ds}\frac{\partial f}{\partial \tau} + \left(\kappa^2 - \tau^2\right)\frac{\partial f}{\partial \kappa} + 2\kappa\tau\frac{\partial f}{\partial \tau} - \kappa f = 0, \tag{2.101}$$

and

$$-\frac{1}{\kappa}\frac{d^3}{ds^3}\frac{\partial f}{\partial \tau} + \frac{2\dot{\kappa}}{\kappa^2}\frac{d^2}{ds^2}\frac{\partial f}{\partial \tau} + 2\tau\frac{d}{ds}\frac{\partial f}{\partial \kappa} + \left(\frac{\tau^2}{\kappa} + \frac{\ddot{\kappa}}{\kappa^2} - \frac{2\dot{\kappa}^2}{\kappa^3} - \kappa\right)\frac{d}{ds}\frac{\partial f}{\partial \tau} + \dot{\tau}\frac{\partial f}{\partial \kappa} - \dot{\kappa}\frac{\partial f}{\partial \tau} = 0. \tag{2.102}$$

Equations (2.101) and (2.102) are considerably more difficult to solve. If, for example, we consider $f = f(\tau)$ and we look only for mathematical helices (so $\kappa = C\tau$), (2.101) and (2.102) become

$$\dot{\tau}^2 f'''(\tau) + \left(\ddot{\tau} - \frac{\dot{\tau}^2}{2\tau}\right) f''(\tau) + C^2\tau^2 f'(\tau) - \frac{C^2\tau}{2} f(\tau) = 0 \tag{2.103}$$

and

$$\dot{\tau}^3 f''''(\tau) + \left(3\dot{\tau}\ddot{\tau} - \frac{2\dot{\tau}^3}{\tau}\right) f'''(\tau) + \left[\dddot{\tau} - \frac{\ddot{\tau}\dot{\tau}}{\tau} - \frac{2\dot{\tau}^3}{\tau^2} - \left(C^2 + 1\right)\tau^2\dot{\tau}\right] f''(\tau) + C^2\dot{\tau}\tau f'(\tau) = 0. \tag{2.104}$$

Where $f' = df/d\tau$. Clearly, if $f(\tau) = \gamma$ for some constant $\gamma > 0$, then equation (2.103) has no solution since we seek curves with nonzero torsion. If instead we take $f(\tau) = \beta\tau + \gamma$, for constants γ and β, then equation (2.103) reduces to

$$\frac{C^2\tau}{2}(\beta\tau - \gamma) = 0.$$

Now τ cannot be equal to γ/β, since κ would be a constant and we then have a mathematical helix on the cylinder not on the sphere. So again there are no solutions.

Since equations (2.103) and (2.104) have no explicit s terms, we may reduce the order by 1 by considering,

$$\begin{aligned} p(s) &= \frac{d\tau}{ds}, \\ \frac{dp}{d\tau} &= \frac{dp}{ds}\frac{ds}{d\tau} \\ \frac{d^2\tau}{ds^2} &= \frac{dp}{d\tau}p, \\ \frac{d^3\tau}{ds^3} &= \left[\frac{d^2p}{d\tau^2}p + \left(\frac{dp}{d\tau}\right)^2\right]p. \end{aligned} \tag{2.105}$$

We obtain

$$p^2 f''' + p\left(\frac{dp}{d\tau} - \frac{p}{2\tau}\right)f'' + C^2\tau^2 f' - \frac{C^2\tau}{2}f = 0, \tag{2.106}$$

and

$$p^2 f'''' + p\left(3\frac{dp}{d\tau} - \frac{2}{\tau}\right)f''' + \left[\frac{d^2p}{d\tau^2}(p) + \left(\frac{dp}{d\tau}\right)^2 - \frac{p}{\tau}\frac{dp}{d\tau} - \frac{2p^2}{\tau^2} - (C^2+1)\tau^2\right] f'' + C^2\tau f' = 0. \tag{2.107}$$

2.3.3.1 $f(\tau) = \alpha\tau^2 + \beta\tau + \gamma$

In this case if $\alpha = 0$ then it corresponds to the above case. However, generally, if $\alpha \neq 0$ there is no mathematical helix at all as a solution. If we substitute this case into (2.103) and (2.104) we obtain

$$2\alpha\ddot{\tau} - \alpha\frac{\dot{\tau}^2}{\tau} + \frac{3}{2}C^2\alpha\tau^3 + \frac{1}{2}C^2\beta\tau^2 - \frac{C^2\gamma}{2}\tau = 0, \tag{2.108}$$

and

$$2\alpha\dddot{\tau} - 2\alpha\frac{\ddot{\tau}\dot{\tau}}{\tau} - \frac{4\alpha\dot{\tau}^3}{\tau^2} - 2\alpha\tau^2\dot{\tau} + C^2\beta\dot{\tau}\tau = 0. \tag{2.109}$$

We reduce the order by 1 by using (2.105), and thus we get

$$\frac{dp}{d\tau} = -\frac{3}{4}\frac{C^2}{p}\tau^3 - \frac{1}{4\alpha}\frac{C^2\beta}{p}\tau^2 + \frac{C^2\gamma}{4\alpha p}\tau + \frac{p}{2\tau}, \tag{2.110}$$

and

$$\frac{d^2p}{d\tau^2} = \frac{1}{p}\left(-(\frac{dp}{d\tau})^2 + \frac{p}{\tau}\frac{dp}{d\tau} + \frac{2}{\tau^2}p^2 + \tau^2 - \frac{C^2\beta\tau}{2\alpha}\right). \tag{2.111}$$

Now we may rewrite (2.110) as

$$\begin{aligned}
p\frac{dp}{d\tau} &= -\frac{3}{4}C^2\tau^3 - \frac{C^2\beta}{4\alpha}\tau^2 + \frac{C^2\gamma}{4\alpha}\tau + \frac{p^2}{2\tau},\\
\frac{1}{2}\frac{d}{d\tau}p^2 &= -\frac{3}{4}C^2\tau^3 - \frac{C^2\beta}{4\alpha}\tau^2 + \frac{C^2\gamma}{4\alpha}\tau + \frac{p^2}{2\tau},\\
\frac{d}{d\tau}p^2 &= -\frac{3}{2}C^2\tau^3 - \frac{C^2\beta}{2\alpha}\tau^2 + \frac{C^2\gamma}{2\alpha}\tau + \frac{p^2}{\tau},\\
\frac{d}{d\tau}\left(-\tau p^2\right) &= \frac{3}{2}C^2\tau^4 + \frac{C^2\beta}{2\alpha}\tau^3 - \frac{C^2\gamma}{2\alpha}\tau^2,
\end{aligned}$$

which can be integrated to give

$$p^2 = -\frac{3}{10}C^2\tau^4 - \frac{C^2\beta}{8\alpha}\tau^3 + \frac{C^2\gamma}{6\alpha}\tau^2 - \frac{C_1}{\tau}, \tag{2.112}$$

where C_1 is the constant of integration. Now if we differentiate (2.112) twice we obtain the first and the second derivatives of p as

$$\begin{aligned}
\frac{dp}{d\tau} &= \frac{1}{2p}\left(-\frac{12}{10}C^2\tau^3 - \frac{3C^2\beta}{8\alpha}\tau^2 + \frac{C^2\gamma}{3\alpha}\tau + \frac{C_1}{\tau^2}\right),\\
\frac{d^2p}{d\tau^2} &= \frac{1}{2p}\left(-2\left(\frac{dp}{d\tau}\right)^2 - \frac{36}{10}C^2\tau^2 - \frac{6C^2\beta}{8\alpha}\tau + \frac{C^2\gamma}{3\alpha} - \frac{2C_1}{\tau^3}\right).
\end{aligned} \tag{2.113}$$

Substituting these into (2.111) we find that solutions (2.112) of (2.110) do not satisfy (2.111), so we conclude there are no energy densities of this case for which mathematical helices are extremal. This suggests nontrivial density functions f are needed.

2.3.3.2 $f(\tau) = \sqrt{\tau}$

Here we consider the transformation in section 2.3.2.3 that comes from the reference [85] and we are looking for curves on the sphere. Based on this transformation, this study obtains Euler-Lagrange equations as follows

$$\frac{1}{\tau}\left(\frac{w'}{\kappa}\right)' + \frac{\kappa}{\tau}w + \left(\frac{k'}{\kappa}\right)' + v = 0, \tag{2.114}$$

and

$$\left[\left(\frac{k'}{\kappa}\right)' + v\right]' = \frac{\tau}{\kappa}w', \tag{2.115}$$

where $v = \kappa k - \tau h$, and w is as defined in (2.85). Here we use the primes to denote differentiation with respect to the arc length s. If the energy density depends on τ only, then (2.114) gives

$$\frac{2\tau}{\kappa}q'' + \left(\frac{\dot{\tau}}{\kappa} - \frac{2\dot{\kappa}\tau}{\kappa^2}\right)q' + 2\kappa\tau q - \kappa f = 0,$$

where $q = \partial f/\partial\tau$. This equation can be written as

$$\left(\frac{\sqrt{\tau}}{\kappa}q'\right)' + \kappa\tau\frac{d}{d\tau}\left(\frac{f}{\sqrt{\tau}}\right) = 0. \tag{2.116}$$

Now if $f(\tau) = \sqrt{\tau}$, then (2.116) gives

$$\frac{\sqrt{\tau}}{\kappa}q' = -\frac{C_1}{4}, \tag{2.117}$$

where C_1 is an arbitrary constant, $q = 1/2\sqrt{\tau}$ and $q' = -\dot{\tau}/(4\tau^{\frac{3}{2}})$. Thus from (2.114) we have $\dot{\tau} = C_1\kappa\tau$ and for $p = 0$, (2.115) reduces to

$$\left(\frac{q'}{\kappa}\right)'' + (\kappa q)' - \frac{\tau^2}{\kappa}q' = 0.$$

Next by using the expressions for q and q' above, we obtain

$$\left(\frac{C_1^2}{4} + 1\right)\left(\frac{\kappa}{\sqrt{\tau}}\right)' + \frac{C_1}{2}\tau^{\frac{3}{2}} = 0,$$

which can be simplified to $\left(\alpha^2 + 1\right)\left(\dot{\kappa} - \alpha\kappa^2\right) + \alpha\tau^2 = 0$, where $\alpha = C_1/2$. This gives $\dot{\kappa} = \alpha\left(\kappa^2 - \beta\tau^2\right)$ where $\beta = 1/(1+\alpha^2)$. Therefore, we need to solve $\dot{\tau} = 2\alpha\kappa\tau$, and $\dot{\kappa} = \alpha\left(\kappa^2 - \beta\tau^2\right)$, which after division becomes

$$\frac{d\tau}{d\kappa} = \frac{2\kappa\tau}{\kappa^2 - \beta\tau^2}.$$

Then by introducing $V = \tau/\kappa$ and integrate this equation to obtain $V = c_2\kappa\left(1 + \beta V^2\right)$, where c_2 is further arbitrary constant. This gives an explicit relation between κ and τ as

$$\tau = c_2(\kappa^2 + \beta\tau^2) \tag{2.118}$$

If we substitute the relation of the mathematical helix $\kappa = \frac{\tau}{c}$ into (2.118) then we solve for τ to get

$$\tau = \frac{1}{c_2\left(\frac{1}{c^2} + \beta\right)}, \tag{2.119}$$

and

$$\kappa = \frac{1}{C}\left(\frac{1}{c_2(\frac{1}{c^2} + \beta)}\right). \tag{2.120}$$

We note that the curvature and the torsion are both constants so this is a regular mathematical helix on a cylinder and not on the sphere.

Now if we do not restrict to mathematical helices, but we take (2.118) and solve it for τ we get

$$\tau = \frac{1 \pm \sqrt{1 - 4\beta c_2^2\kappa^2}}{2\beta c_2}, \tag{2.121}$$

then we substitute (2.121) into (2.5) we have

$$\dot{\kappa} = \frac{1}{2\beta c_2}\kappa\left(\kappa - 1\right)\left(1 + \sqrt{1 - 4\beta c_2^2\kappa^2}\right), \tag{2.122}$$

which is

$$\frac{d\kappa}{\kappa(\kappa - 1)(1 + \sqrt{1 - 4\beta c_2^2\kappa^2})} = \frac{1}{2\beta c_2}ds. \tag{2.123}$$

If we use the substitution

$$\cos\theta = 2c_2\sqrt{\beta}\kappa,$$
$$\kappa = \frac{\cos\theta}{2c_2\sqrt{\beta}},$$
$$d\kappa = -\frac{\sin\theta}{2c_2\sqrt{\beta}}d\theta,$$

equation (2.123) becomes

$$\frac{-\sin\theta}{\cos\theta\left(\frac{\cos\theta}{2c_2\sqrt{\beta}} - 1\right)(\sin\theta + 1)}d\theta = \frac{1}{2\beta c_2}ds. \tag{2.124}$$

Now we use the substitution, namely

$$\begin{aligned}\tan\frac{\theta}{2} &= t,\\ \sin\theta &= \frac{2t}{1+t^2},\\ d\theta &= \frac{2dt}{1+t^2},\\ \cos\theta &= \frac{1-t^2}{1+t^2},\end{aligned}$$

equation (2.124) becomes

$$-4\int \frac{tc_2\sqrt{\beta}(1+t^2)}{(1-t^2)(1+t)^2\left(\frac{1}{2}(1-t^2)-(1+t^2)c_2\sqrt{\beta}\right)}dt = \int \frac{1}{2\beta c_2}dt. \tag{2.125}$$

Using partial fractions and integrating the above equation, we have

$$\begin{aligned}&-\frac{1}{4}\ln(t+1)(\frac{1}{c_2^2\beta}-1)-\frac{1}{(t+1)}(1-\frac{1}{c_2\sqrt{\beta}})-\frac{1}{4}\ln(t-1)+\frac{1}{(t+1)^2}\\ &-\frac{1}{4}\frac{\tan^{-1}(\frac{(1+2c_2\sqrt{\beta})t}{\sqrt{4c_2^2\beta-1}})}{\sqrt{4c_2^2\beta-1}}(\frac{1}{c_2^2\beta}-4)+\frac{1}{4}\frac{\ln(2c_2\sqrt{\beta}(1+t^2)+t^2-1)(1+2c_2\sqrt{\beta})}{c_2^2\beta(1+2c_2\sqrt{\beta})}=\frac{s}{2\beta c_2}+\tilde{C},\end{aligned}$$

where $\tilde{C}$ is the integration constant. Now we substitute $\tan\frac{\theta}{2}=t$ and then $\kappa=\frac{\cos\theta}{2c_2\sqrt{\beta}}$ and simplify to obtain

$$\begin{aligned}&\frac{1}{4}\ln(A+1)(\frac{1}{c_2^2\beta}-1)+\frac{1}{c_2\sqrt{\beta}(A+1)}-\frac{1}{4}\ln(A-1)-\frac{1}{8}\frac{\cos^{-1}(2c_2\sqrt{\beta}\kappa)(1+2c_2\sqrt{\beta})}{(4c_2^2\beta-1)}(\frac{1}{c_2^2\beta}-4)\\ &+\frac{1}{A+1}+\frac{1}{4c_2^2\beta}\ln(2c_2\sqrt{\beta}(1+A^2)+A^2-1)=\frac{s}{2\beta c_2}+\tilde{C},\end{aligned}$$

where $A=\frac{1-2c_2\sqrt{\beta}\kappa}{(1-4c_2^2\beta\kappa^2)^{\frac{1}{2}}}$. This equation gives implicitly the curvature as a function of s, τ is then given via (2.121). This is a parameterized curve on sphere, not a mathematical helix but satisfying Euler Lagrange equations in the case of $f(\tau)=\sqrt{\tau}$. While it could be argued that energy densities could not depend only on torsion the above case gives an example of the sort of complexities that could arise when f does depend on torsion.

2.3.3.3 Energy densities of the form $f = f\left(\frac{\kappa}{\tau}\right)$

From the study in [85], equation (2.86) is in terms of κ and τ as

$$\left[\frac{d}{ds}\frac{df}{d\xi}\right]^2 + \kappa^2\left[\left(\frac{df}{d\xi}\right)^2 + \left(\xi\frac{df}{d\xi} - f\right)^2\right] = C\kappa^2, \tag{2.126}$$

where $\xi = \tau/\kappa$ and C denotes an arbitrary constant. Observing that

$$f(\xi) = A\xi, \tag{2.127}$$

is a solution for (2.126) where $C = A^2 > 0$ we can calculate that $\frac{df}{d\xi} = A$, $\frac{d}{ds}\frac{df}{d\xi} = 0$, and observe that (2.126) is satisfies provided $A^2 = C$.

2.4 Conclusion

f	Mathematical helices	Revolutionary curves on a sphere	Other cases
$f(\kappa)$	None	(2.23)	(2.53) and (2.59)
$f(\kappa, \dot{\kappa})$	(2.71)	(2.84)	(2.91) and (2.97)
$f(\tau)$	None	$f(\tau) = \sqrt{\tau}$	None
$f(\kappa, \tau)$	None	None	(2.127)

Table 2.1: Summary of energy density functionals for extremal helical curves on a sphere.

In summary, we adopt the calculus of variations to extremise mathematical curvature-dependent energies for curves in three-dimensional space. Throughout this research, we investigate and determine the energy density functions that show spherical helices as solutions for Euler-Lagrange equations. In particular, three special cases of the energy density are considered; firstly, the energy depends on the curvature only. Secondly, the energy depends on the curvature and its first derivative. Finally, the energy depends on the torsion only. Further, two types of curves are studied in this research, mathematical helices on a sphere and revolutionary curve on a sphere. As summarized in Table 2.1, we find classes of such energies for mathematical spherical helices and the class of curves on the sphere which give rise to helices on the sphere as extremal curves. Such curves are relevant in modelling spherical nanoantennas.

Furthermore, we comment that in this thesis we focus on geometrically inspired energy functions. It is possible also to include an electrostatic term in the energy that measures interaction between atoms, as for example in [29]. This is a potential avenue for future work.

Chapter 3

Determination of join regions between carbon nanostructures using calculus of variations

3.1 Introduction

Joining between carbon nanostructures gives rise to new applications for the joined materials. Importantly, carbon nanostructures offer the possibility of combining and joining other types of nanomaterials for the purpose of obtaining different properties from the new structure [77]. Joining between nanostructures can enhance the physicochemical and electrochemical performances of the combined materials [64, 31, 100]. Much research has been conducted in nanomaterials synthesis. This gives better prosperities and a wide range of useful applications. For example, joining fullerenes and nanotubes can lead to nanobuds which is applicable for field-emission devices [10]. Joining carbon nanotubes and graphene sheets can lead to useful applications in communication systems like connecting to an electronic platform [30]. Also, joining between two fullerenes can create more efficient storage devices [14]. Furthermore, a variational approach such as that used in the joining of carbon nanostructures can also be used in partial differential equation blending of surfaces [58].

The following literature review focusses on carbon nanostructures and gives a brief snapshot for each type of carbon nanostructures, namely fullerene, carbon nanocones and graphene. In particular, we summarise their structures, types, properties and potential applications.

3.1.1 Fullerenes

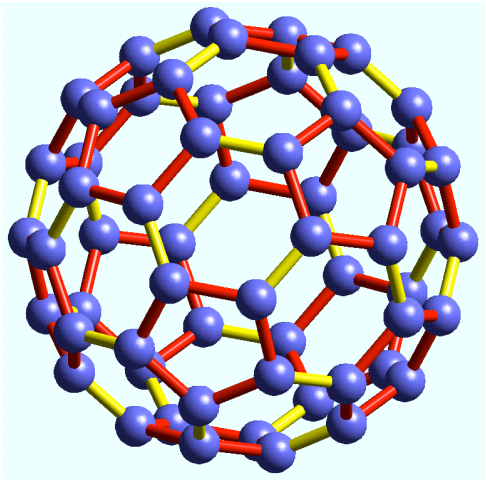

Figure 3.1: Fullerene structure [90].

Since the discovery of their structures in 1980s, fullerenes have been attracting enormous attention in the scientific community. As they have applications in many areas [79]. Fullerenes are important forms of carbon nanomaterials that have special properties based on their shape and size [90]. In particular, they were observed by a group of scientists including Richard Smalley, Harry Kroto and Robert Curl who shared a Nobel prize in 1996 for their discovery [90]. There are three different basic forms of fullerenes which are spherical, elliptical and in the form of tubes [90].

They have a similar structure to graphene, which is formed by linking hexagonal rings, but fullerenes contain pentagonal rings that are required to close the spherical shell [10] as shown in Figure 3.1. They contain 20 hexagonal and 12 pentagonal rings as the basis of an icosahedral symmetry closed cage structure where each carbon atom is bonded to three others and is sp^2 hybridized [95].

Fullerenes also have many interesting chemical, optical and physical properties, which have been exploited to develop different important applications, including drug delivery such as Prozac and steroid hormones [49], osteoporosis therapy, X-ray contrast agents to reduce toxicity [32, 38, 80, 19], solar cells, hydrogen gas storage, optical and sensors applications [90]. Moreover, they have electrical properties that show a great promise in electronics-related applications such as data storage, fuel cells, memory devices and solar cells [49].

In terms of health and personal applications they reinforce the controlling of the neurological damage of some diseases for example Alzheimer's disease and Lou Gehrig's disease which are caused by radical damage [95]. During the 1990s, scientists proved that fullerenes have biological activities like therapeutic products in the treatment of many different diseases, for example a private bio-pharmaceutical company 'C sixty Inc' created a new class of therapeutics that depends on the fullerenes molecular for cancer treatment, AIDS and neurodegenerative diseases [79].

The most popular type of fullerenes is called Buckyball C_{60} which includes 60 carbon atoms. This type of fullerenes is the easiest type in the production process and the cheapest comparing to other larger fullerenes [90]. It has a diameter of only 0.7 nm and it is symmetrical and approximately spherical as a soccer ball [84]. Furthermore, a single C_{60} molecule has an effective bulk modulus of 668 GPa when compressed to 70% of its size, this feature makes this type of fullerenes harder than a diamond with 442 GPa and steel with 160 GPa [90]. The structure of the molecule is shown in Figure 3.1. Also the average C-C bond distance measured by using nuclear magnetic resonance is 1.44 Å[90].

3.1.2 Graphene

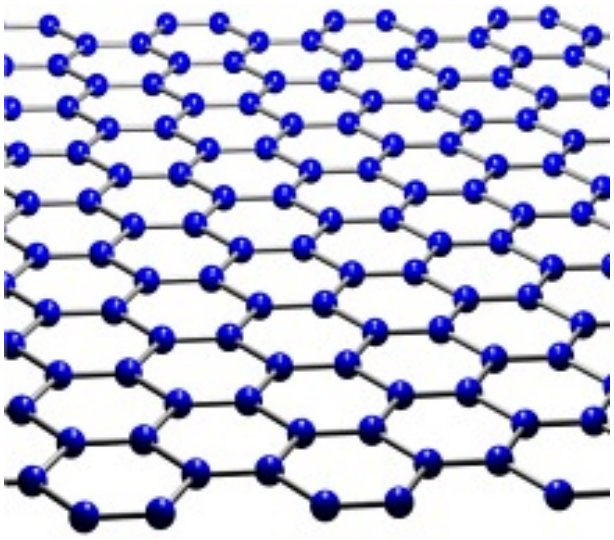

Figure 3.2: Structure of graphene [33].

Graphene is defined as allotropes of carbon that is a two-dimensional layer of carbon atoms

which are arranged as a honeycomb lattice with a carbon-carbon bond length of about 0.142 nm [46]. Graphene is a one atom thick carbon sheet composed of six member rings [77] as seen in Figure 3.2. Since 2004, scientists have isolated graphene by the exfoliation of graphite, and graphene has attracted considerable attention among the carbon family [6]. Based on its unique structure, there are significant studies on its properties and applications [103]. The distinctive properties of graphene such as physical, optical high mechanical strength, stiffness, high elasticity, high electrical and thermal conductivity promise numerous and broad applications in aerospace, medicine, environmental, energy generation and storage, batteries, fuel cells, sensors and metrology, bio-applications, engineering, mechanical, electronic, pollutant removal in environmental remediation and food and beverage industries [71] [46] [6] [35] [78] [63].

Therefore, other important properties make it a more attractive member of carbon nanomaterials, for example it has high Young's modulus which is about 1100 GPa. Also fracture strength about 125 GPa, thermal conductivity about 5000 $Wm^{-1}K^{-1}$, mobility of charge carriers 200000 $cm^2V^{-1}s^{-1}$, chemical stability and theoretical value of 2630 m^2 g^{-1} [63]. In addition, graphene may be used as a photo-detector because of the wide absorption range, high mobility of carriers, thinness and low cost of the material and the ability to operate at ambient temperature [6].

Graphene has been synthesized by many methods. For example, micro-mechanical cleavage, chemical vapor deposition, plasma discharge etching of graphite, chemical reduction of graphene oxides, total organic synthesis, electrochemical synthesis, unzipping of carbon nanotubes, arc discharge and epitaxial growth on silicon carbide [63].

3.1.3 Carbon nanocones

Due to the similar structures and properties of carbon nanotubes, much study has been made by scientists, and [41] Ge et al. were the first who proved that carbon nanocones have five possible types with different angles [5]. After that the studies in [60] [97] have discovered the reality and existence of the five types of carbon nanocones based on the apex angles of $19.2°, 38.9°, 60°, 83.60°$ and $112.9°$. Carbon nanocones have been defined as curved graphene

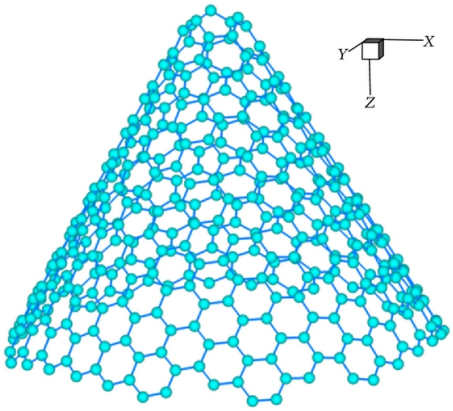

Figure 3.3: Carbon nanocones structure [4].

sheets with the addition of pentagons at the cone-tips [93]. In particular, they might be found on the caps of nanotubes like free-standing structures in a carbon arc [5].

Nanocones are conical graphitic structures with disclination number of pentagons $N_p = 1, 2, 3, 4$ or 5. For a polyhedron consisting of only hexagons and pentagons, Euler's theorem of polyhedron gives $N_p = 6$ for any closed cap where $N_p = 0$ for a graphene sheet. If γ is the cone vertex angle, then Table 3.1 shows the values of γ [11][97].

Table 3.1: Relation of number of pentagons N_p and open angle γ for carbon nanocones.

N_p	0	1	2	3	4	5	6
γ	180°	112.90°	83.60°	60.00°	38.90°	19.2°	0°

There are many different methods to synthesize carbon nanocones, for example, chemical vapor and arc-discharge schemes [96]. In particular, they are useful for high resolution and/or high intensity applications because of their small size. Moreover, highly sensitive and conical geometry make them candidates for scanning probe tips (in atomic force microscope and scanning tunneling microscope probes), electron field emitters and in nanoindentation applications [17][97]. Some researchers have also found other useful applications of carbon nanocones in different areas, for example, in engineering applications [61], cold electron and field emitter [101], adsorbent[65], mechanical sensors [50] and they can be useful as high sensitive resonators [98]. They also have useful applications in deformation problems [16]. Further, theoretical studies suggest that the oscillation of nanocones inside carbon nanotubes can create gigahertz frequency which can be used as ultra-sensitive nanoantennas and ultra-fast signalling devices [11] [3]. Other applications

in the engineering field include carbon nanocones are important in nanoelectronics, bio-sensors and composites [96].

The researchers in [77] [64] [31] [100] [10] [30] and [14] used a particular variational technique to determine the join region between two different carbon nanostructures. As carbon nanotubes deform according to perfect elasticity, the elastic energy is used to determine the join region involving a finite number of discrete bonds [13] [102]. Based on that, they adopted calculus of variations to minimize the elastic energy to obtain Euler-Lagrange equation that determines the joining area between two carbon nanostructures. Moreover, they determined the values of the geometric parameters for the connected structures. By noting that the defects on the nanostructures have been assumed to be axially symmetric this gave rise to the problem in a two-dimensional plane. Because the curvature of the joining area can be both positive or negative curvature, two different models need to be examined.

In this chapter we use the same procedure as above to join other different nanostructures. Following [10] [11] [14] [12], this chapter considers a mathematical model using the calculus of variations to determine the shape of the join between nanostructures; a carbon nanocone with a fullerene, two nanocones, a plane sheet of graphene with nanocones, a fullerene with plane sheet of graphene and a nanocone with two parallel sheets of graphene.

In the following section, we give fundamental equations using calculus of variations to model the joining between these particular nanostructures. Model I is studied where the curvature is assumed to remain positive in the join region. When the curvature is assumed to have two regions, positive and negative curvature, we refer to this case as Model II. In section 3.3, we investigate the values of the characteristic parameter μ. In section 3.4 we give the results of the joining structures where in subsection 3.4.1 we consider the joining between a carbon nanocone and a fullerene. In subsection 3.4.2 the joining between two carbon nanocones is examined. Subsection 3.4.3 studies the joining between a carbon nanocone and a flat sheet of graphene. Next, the case of a fullerene and a flat sheet of graphene is investigated in subsection 3.4.4. In subsection 3.4.5.1 we join a carbon nanocone with two parallel sheets of graphene. In subsection

3.4.5.2 we join fullerene with two parallel sheets of graphene. Finally, summary of the chapter is presented in section 3.5.

3.2 Model and mathematical background

This section presents the method developed by Hill et al. [30] and Baowan et al. [13] to study the join regions between carbon nanostructures. In the next subsection, calculus of variations is used specifically to derive the appropriate Euler-Lagrange equation to determine the joining curve between two carbon nanostructures. In subsection 3.2.2 the joining region between carbon nanostructures is determined where the curvature of the joining region is studied which has two different cases; in subsubsection 3.2.2.1 Model I is studied where the curvature is assumed to remain positive however, in subsubsection 3.2.2.2 when there are two disjoint regions wherein curvature has positive and negative sign we refer to this case as Model II.

3.2.1 Calculus of variations

We use calculus of variations to find the curve $y(x)$, with an element of arc length ds, which minimizes the energy functional $I[y]$ that is given by

$$I[y] = \int_0^l \kappa^2 ds + \lambda \int_0^l ds, \tag{3.1}$$

where κ is the curvature and λ is a Lagrange multiplier corresponding to the fixed length constraint, l is the length of the joining curve and the boundaries of the join region are x_0 and x_1 where at $x = x_0$ we have $s = 0$ and at $x = x_1$ we have $s = l$. For a curve in two-dimensions described as a graph $y = y(x)$, we have $\kappa = \ddot{y}/\left(1+\dot{y}^2\right)^{3/2}$ and $ds = \left(1+\dot{y}^2\right)^{1/2} dx$, so that equation (3.1) becomes

$$I[y] = \int_{x_0}^{x_1} \frac{\ddot{y}^2}{(1+\dot{y}^2)^{5/2}} dx + \lambda \int_{x_0}^{x_1} (1+\dot{y}^2)^{1/2} dx, \tag{3.2}$$

where throughout this chapter, dot denotes differentiation with respect to x. After integrating by parts twice, we may derive the standard equation

$$\delta I[y] = \left[\left(F_{\dot{y}} - \frac{d}{dx}F_{\ddot{y}}\right)\delta y + F_{\ddot{y}}\delta\dot{y}\right]_{x_0}^{x_1} + \int_{x_0}^{x_1} \left(F_y - \frac{d}{dx}F_{\dot{y}} + \frac{d^2}{dx^2}F_{\ddot{y}}\right)\delta y dx, \tag{3.3}$$

where subscripts denote partial derivatives and here the function F is given by

$$F\left(\dot{y},\ddot{y}\right)=\frac{\ddot{y}^2}{(1+\dot{y}^2)^{5/2}}+\lambda\left(1+\dot{y}^2\right)^{1/2}. \tag{3.4}$$

The natural boundary condition is given by

$$\left(F_{\dot{y}}-\frac{d}{dx}F_{\ddot{y}}\right)|_{x=x_1}=0, \tag{3.5}$$

which applies when the y-coordinate at the $x=x_1$ boundary is not prescribed [13].

3.2.1.1 The Euler-Lagrange equation

From equation (3.3) we have the usual Euler-Lagrange equation for $F(x,y,\dot{y},\ddot{y})$, which is given by

$$F_y-\frac{d}{dx}F_{\dot{y}}+\frac{d^2}{dx^2}F_{\ddot{y}}=0. \tag{3.6}$$

Thus, integrating the above equation gives

$$F_{\dot{y}}-\frac{d}{dx}F_{\ddot{y}}=C_1,$$

where C_1 is an arbitrary constant of the integration. We note from (3.5) that at the boundary $x=x_1$, $C_1=0$ and thus for the entire domain we have

$$F_{\dot{y}}=\frac{d}{dx}F_{\ddot{y}}. \tag{3.7}$$

Using definition of the full derivative we have

$$\frac{d}{dx}F=F_x+\dot{y}F_y+\ddot{y}F_{\dot{y}}+\dddot{y}F_{\ddot{y}}.$$

Since $F_x\equiv F_y\equiv 0$ and from (3.7) we obtain that

$$\frac{d}{dx}\left(F-\ddot{y}F_{\ddot{y}}\right)=0,$$

which upon integrating this with respect to x we get

$$F-\ddot{y}F_{\ddot{y}}=-\alpha, \tag{3.8}$$

where α is an arbitrary constant of the integration. Now we substitute (3.4) into (3.8) and obtain

$$\frac{\ddot{y}^2}{(1+\dot{y}^2)^3} = \lambda + \frac{\alpha}{(1+\dot{y}^2)^{1/2}}.$$

As a result, we can write the curvature κ as

$$\kappa = \pm\left(\lambda + \frac{\alpha}{(1+\dot{y}^2)^{1/2}}\right). \tag{3.9}$$

.

3.2.2 Curvature effects at the join region

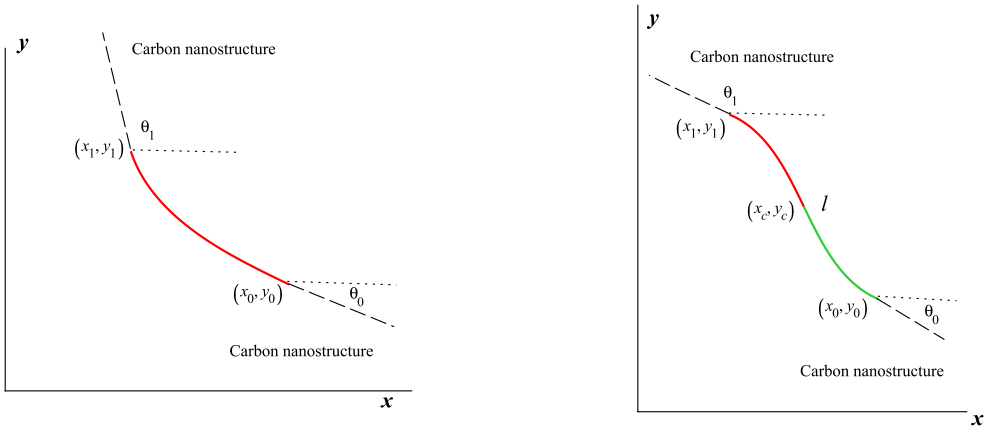

(a) Model I. (b) Model II.

Figure 3.4: Model I curvature positive; and Model II, curvature both positive and negative [13].

In this subsection we investigate the general formulation for the join region which connects the two carbon nanostructures. Considering Figure 3.4, the joining starts at a prescribed location (x_0, y_0) where the boundary makes an angle θ_0 with positive direction of x. The second boundary point of the join region is at (x_1, y_1) where here the boundary makes the angle θ_1 with the positive x-direction. Note that x_1 and θ_1 are prescribed, whereas y_1 is obtained using the natural boundary condition given in equation (3.5). Based on Figures 3.4 Model I and II can be distinguished based on the sign of the curvature κ. In Model I, the sign of the curvature does not change during the joining and we assume that in this case the curvature always remains positive. In Model II, the curvature of the join region changes the sign during the joining, and as a result, we assume that the curvature is positive adjacent to (x_0, y_0) and becomes negative before reaching (x_1, y_1) [13].

3.2.2.1 Model I: positive curvature

As shown in Figure 3.4(a), the curvature in Model I is positive along the entire arc of length l. Thus, we only consider the positive case in equation (3.9). By using $\dot{y} = \tan\theta$, equation (3.9) becomes

$$\kappa = (\lambda + \alpha\cos\theta)^{\frac{1}{2}}. \tag{3.10}$$

From the definition of the curvature $\kappa = \ddot{y}/(1+\dot{y}^2)^{\frac{3}{2}}$, and making the same substitution for $\dot{y}$, we may deduce

$$\frac{dy}{d\theta} = \frac{\sin\theta}{(\lambda + \alpha\cos\theta)^{\frac{1}{2}}}. \tag{3.11}$$

Next, we now introduce a new parametric variable ϕ which is defined via

$$\cos\theta = 1 - 2k^2\sin^2\phi, \tag{3.12}$$

where $k = [(\lambda+\alpha)/2\alpha]^{\frac{1}{2}}$, we obtain

$$\frac{dy}{d\phi} = 2\beta k\sin\phi, \tag{3.13}$$

where $\beta = (2/\alpha)^{\frac{1}{2}}$. Integrating equation (3.13) and using the boundary condition at the point (x_0, y_0) we get

$$y(\phi) = y_0 + 2\beta k\left(\cos\phi_0 - \cos\phi\right), \tag{3.14}$$

where

$$\phi_0 = \sin^{-1}\left(\frac{1 - cos\theta_0}{2k^2}\right)^{\frac{1}{2}}.$$

Similarly, we can show that

$$\frac{dx}{d\theta} = \frac{\cos\theta}{(\lambda + \alpha\cos\theta)^{\frac{1}{2}}},$$

and in terms of the variable ϕ, we have

$$\frac{dx}{d\phi} = \beta\frac{(1-2k^2\sin^2\phi)}{(1-k^2\sin^2\phi)^{\frac{1}{2}}} = \beta\left[2(1-k^2\sin^2\phi)^{\frac{1}{2}} - (1-k^2\sin^2\phi)^{-\frac{1}{2}}\right].$$

By integrating the above equation gives,

$$x(\phi) = x_0 + \beta(2\left[E(\phi,k) - E(\phi_0,k)\right] - \left[F(\phi,k) - F(\phi_0,k)\right]), \tag{3.15}$$

where $F(\phi,k)$ and $E(\phi,k)$ denote the usual Legendre incomplete elliptic integrals of the first and second kinds, respectively as defined in [20]. Since $\phi_1 = \sin^{-1}\left[(1-\cos\theta_1/(2k^2))\right]^{\frac{1}{2}}$, using equations (3.14) and (3.15) we obtain

$$\begin{aligned} x_1 &= x_0 + \beta(2\left[E(\phi_1,k) - E(\phi_0,k)\right] - \left[F(\phi_1,k) - F(\phi_0,k)\right]) \\ y_1 &= y_0 + 2\beta k\left(\cos\phi_0 - \cos\phi_1\right). \end{aligned} \tag{3.16}$$

From the definition of the arc length, we have

$$l = \int_{x_0}^{x_1} \left(1+\dot{y}^2\right)^{\frac{1}{2}} dx.$$

Upon substituting $\dot{y} = \tan\theta$, changing the parameter to ϕ as in $\cos\theta = 1 - 2k^2\sin^2(\phi)$, and integrating, we have

$$l = \beta\left[F(\phi_1,k) - F(\phi_0,k)\right]. \tag{3.17}$$

Now, we define a dimensionless parameter $\mu = (x_1 - x_0)/l$ which can be shown to be

$$\mu = \frac{2\left[E(\phi_1,k) - E(\phi_0,k)\right]}{F(\phi_1,k) - F(\phi_0,k)} - 1. \tag{3.18}$$

For prescribed values of x_0, x_1 and l, equation (3.18) can be solved numerically to determine the value of k. Then by substituting k into equation (3.17), the value of β can be determined and therefore y_1 can be obtained from (3.16).

3.2.2.2 Model II: positive and negative curvature

For this model, the curvature is positive at the point (x_0, y_0) up until the point (x_c, y_c) where the curvature changes to be negative until the point (x_1, y_1) is reached (see Figure 3.4(b)). At (x_c, y_c), $\kappa = 0$ and by solving equation (3.10) we obtain $\theta_c = \cos^{-1}(\frac{-\gamma}{\alpha})$. By making the substitution used in equation (3.12) for ϕ, we have $\phi_c = \frac{\pi}{2}$. By substituting ϕ_c into equations (3.14) and (3.15) we can calculate x_c and y_c as below:

$$\begin{aligned} x_c &= x_0 + \beta\{2[E(k) - E(\phi_0,k)] - [K(k) - F(\phi_0,k)]\}, \\ y_c &= y_0 + 2\beta k\cos\phi_0, \end{aligned}$$

noting that $K(k)$ and $E(k)$ are the complete elliptic integrals of the first and second kinds respectively. In the joining region between (x_c, y_c) and (x_1, y_1), we take the negative sign of equation (3.9), and through the same method used in Model I, we obtain

$$\frac{dx}{d\phi} = -\beta \frac{(1 - 2k^2 \sin^2 \phi)}{(1 - k^2 \sin^2 \phi)^{\frac{1}{2}}},$$
$$\frac{dy}{d\phi} = -2\beta k \sin \phi.$$

Thus, in this region $x(\phi)$ and $y(\phi)$ are given by

$$x(\phi) = x_0 + \beta\{2[E(k) - E(\phi, k)] - [K(k) - F(\phi, k)]\},$$

$$y(\phi) = y_c + 2\beta k \cos \phi.$$

As a result, the second boundary (x_1, y_1) is given by

$$x_1 = x_0 + \beta\{2[2E(k) - E(\phi_0, k) - E(\phi_1, k)] - [2K(k) - f(\phi_0, k) - F(\phi_1, k)]\}, \tag{3.19}$$

$$y_1 = y_0 + 2\beta k(\cos \phi_0 + \cos \phi_1). \tag{3.20}$$

In Model II, the arc length is determined in two parts, which is given by

$$\begin{aligned} l &= \int_{x_0}^{x_c} (1 + \dot{y}^2)^{\frac{1}{2}} dx + \int_{x_c}^{x_1} (1 + \dot{y}^2)^{\frac{1}{2}} dx \\ &= \beta \int_{\phi_0}^{\frac{\pi}{2}} (1 - k^2 \sin^2 \phi)^{-\frac{1}{2}} d\phi + \beta \int_{\phi_1}^{\frac{\pi}{2}} (1 - k^2 \sin^2 \phi)^{-\frac{1}{2}} d\phi \\ &= \beta \left[2K(k) - F(\phi_0, k) - F(\phi_1, k)\right]. \end{aligned} \tag{3.21}$$

As a result, we find a dimensionless parameter $\mu = (x_1 - x_0)/l$, for Model II to be given by

$$\mu = 2\left(\frac{2E(k) - E(\phi_0, k) - E(\phi_1, k)}{2K(k) - F(\phi_0, k) - F(\phi_1, k)}\right) - 1. \tag{3.22}$$

Again, for prescribed values of x_0, x_1 and l we can solve equation (3.22) numerically to find the value of k, and by substituting k into equation (3.21), we can determine the value of β so that y_1 can be determined from equation (3.19).

3.3 The characteristic parameter μ

In this section we follow the study in [13]. The numerical solution for (3.18) and (3.22) is obtained when they are characterized by the non-dimensional parameter $\mu = (x_1 - x_0)/l$ and

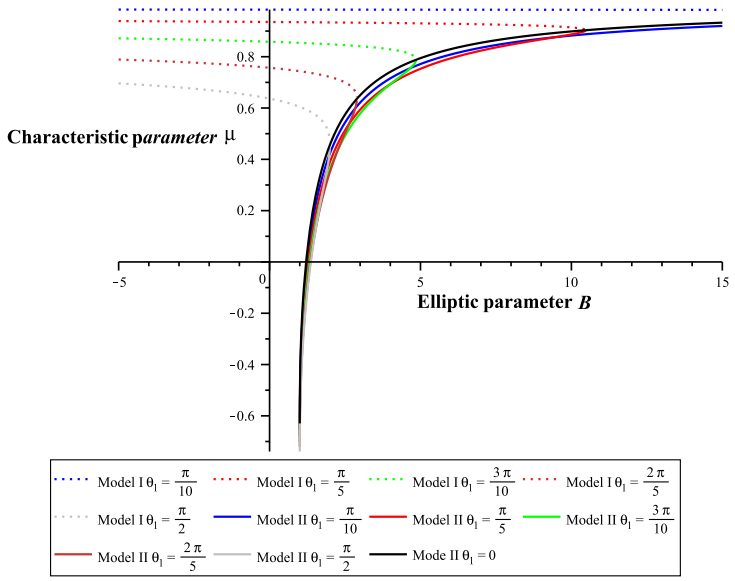

Figure 3.5: The characteristic parameter μ for various values of the elliptic parameter B for $\theta_0 = 0$ and θ_1 as indicated in the legend.

subject to the constraint $-1 < \mu < 1$. In Figure 3.5, the relation between the parameter μ and $B = 1/k^2$ is shown, assuming the angle at the beginning of the join is $\theta_0 = 0$ and varying values for θ_1. All curves have a critical value at $\mu = \mu_1$ except when $\theta_1 = 0$. Model I applies when $\mu > \mu_1$, and Model II applies when $\mu < \mu_1$. For the special case $\theta_1 = 0$, we have $\mu_1 = 1$. Figure 3.6 shows the relation between μ and B. In the figure, the angle at the end of the join

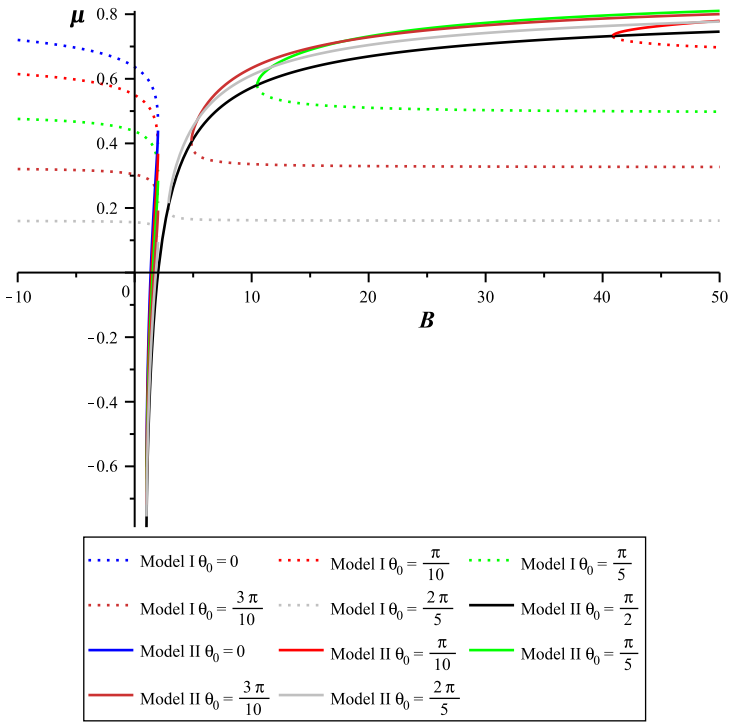

Figure 3.6: The characteristic parameter μ for various values of the elliptic parameter B for $\theta_1 = \pi/2$ and θ_0 as indicated in the legend.

region is fixed to be $\theta_1 = \pi/2$, while the angle θ_0 is varied. For this case, there are a number of the critical values for μ. In particular, there are μ_1 and μ_2, where Model I applies in the range $\mu_1 < \mu < \mu_2$ and Model II applies when $\mu < \mu_1$ and $\mu > \mu_2$. For all cases except the special case $\theta_0 = 0$, there is a discontinuity in the Model I for which the gradient of the graph jumps from $-\infty$ to ∞. This point of discontinuity occurs at $\mu = \mu_0$. For all curves in Figure 3.6, when $\mu_1 < \mu < \mu_0$, B must satisfy $B < 2$, and for $\mu_0 < \mu < \mu_2$ the curves lie strictly in the range $B > 2$. Finally, $\mu = \mu_3$ occurs at $B = 0$. In both Figures 3.5 and 3.6, we see that the crossing of the μ-axis only occurs for curves in Model I. This is due to the fact that $B = 0$ is the special case where the elliptic functions degenerate into the standard trigonometric functions and the join region is a circular arc. As there is no change in the sign of the curvature in the circular arc, μ_3 must occur in Model I, and since it occurs in the range $B < 2$, μ must be in the region $\mu_1 < \mu_3 < \mu_0$ [13].

3.4 Results

This thesis extends the investigation in [13] to consider the joining of various carbon nanostructures.

3.4.1 Joining carbon nanocones and fullerenes

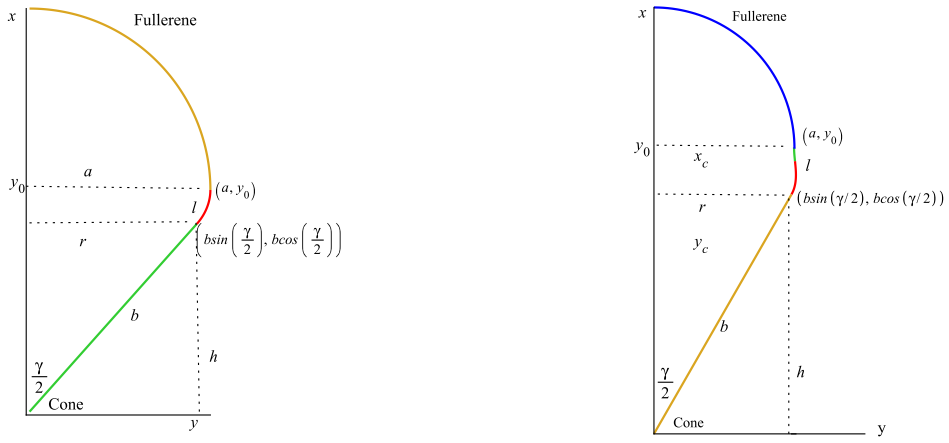

(a) Model I.

(b) Model II.

Figure 3.7: Axially symmetric geometries for Model I and Model II.

Here we consider two different models, illustrated in Figure 3.7. The curvature in Model I is assumed to be positive throughout the join, while in Model II the curvature contains two regions

of positive and negative sign. We position the nanocone of radius r such that the cone vertex is assumed to be located at the origin of the xz-plane. Moreover, the fullerene of radius a is located with its center on the y-axis, starting from an unknown positive distance above xz-plane, denoted by y_0 . In this case we note that the nanocone and the fullerene are rotationally symmetric about the y-axis, which allow us to consider it as a two dimensional problem in (xy)-plane. The total arc length l is assumed to connect the cone at $(r, h) = (b\sin(\gamma/2), b\cos(\gamma/2))$ and the fullerene at (a, y_0), where γ is the cone angle and $b = r\csc(\gamma/2)$. Noting that $(b\sin(\gamma/2), b\cos(\gamma/2))$ is the nearest atomic position of the joined atoms on the cone and (a, y_0) is the nearest atomic position of the joined atoms on the fullerene. Moreover, we consider the five possibilities of the cone angle γ as shown in Table 3.1. In this case, the angles at the boundaries of the join region are $\theta_0 = \gamma/2$ and $\theta_1 = \pi/2$ and the boundary conditions at x_0 are

$$y(b\sin\frac{\gamma}{2}) = b\cos\frac{\gamma}{2}, \quad \dot{y}(b\sin\frac{\gamma}{2}) = \cot\frac{\gamma}{2}. \tag{3.23}$$

At x_1 for Model I the boundary condition is

$$\dot{y}(a) = \infty, \tag{3.24}$$

and for Model II at x_1 we have

$$\dot{y}(a) = -\infty. \tag{3.25}$$

We note that equation (3.18) coincides with equation (3.22) for two values of k, that are $k = 1/\sqrt{2}$ and $k = [(1 - \sin(\gamma/2))/2]^{\frac{1}{2}}$. First, when $k = 1/\sqrt{2}$, μ can be written as μ_1 which is given by

$$\mu_1 = 2\left(\frac{E(1/\sqrt{2}) - E(\sin^{-1}(\sqrt{1-\sin(\gamma/2)})), 1/\sqrt{2}}{K(1/\sqrt{2}) - F(\sin^{-1}(\sqrt{1-\sin(\gamma/2)})), 1/\sqrt{2}}\right) - 1.$$

Secondly, when $k = [(1 - \sin(\gamma/2))/2]^{\frac{1}{2}}$, μ can be written as μ_2 which is given by

$$\mu_2 = 2\left(\frac{E(\sqrt{[1-\sin(\gamma/2)]/2}) - E(\sin^{-1}[1/\sqrt{1-\sin(\gamma/2)}], \sqrt{[1-\sin(\gamma/2)]/2})}{K(\sqrt{[1-\sin(\gamma/2)]/2}) - F(\sin^{-1}[1/\sqrt{1-\sin(\gamma/2)}], \sqrt{[1-\sin(\gamma/2)]/2})}\right) - 1.$$

The solution of this problem is characterised by the nondimensional parameter $\mu = [a - b\sin(\gamma/2)]/l$. Figure 3.8 shows the relation between $\mu = a - b\sin(\gamma/2)/l$ where $-1 < \mu < 1$ and $B = 1/k^2$. In particular, we have two regions, the first region is $\mu < \mu_0$ which corresponds

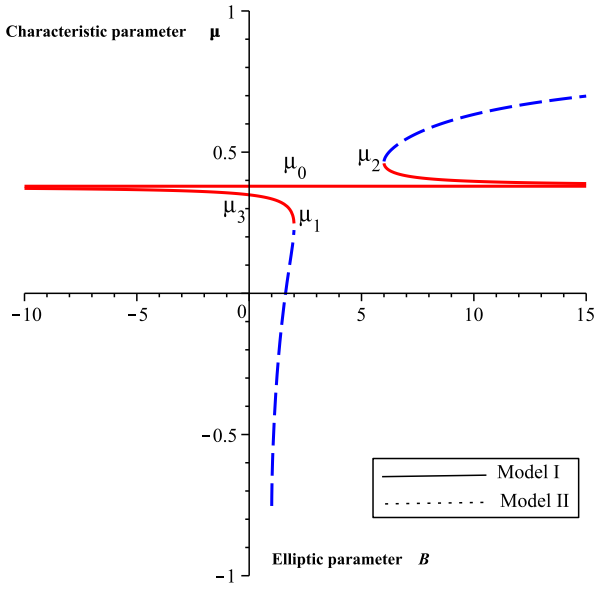

Figure 3.8: Relation between the parameters $\mu = (a - b\sin(\gamma/2))/l$ and $B = 1/k^2$.

to the value of $B < 2$ where μ_0 is the asymptotic value for μ when k tends to zero, which is determined in the Appendix C, which can be written as

$$\mu_0 = 1 + \frac{\sqrt{2}(1 - \sqrt{2}\cos\omega)}{\ln[(\sqrt{2}-1)/(\tan(\omega/2))]},$$

where $\omega = (\pi - \gamma)/4$. This region can be divided to three subregions; the first subregion is when $\mu_3 < \mu < \mu_0$ where μ_3 is the asymptotic value of μ when k tends to ∞. As shown in the Appendix C, μ_3 can be written as

$$\mu_3 = \frac{2}{\gamma}(1 - \cos(\gamma/2)).$$

In this subregion the value of the parameter B is negative. The second subregion is $\mu_1 < \mu < \mu_3$ where the value of the parameter B corresponds to $0 < B \leq 2$. The last subregion is $-1 < \mu < \mu_1$ where the value of the parameter B is between $1 < B \leq 2$.

The second region is when $\mu > \mu_0$ which corresponds to the value of $B > 2/1 - \sin(\gamma/2)$. This region also contains two subregions, which are $\mu_0 < \mu < \mu_2$ and $\mu_2 < \mu < 1$ for Model I and Model II, respectively. The values of the parameter B for two the subregions are positive values.

3.4.1.1 Joining carbon nanocones with half spherical fullerenes.

From the above results, the parameter B in Model I has negative value so we choose $B = -4$. Here, we join fullerenes with five possible cases of carbon nanocones which have half angles

$112.9°, 83.6°, 60°, 38.9°$ and $19.2°$. In Figure 3.9, the arc length is assumed to be $l = 2$ and the fullerenes are centered at

$(0, 11.66), (0, 11.81), (0, 11.91), (0, 11.97)$ and $(0, 11.99)$ with radii $10.04, 9.67, 6.3, 3.88$ and 1.86 Å, respectively.

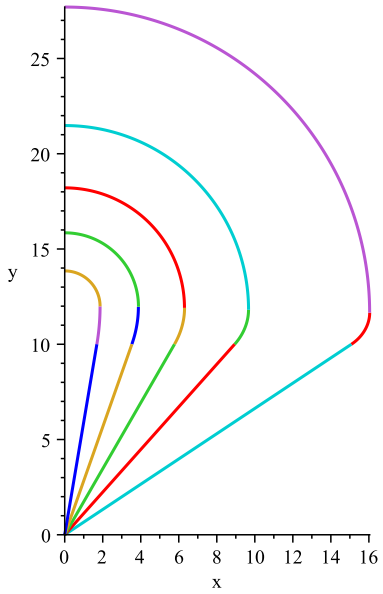

Figure 3.9: Plot of joining $y = y(x)$ for Model I for five possible carbon nanocones with $l = 2$ and $B = -4$, and fullerenes are centered at $(0, 11.66), (0, 11.81), (0, 11.91), (0, 11.97)$ and $(0, 11.99)$ with radii $10.04, 9.67, 6.3, 3.88$ and 1.86 Å, respectively

For Model II the parameter B has positive value and we choose $B = 1.7$. The five possible cases of the nanocones are taken into account to join with fullerenes. In Figure 3.10 the arc length of the joining curve again is assumed to be $l = 2$ and the fullerenes are centered at $(0, 11.66), (0, 11.81), (0, 11.91), (0, 11.97)$ and $(0, 11.99)$ with radii $15.3, 9.15, 5.9, 3.53$ and 1.6 Å respectively.

3.4.1.2 Join nanocones with fullerene caps

In the previous section we joined nanocones with exactly half of spherical fullerenes. In this section, we join nanocones with more than half and less than half a spherical fullerene, for each of Models I and II. We match the coordinates and the slope to have a continuous curve at the join. Model I concerns joining the nanocone with more than a half of a spherical fullerene. We consider two cases where the values of $\theta_0 = 112.2°$ and $\theta_1 = -15°$ and $-30°$, and the boundary conditions at x_1 are $\dot{y}(x_1) = 5$ and $\dot{y}(x_1) = 2$ respectively. The joining profiles are shown in

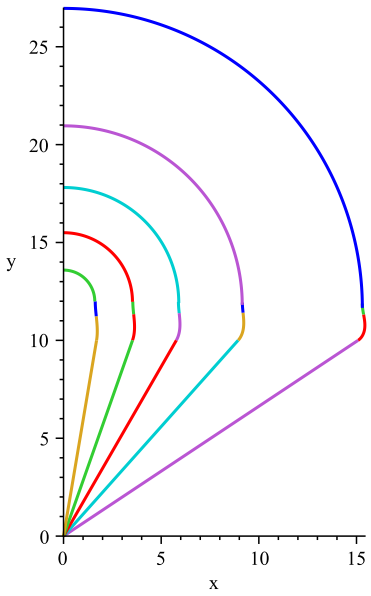

Figure 3.10: Plot of joining $y = y(x)$ for Model II for five possible carbon nanocones, $l = 2$ and $B = 1.7$, fullerenes centered at $(0, 11.66), (0, 11.81), (0, 11.91), (0, 11.97)$ and $(0, 11.99)$ with radii $15.3, 9.15, 5.9, 3.53$ and 1.6 Å respectively.

Figure 3.11. Model II concerns the joining of nanocones with less than a half of a spherical fullerene. In this case we consider four values of θ_1 that are $\theta_1 = 70°, 75°, 80°$ and $85°$. The corresponding boundary conditions are $\dot{y}(x_1) = -2.7, -3.7, -5.6$ and -11.4 respectively. The join profiles are as shown in Figure 3.12.

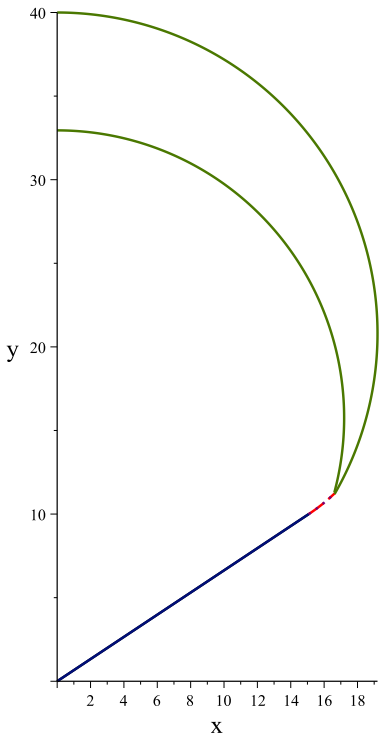

Figure 3.11: Plot of join curve $y = y(x)$ for Model I with positive gradient; the first fullerene is assumed to be centered at $(0, 15.75)$ with radius 17.2 Å and the fullerene is centered at $(0, 20.8)$ with radius 19.2 Å respectively .

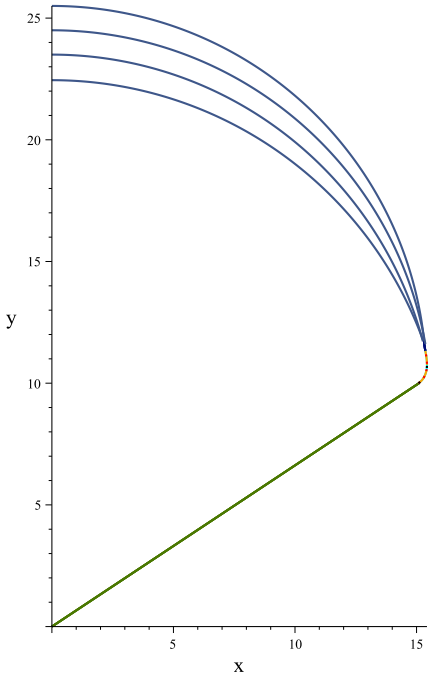

Figure 3.12: Plot of join $y = y(x)$ for Model II with negative gradient and the fullerenes are assumed to be centered at $(0, 6.2), (0, 7.6), (0, 8.9)$ and (10.1) with radii $16.25, 15.8, 15.6$ and 15.4 Å respectively.

3.4.1.3 Perfect join of fullerene and nanocone

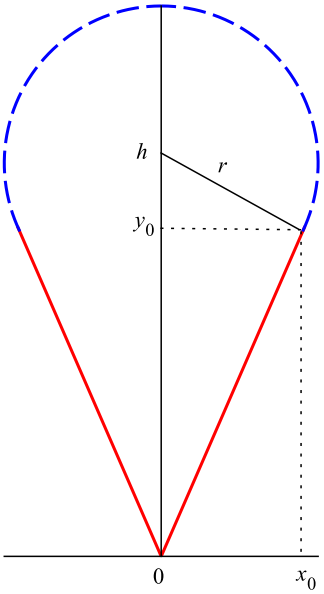

Figure 3.13: Perfect joining of nanocone and fullerene centered at $(0, h)$ with radius r.

Without using calculus of variations, here we show a special case of joining a fullerene with a nanocone, where at the joining region the generating curve is continuous with the slopes matching perfectly at the join (i.e. the first derivatives of the graph functions are equal). As shown in Figure 3.13 we assume in this case that horizontally, the apex of the cone and the center of fullerene are aligned. Furthermore, we assume that $(0, h)$ is the center of the fullerene, r is the radius of the fullerene and (x_0, y_0) is the coordinates of the cone. The circle with center at $(0, h)$ can be represented by

$$x^2 + (y - h)^2 = r^2, \tag{3.26}$$

and the cone equation is $y = k|x|$, where $k > 0$. At (x_0, y_0), we have $y_0 = kx_0$ so that the gradient $k = y_0/x_0$. Thus, the cone equation becomes

$$y = \frac{y_0}{x_0}|x|.$$

Next, we need to show that the gradient (which is the ratio of the change on y over the change on x) of the generating curve of the lower half of the circle is y_0/x_0 at (x_0, y_0). This requires suitable choices of r and h.

3.4.1.4 Joining a fullerene with nanocone perfectly by specifying the center and radius of the fullerene

If we substitute (x_0, y_0) into equation (3.26), we obtain an equation in terms of h and r, namely

$$x_0^2 + (y_0 - h)^2 = r^2. \tag{3.27}$$

Then by differentiating equation (3.26) with respect of x we obtain

$$x + (y - h)\frac{dy}{dx} = 0. \tag{3.28}$$

since

$$\frac{dy}{dx} = \frac{y_0}{x_0},$$

equation (3.28) at (x_0, y_0) becomes

$$x_0 + (y_0 - h)\frac{y_0}{x_0} = 0. \tag{3.29}$$

Now, we have two equations (3.27) and (3.29), solving them simultaneously we have

$$x_0^2 = -(y_0 - h)y_0, \tag{3.30}$$

and by substituting equation (3.30) into equation (3.27) we have

$$-(y_0 - h)y_0 + (y_0 - h)^2 = r^2,$$

which is simplified to

$$y_0 = -\Big(\frac{r^2}{h}\Big) + h. \tag{3.31}$$

To find x_0, we substitute equation (3.31) into equation (3.30),

$$x_0^2 = -\Big[(-\frac{r^2}{h} + h - h)\Big]\Big(-\frac{r^2}{h} + h\Big),$$

which is simplified to

$$x_0 = \Big[-\big(\frac{r^2}{h}\big)^2 + r^2\Big]^{\frac{1}{2}}. \tag{3.32}$$

As a result, we obtain the cone coordinates (x_0, y_0) in terms of the radius of the fullerene r and the fullerene's center $(0, h)$.

As an example, if we suppose that, the center of the fullerene at $(0, 15)$ so $h = 15$ and the radius of the fullerene is $r = 6$ then by using equations (3.31) and (3.32) we can determine the coordinates of the $(x_0, y_0) = (5.5, 12.6)$. Clearly, the fullerene and the cone are connected perfectly and matching exactly as shown in Figure 3.14.

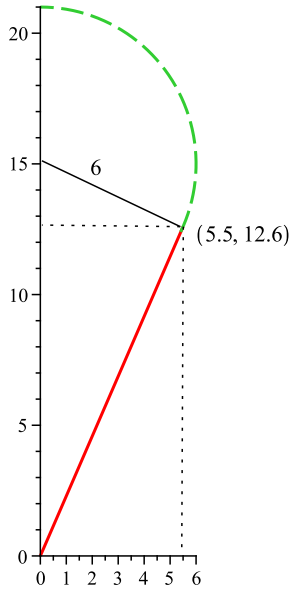

Figure 3.14: Perfect joining of fullerene with center $(0, 15)$ and radius 6 and cone with $(x_0, y_0) = (5.5, 12.6)$ coordinates.

3.4.1.5 Joining a fullerene with nanocone perfectly by specifying the nanocone coordinates

In this case we determine the center $(0, h)$ and the radius r of the fullerene based on the cone's coordinates (x_0, y_0). By using the cone's coordinates equations in the previous section, equation (3.31), we have

$$h^2 - y_0 h - r^2 = 0, \tag{3.33}$$

so

$$y_0 = h - \frac{r^2}{h}, \tag{3.34}$$

which is can be written as

$$\frac{r^2}{h} = h - y_0. \tag{3.35}$$

Also from (3.32)

$$x_0^2 = \frac{r^2}{h}\Big(- \frac{r^2}{h} + h\Big),$$

by using (3.34), we obtain

$$x_0^2 = \frac{r^2}{h} y_0,$$

which gives

$$\frac{r^2}{h} = \frac{x_0^2}{y_0}. \tag{3.36}$$

From (3.35) and (3.36) we obtain

$$h = \frac{x_0^2}{y_0} + y_0, \tag{3.37}$$

and from (3.33) we have

$$r^2 = h(h - y_0). \tag{3.38}$$

Using equation (3.37) we get

$$r = \frac{x_0}{y_0}\sqrt{x_0^2 + y_0^2}. \tag{3.39}$$

As a result, we can determine the fullerene's center $(0, h)$ using equation (3.37) and the fullerene's radius r using equation (3.39). As shown in the previous subsubsection, if the coordinates of the cone $(x_0, y_0) = (5.5, 12.6)$, by using equations (3.37) and (3.39) we obtain $h = 15$ and $r = 6$, as expected.

For this method of joining, given more than half a sphere, and a point on the same vertical axis as the center of the sphere, there is a cone which can be joined perfectly (ie the slopes match as well as the position). To join a small piece of the cone to a sphere, the natural way would be to extend the cone by a straight line. In this case, the integral curvature term in (3.1) is exactly equal to zero, and we know that for all curves joining two points by a straight line has the shortest length, so in this way we have found a global minimizer. It works only in this special scenario where the cone is extended to match up exactly with the spherical part. Given a cone

angle, there is a family of more-than-half sphere that can be joined in a similar way, depending on how far we wish to extend the cone from its apex.

Finally, we note that the above results can also be derived from setting $\kappa = 0$ at the join. Since $\kappa = \ddot{y}/(1+\dot{y}^2)^{\frac{3}{2}}$, then we have $\ddot{y}(x) = 0$ which gives rise to $y(x) = C_0 x + C_1$, where C_0 and C_1 are arbitrary constants. Using the boundary conditions at the joining point x_0, which are $y(x_0) = y_0$ and $\dot{y}(x_0) = \cot(\gamma/2)$, we find $C_0 = \cot(\gamma/2)$ and $C_1 = y_0 - x_0 \cot(\gamma/2)$.

All Maple codes for this section are presented in Appendix D.1.

3.4.2 Joining two carbon nanocones

(a) Model I. (b) Model II.

Figure 3.15: Axially symmetric geometries for Model I and Model II.

To study the joining area between two carbon nanocones we consider the same method as shown in the subsection 3.4.1. The first nanocone is assumed to be located at the origin with the radius r. The second nanocone has the radius a and is assumed to be located with its center on the y-axis starting from y_0 which is unknown positive distance above xy-plane.

3.4.2.1 Joining two symmetric carbon nanocones

In this case, we join two symmetric nanocones. Here the curvature of the joining curve must remain positive to connect the cones. This situation can be described as Model I in Figure 3.15(a). Also the parameter B in this region has negative value as in Figure 3.8. We specify $\theta_0 = \frac{\gamma}{2}$ and $\theta_1 = -\frac{\gamma}{2}$ and the boundary conditions at x_0,

$$y(b\sin\frac{\gamma}{2}) = b\cos\frac{\gamma}{2},$$
$$\dot{y}(b\sin\frac{\gamma}{2}) = \cot\frac{\gamma}{2},$$

and at x_1 the boundary condition is

$$\dot{y}(a) = -\infty.$$

In Figure 3.16, we plot the join for two symmetric nanocones where five possible nanocone's angles ($112.9°, 83.6°, 60°, 38.9°$ and $19.2°$) are considered.

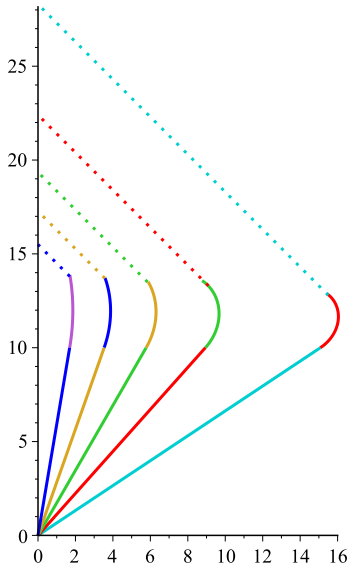

Figure 3.16: Plot of joining $y = y(x)$ for Mode I for five possible nanocones with $B = -4$ and $l = 2$.

3.4.2.2 Joining two different angle nanocones

In this case, we consider two nanocones that have different angles. Here we assume the join curve to have both positive and negative curvature to connect the cones. This case can be described by Model II in Figure 3.15(b). The parameter B is positive for the two subregions of Model II. In Figure 3.17 we show the joining curves which connect the nanocones for all five possible cases for chosen different values of the parameter B ($B = 1.0001, 1.001, 1.01, 1.1, 1.2, 1.3$ and 1.5) respectively.

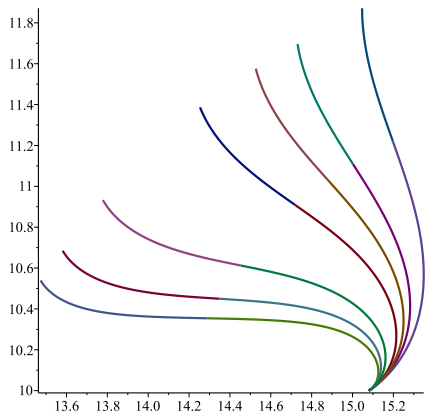

(a) The first nanocone angle is 112.9°

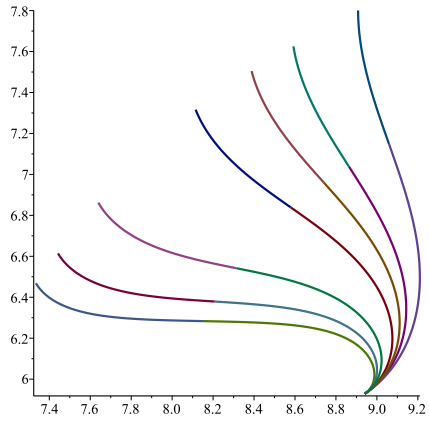

(b) The first nanocone angle is 83.6°

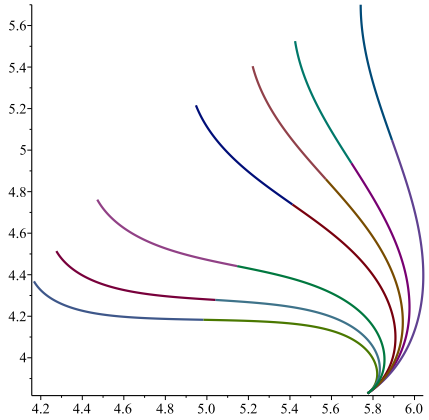

(c) The first nanocone angle is 60°

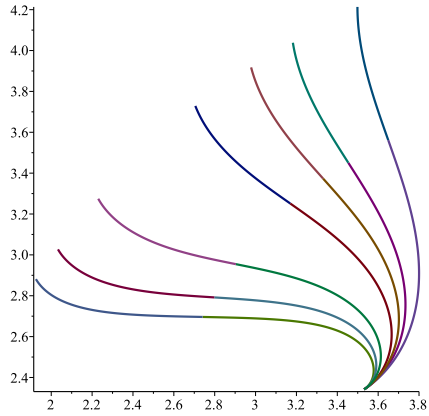

(d) The first nanocone angle is 38.9°

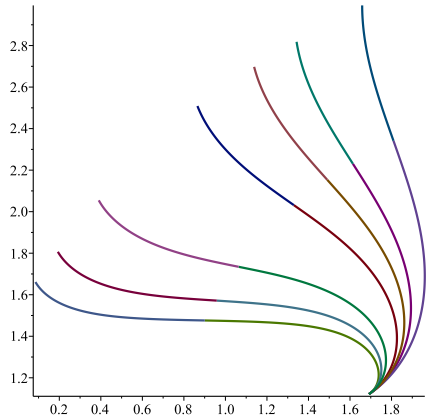

(e) The first nanocone angle is 19.2°

Figure 3.17: Joining curves for $B = 1.0001, 1.001, 1.01, 1.1, 1.2, 1.3$ and 1.5 respectively for all five angles of the nanocones.

3.4.2.3 Joining two different nanocones

In this subsection we join nanocones of two different angles. The first nanocone has varied angles as shown in Table 3.1, so $\theta_0 = 112.9°, 83.6°, 60°, 38.9°, 19.2°$. The second carbon nanocone has a fixed angle, which is assumed to be $\theta_1 = 60°$ with gradient of $\dot{y}(a) = -1.7$. Moreover, in this case the parameter B is assumed to have three particular different values for the joining where $B = 1.0001, 1.01$ and 1.1. Based on that we obtain Figure 3.18 when $\theta_0 = 112.9°$, Figure 3.19 is when $\theta_0 = 83.6°$, Figure 3.20 when the angle $\theta_0 = 60°$, Figure 3.21 shows the join when $\theta_0 = 38.9°$ and Figure 3.22 when the angle is $\theta_0 = 19.2°$. Noting that, Appendix D.2 shows Maple codes for these joinings.

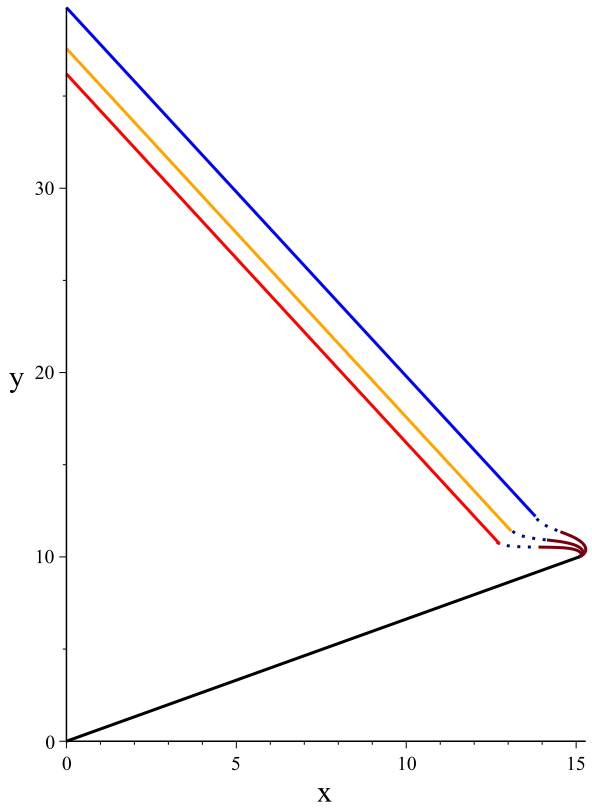

Figure 3.18: Nanocone angle $112.9°$ with $l = 3$ and $B = 1.0001, 1.01$ and 1.1.

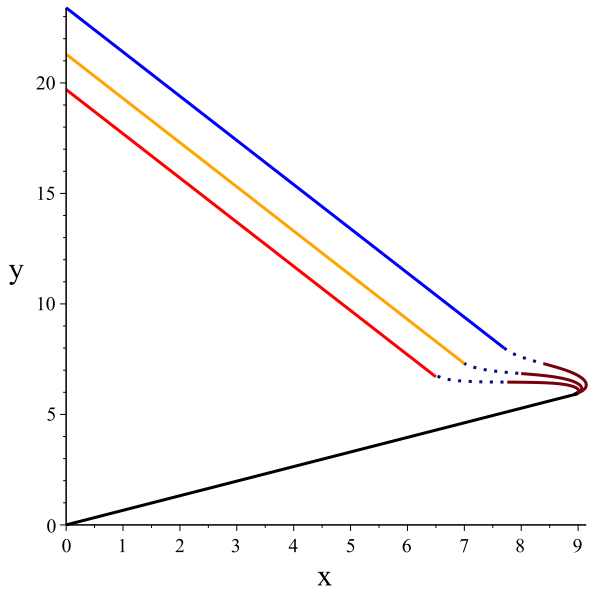

Figure 3.19: Nanocone angle 83.6° with $l = 3$ and $B = 1.0001, 1.1$ and 1.01.

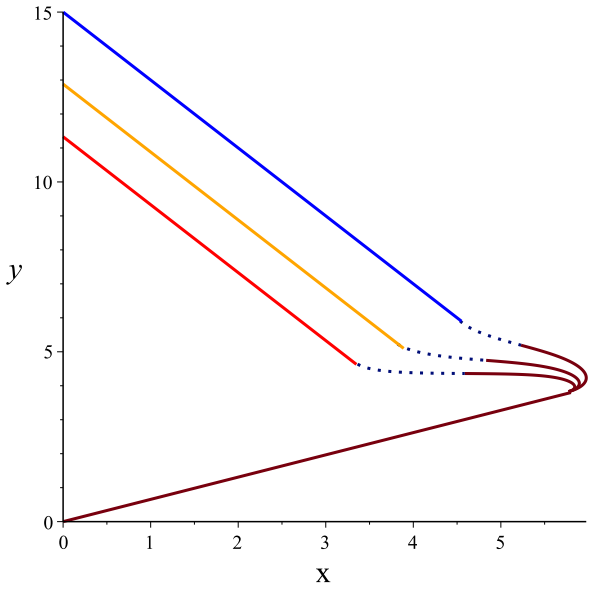

Figure 3.20: Nanocone angle 60° with $l = 3$.

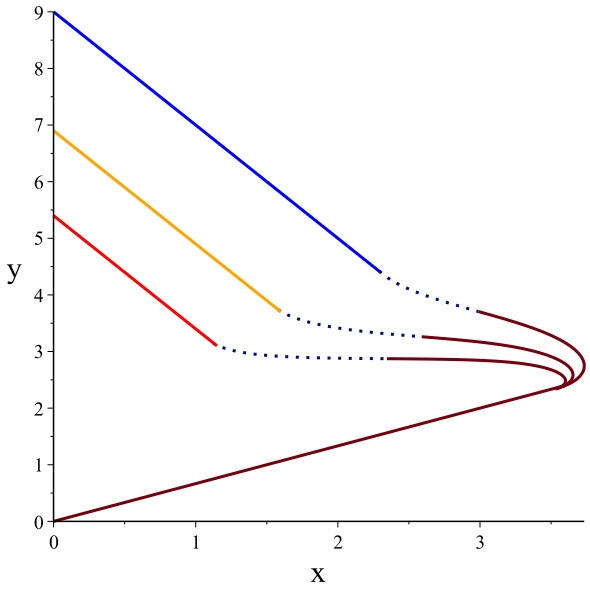

Figure 3.21: Nanocone angle 38.9° with $l = 3$.

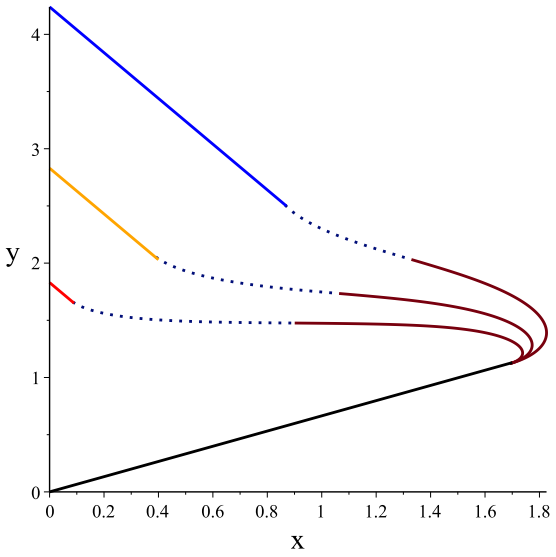

Figure 3.22: Nanocone angle 19.2° with $l = 2$.

3.4.3 Joining carbon nanocones and flat sheet of Graphene

(a) Model I. (b) Model II.

Figure 3.23: Geometries for Model I and Model II.

Here we join carbon nanocone with the flat sheet of graphene. Again we use the same method as in subsection 3.2. In particular, x_0 is the graphene radius and a is the radius of the nanocone. The attachment points are at $(x_0, 0)$ for the graphene and at (a, y_0) for the nanocone, as shown in Figure 3.23. The angle of graphene is assumed to be $\theta_0 = 0$ and the angle of the carbon nanocone θ_1 is one of the five possible angles as indicated in Table 3.1. As a result, the boundary conditions at the graphene sheet are

$$y(x_0) = 0, \quad \dot{y}(x_0) = 0.$$

For the boundary conditions at the carbon nanocone for Model I, the value of $\dot{y}$ ranges from 0 at $x = x_0$ to a negative value depending on the angle of the cone at $x = a$. In Model II the value of $\dot{y}$ ranges from 0 at $x = x_0$ to ∞, then it changes the sign from $-\infty$ to negative value depending on the angle of the cone.

3.4.3.1 The characteristic parameter μ

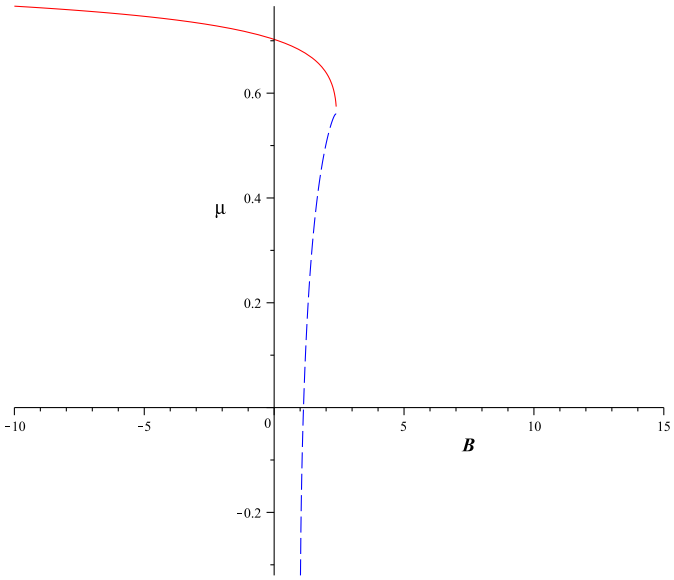

Figure 3.24: Relation between the parameters $\mu = (x_0 - a)/l$ and $B = 1/k^2$.

Based on Figure 3.24, three distinct regions are evident. The first region where the parameter B is negative corresponds to Model I. The second region is $0 < B \leq 2$ which also corresponds to Model I, and the third region is $1 < B \leq 2$ which corresponds to Model II [30].

For particular values of the parameter B, we join the graphene with nanocones for Model I as in Figure 3.25 and Model II as in Figure 3.26. Appendix D.3 presents Maple codes of these joining.

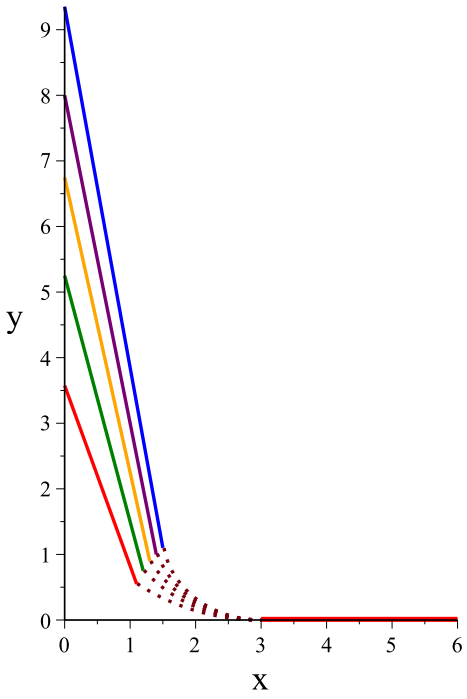

Figure 3.25: Plot of joining $y = y(x)$ for Model I for five possible nanocones $112.9°, 83.6°, 60°, 38.9°$ and $19.2°$ with graphene where $B = -4$ and $l = 2$.

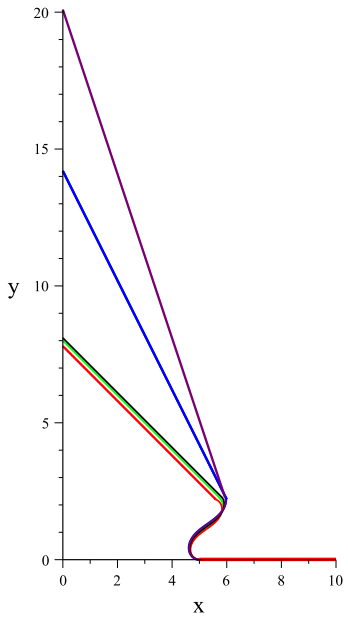

Figure 3.26: Plot of joining $y = y(x)$ for Model II for five possible nanocones $112.9°, 83.6°, 60°, 38.9°$ and $19.2°$ with graphene where $B = 1.1$ and $l = 3$.

3.4.4 Joining between fullerene and flat sheet of graphene

(a) Model I. (b) Model II.

Figure 3.27: Geometries for Model I and Model II.

Again we use the same analysis mentioned in section 3.2. We assume that that x_0 is the graphene radius and a is the fullerene radius. The attachment points of the two carbon nanomaterials are assumed to be at $(x_0, 0)$ and (a, y_0) for the graphene and fullerene respectively, as shown in Figure 3.27. The angle of the graphene is chosen to be $\theta_0 = 0$ and the angle of the fullerene is assumed to be $\theta_1 = -\frac{\pi}{6}$ with gradient $\dot{y}(x_1) = 0.5$. Moreover, the boundary conditions at the graphene sheet are

$$y(x_0) = 0,$$

$$\dot{y}(x_0) = 0.$$

The range of the values of the parameter B is the same as that described in Figure 3.24.

In Model I, the value of the parameter B is valid for both positive and negative values as investigated in Figure 3.24. As a result, there are two different joining structures corresponding to positive and negative values of the parameter B. For the positive value of the parameter B, here we assume $B = 1$ so we have the joining structure as shown in Figure 3.28. Furthermore for the negative value of B, which is assumed to be $B = -1$, the join profile is given in Figure 3.29.

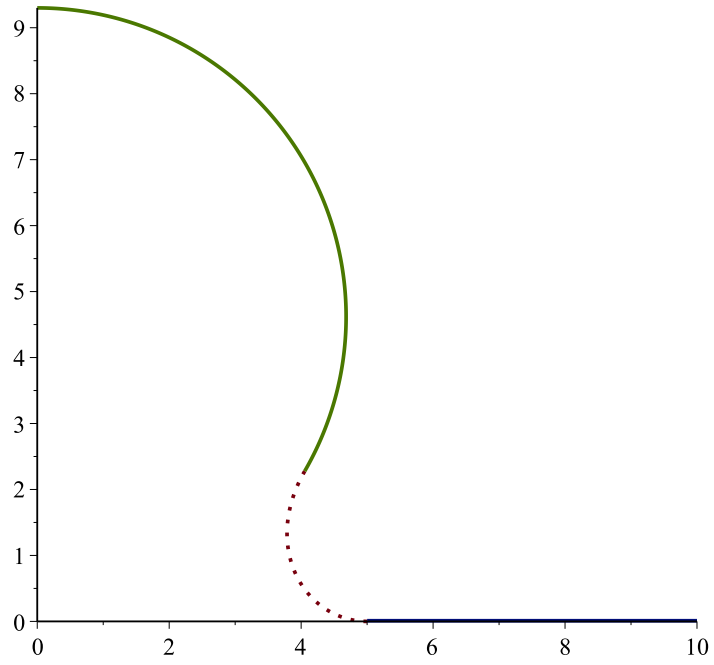

Figure 3.28: Plot of the join curve $y = y(x)$ of Mode I for joining fullerene with graphene when $l = 3$ and $B = 1$.

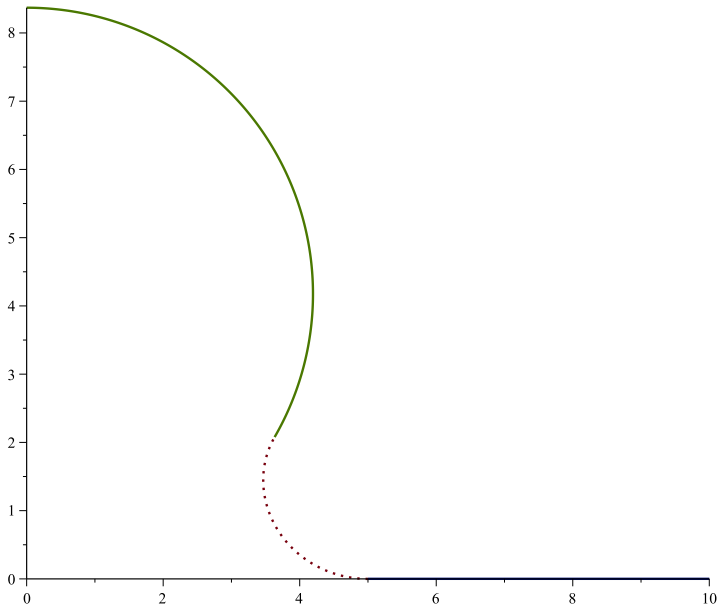

Figure 3.29: Plot of the join curve $y = y(x)$ of Mode I for joining fullerene with graphene where $l = 3$ and $B = -1$.

For Model II, the parameter B is valid only for the positive value. As a result, we have the join structure with positive value of B which is assumed to be $B = 1.1$, as shown in Figure 3.30.

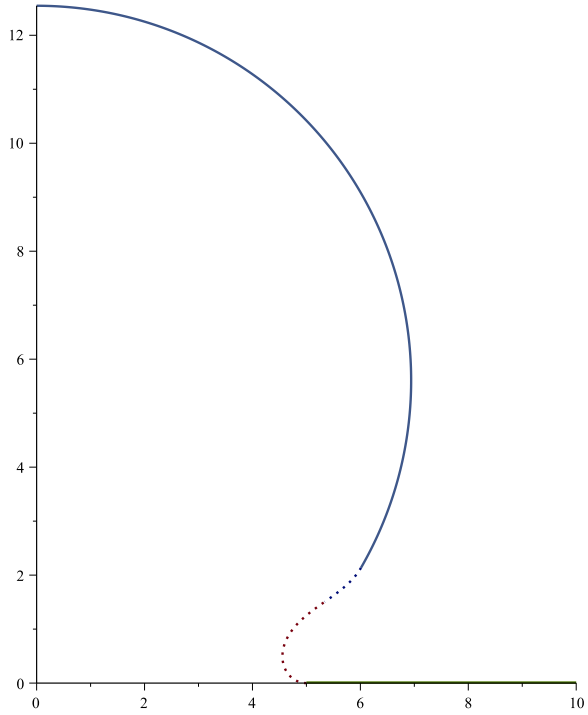

Figure 3.30: Plot of the join curve $y = y(x)$ of Mode II for joining fullerene with graphene where $B = 1.1$ and $l = 3$.

Maple codes corresponding to these joinings are given in Appendix D.4

3.4.5 Joining between two parallel sheets of graphene with nanocone and fullerene

Here we join carbon nanocone and fullerene with two parallel sheets of graphene. By using both of Model I and Model II we join other nanomaterials. Model I joins nanocone and fullerene with the second graphene sheet and Model II joins nanocone and fullerene with the first graphene sheet. The value of the parameter μ is the same in Figure 3.8.

3.4.5.1 Joining between two parallel sheets of graphene with carbon nanocone

In this case we join two parallel sheets of graphene with carbon nanocone. Model I has $\theta_0 = \pi/2$ and $\theta_1 = 0$ with gradient $\dot{y}(x_1) = 0$. Model II has $\theta_0 = \frac{\pi}{90}$ and $\theta_1 = \frac{\pi}{2.11}$ with positive gradient. The joining structure of this case is determined as in Figure 3.31. Appendix D.5 presents the codes of this joining.

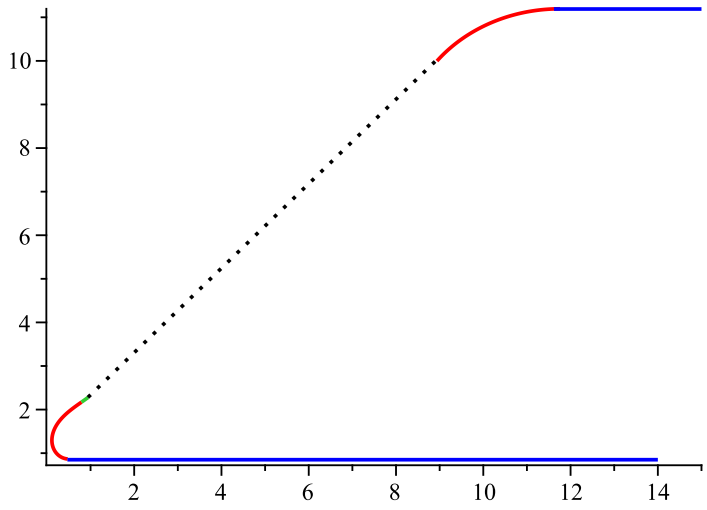

Figure 3.31: Plot of joining between nanocone and two parallel sheets of graphene.

3.4.5.2 Joining between two parallel sheets of graphene with part of fullerene

This case is joining two parallel sheets of graphene with part of fullerene. In Model I we consider $\theta_0 = \frac{\pi}{2}$ and $\theta_1 = 0$ and in Model II we use $\theta_0 = \frac{\pi}{2}$ and $\theta_1 = \frac{\pi}{2}$ with positive gradient. As a result, the joining structure of these carbon nanomaterials is determined as in Figure 3.32. Maple codes in Appendix D.6 are used to produce this joining profile.

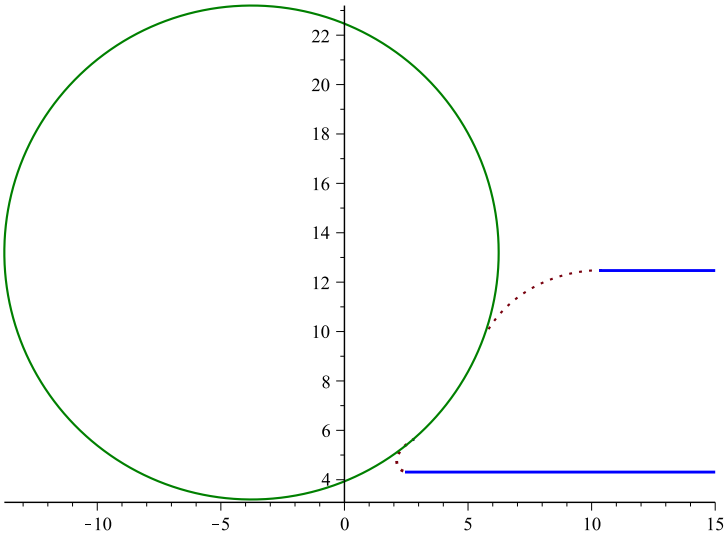

Figure 3.32: Plot of joining between fullerene centred at $(-3.76, 13.2)$ with radius 10 Å and two parallel sheets of graphene.

3.5 Conclusion

This chapter gives an approximate analytical solution to a discrete problem for the determination of the surface which joins two carbon nanostructures. We use a variational approach that depends on minimization of covalent bond energy. Two different models are assumed which depend on the sign of the curvature. Model I refers to positive curvature only, and Model II refers to both positive and negative curvatures. Based on that, we join various different nanostructures to obtain new configurations which may enhance their intrinsic properties leading to new applications. Specifically, we join carbon nanocones with fullerenes and nanocones and flat sheets of graphene. We join fullerene with flat sheets of graphene and finally, joining nanocones and part of fullerene with two parallel sheets of graphene. The new nanostructures may be useful as a probe for scanning tunneling microscopy.

Chapter 4

Comparison of two different energies for modelling the joining between carbon nanostructures

4.1 Introduction

The research in theory of minimal surfaces in $\mathbb{R}^3$ is an important and active field. The investigations of minimal surfaces in $\mathbb{R}^3$ began with Lagrange in 1762 when he considered the problem of determining a graph with least area over a domain in $\mathbb{R}^2$ and taking prescribed values on the boundary. As a result, he obtained the partial differential equation to be satisfied by the solution. After that, in 1776 Meusnier recognized the geometric meaning of that equation by specifying the mean curvature $H = 0$. Throughout the nineteenth century, research topics involving minimal surfaces have attracted much attention. The physicist Plateau obtained that minimal surfaces may be recognised as soap film. In 1930 the Plateau's problem which determined a minimal disk bounded by a given Jordan curve was solved by Douglas and Rado [81]. Importantly, minimal surfaces have many applications in physical and biological sciences. In particular, they have an important role to nanotechnology in molecular engineering and material science. Minimal surfaces have least surface area which enables wide usage in large scale and light roof constructions [72]. For example, minimal surfaces are used in architecture and art such as the olympic stadium in Munich [106] [56].

There are many examples of minimal surfaces such as the plane, catenoids, helicoids, Schwarz, Riemann's, Enneper and Henneberg surfaces [56].

Now we have a generalization of minimal surfaces called Willmore surfaces. This energy func-

tional is defined as

$$W = \int_M H^2 d\mu,$$

where H denotes the mean curvature of surface M and $d\mu$ is the area element. Willmore energy has important applications in the fields of science and nanotechnology [47]. For example, in biology Helfrich surface models the shape of the red blood cell [88]. It also appears as a surface energy for lipid bilayers [88]. Willmore energy is another natural generalisation of elastic energy used in mechanics [88]. This energy has useful applications in optical design [88]. Furthermore minimal surfaces as catenoid has nanomagnetism applications [23] [24].

In this chapter, we compare the joining between carbon nanostructures based on two different energies. First is the energy described by equation (3.1) which depends on the axial curvature only. Secondly, we use Willmore energy that depends on the axial curvature and the rotational curvature, which is given by

$$I[y] = \int (\kappa_a + \kappa_r)^2 d\mu + \lambda \int d\mu, \tag{4.1}$$

we use the convention that the mean curvature is the sum of the principal curvatures. In the next section, first and second energies are addressed in detail. The comparison and discussion for the two energies is given in Section 4.3. Finally, the conclusion of this chapter is presented in section 4.4.

4.2 Model and mathematical background

For the first energy we consider the same case as in section 3.2.2.1 with suitable boundary conditions. For the second energy, if we have the surface $z(r,\theta) = f(r,\theta)$, which the curve depends on (r,θ), we can describe surface parameterically by $S = \{(x,y,z) : x = r\cos\theta, y = r\sin\theta, z = f(r,\theta)\}$ with $0 < r \leq a$ where H is the mean curvature of surface which is $H = \kappa_a + \kappa_r$, where κ_a is the axial curvature and κ_r is the rotational curvature. For cross section, the position vector of point on curve is denoted by $\tilde{\mathbf{r}}(x) = (x, f(x))$. If the curve revolves around the $z-$axis, the position vector is

$$\tilde{\mathbf{r}}(r,\theta) = (r\cos\theta, r\sin\theta, f(r)). \tag{4.2}$$

First, we find the tangent vectors as $\tilde{\mathbf{r}}_r = (\cos\theta, \sin\theta, f'(r))$ and $\tilde{\mathbf{r}}_\theta = (-r\sin\theta, r\cos\theta, 0)$.

Second, the unit normal is

$$-\frac{(\cos\theta f'(r)i + \sin\theta f'(r)j - k)}{\sqrt{f'^2(r)+1}}.$$

Then, the metric g_{ij} is

$$\begin{pmatrix} 1+f'^2(r) & 0 \\ 0 & r^2 \end{pmatrix},$$

and $\det(g_{ij}) = r^2\left(1+f'^2(r)\right)$. The inverse metric $g^{ij} = (g_{ij})^{-1}$ is

$$\begin{pmatrix} \frac{1}{1+f'^2(r)} & 0 \\ 0 & \frac{1}{r^2} \end{pmatrix},$$

and the second fundamental form h_{ij} is

$$\begin{pmatrix} \frac{f''^2(r)}{\sqrt{f'^2(r)+1}} & 0 \\ 0 & \frac{rf'(r)}{\sqrt{f'^2(r)+1}} \end{pmatrix},$$

then $(g_{ij})^{-1}(h_{ij})$ is

$$\begin{pmatrix} \frac{f''(r)}{(1+f'^2(r))^{\frac{3}{2}}} & 0 \\ 0 & \frac{f'(r)}{r\sqrt{f'^2(r)+1}} \end{pmatrix}.$$

Thus we obtain $H = \frac{f''(r)}{(1+f'^2(r))^{\frac{3}{2}}} + \frac{f'(r)}{r\sqrt{f'^2(r)+1}}$ where $\kappa_a = \frac{f''(r)}{(1+f'^2(r))^{\frac{3}{2}}}$ and $\kappa_r = \frac{f'(r)}{r\sqrt{f'^2(r)+1}}$. The Euler-Lagrange equation is

$$\Delta_m H + \mid A^\circ \mid^2 H + \lambda H = 0, \tag{4.3}$$

where

$$\begin{aligned} \mid A^\circ \mid^2 &= \frac{1}{2}(\kappa_a - \kappa_r)^2 \\ &= \left(\frac{f''(r)}{(1+f'^2(r))^{\frac{3}{2}}} - \frac{f'(r)}{r\sqrt{f'^2(r)+1}}\right)^2, \end{aligned} \tag{4.4}$$

and

$$\Delta_m = \frac{1}{\sqrt{\det(g_{ij})}} \sum_{i,j} \frac{\partial}{\partial x_i}\left\{\sqrt{\det(g_{ij})}g^{ij}\frac{\partial}{\partial x_j}\right\},$$

so

$$\Delta_m H = \frac{1}{r\sqrt{1+\dot{f}^2(r)}}\frac{\partial}{\partial r}\left[\frac{r\frac{\partial H}{\partial r}}{\sqrt{1+f'^2(r)}}\right]. \tag{4.5}$$

Substituting (4.4) and (4.5) into (4.3) we obtain

$$\frac{1}{r\sqrt{1+p^2}}\frac{\partial}{\partial r}\left[\frac{r\frac{\partial}{\partial r}H}{\sqrt{1+p^2}}\right]+\left(\frac{1}{2}\left[\frac{\dot{p}}{(1+p^2)^{\frac{3}{2}}}-\frac{p}{r\sqrt{1+p^2}}\right]^2+\lambda\right)H=0, \tag{4.6}$$

which is

$$\frac{\partial}{\partial r}\left[\frac{r\frac{\partial}{\partial r}H}{\sqrt{1+p^2}}\right]=-\left[\frac{r}{2}\left(\frac{\dot{p}}{\sqrt{1+p^2}}-\frac{p\sqrt{1+p^2}}{r}\right)^2+\lambda(r\sqrt{1+p^2})\right]H, \tag{4.7}$$

where $p=f'(r)$. Now if $\lambda=0$ and we use the catenoid as shown in Figure 4.1 (as it is a minimal surface and local minimizer of the area functional), that is $H=0$, we obtain surface that is an absolute minimizer of the Willmore energy. However, this result could be energy minimizing for a whole class of energies not just the Willmore energy. These include the surface area (leading to minimal surfaces) and energy of the form $\int H^k d\mu$, for any constant $k\geq 0$. It makes sense to consider joining different rotationally symmetric carbon nanostructures with pieces of the catenoid. Thus in the following section we use a piece of catenoid for joining different carbon nanostructures.

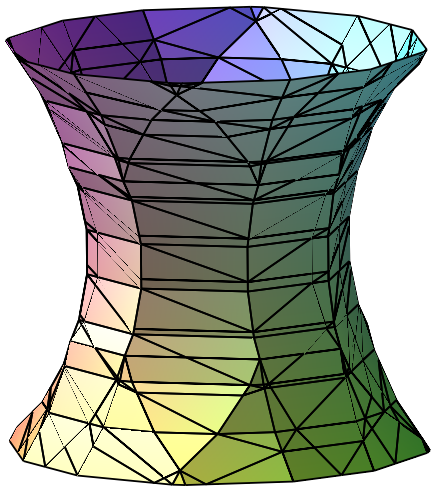

Figure 4.1: Catenoid

4.3 Results

Here we compare the joining between carbon nanostructures considering two energies mentioned in the previous section.

4.3.1 Modelling the joining between carbon nanocones and carbon nanotubes

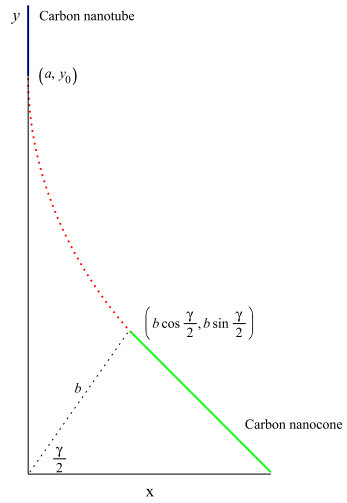

Figure 4.2: Model I for joining between carbon nanotube and carbon nanocone (first energy).

For the first energy, we consider Model I as shown in Figure 4.2 to have the boundary conditions at the carbon nanocone as follows:

$$y(b\cos\gamma/2) = b\sin\gamma/2,$$

$$\dot{y}(b\cos\gamma/2) = -\cot\gamma/2.$$

The value of $\dot{y}$ ranges from $-\cot\gamma/2$ at $x = b\cos\gamma/2$ to $-\infty$ at $x = a$, and therefore the boundary condition at the carbon nanotube is $\dot{y}(a) = -\infty$.

For the second energy, catenoids are absolute minimisers and we may consider joining catenoids of the form

$$y(x) = A\cosh^{-1}(x+1) + h, \tag{4.8}$$

where A and h are constants as shown in Figure 4.3. The codes for this join is given in Appendix E.

Here we match the gradient and join carbon nanocones with carbon nanotubes for five cases that are based on angles of carbon nanocones as identified in Table 3.1. Figure 4.4(a) is when

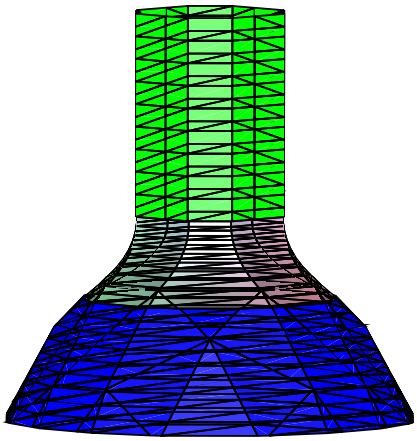

Figure 4.3: Joining carbon nanocone and carbon nanotube with a piece of catenoid.

$\gamma = 112.9°$ and Figure 4.4(b) is when $\gamma = 83°$. Figure 4.5(a) is when $\gamma = 60°$ and Figure 4.5(b) is when $\gamma = 38°$. Figure 4.6 corresponds to the case when $\gamma = 19°$. In addition, by using numerical integration, Simpson's rule, the difference between the two energies is calculated for each angle of the nanocone as shown in Appendix E. For the first angle 112.9° the relative error is 0.09%, for the angle 83.6° is 0.15%, for the angle 60° is 0.18%, for the angle 38.9° is 0.5% and for the angle 19.2° is 0.9%. As a result, the rotational curvature does not contribute much in the total energy. In addition, because one of the joins is at the neck of the catenoid, we can get the same results if we join to a half sphere of the appropriate size, or, if we join two pieces of cones in the opposite orientation as in the following subsections.

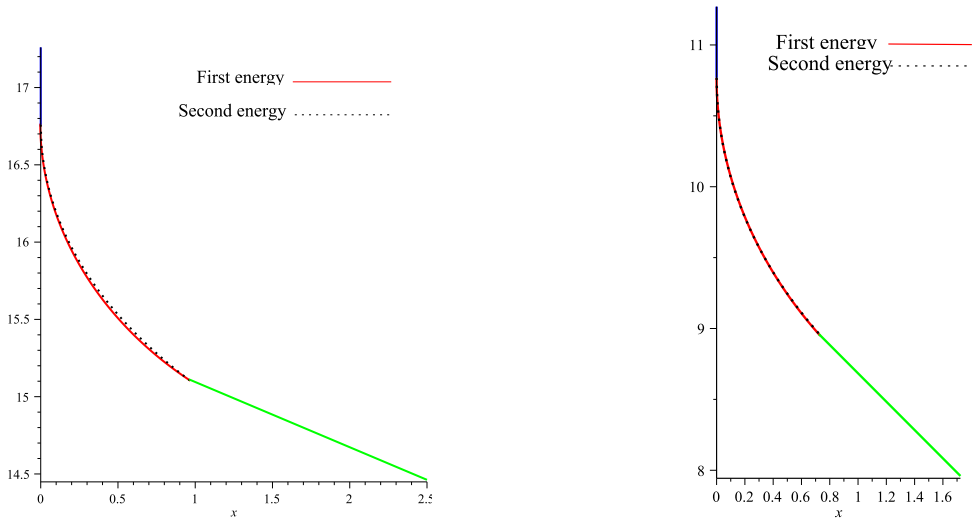

(a) 112.9° (b) 83.6°

Figure 4.4: The joining based on first and second energies for nanocones with angles 112.9° and 83.6°.

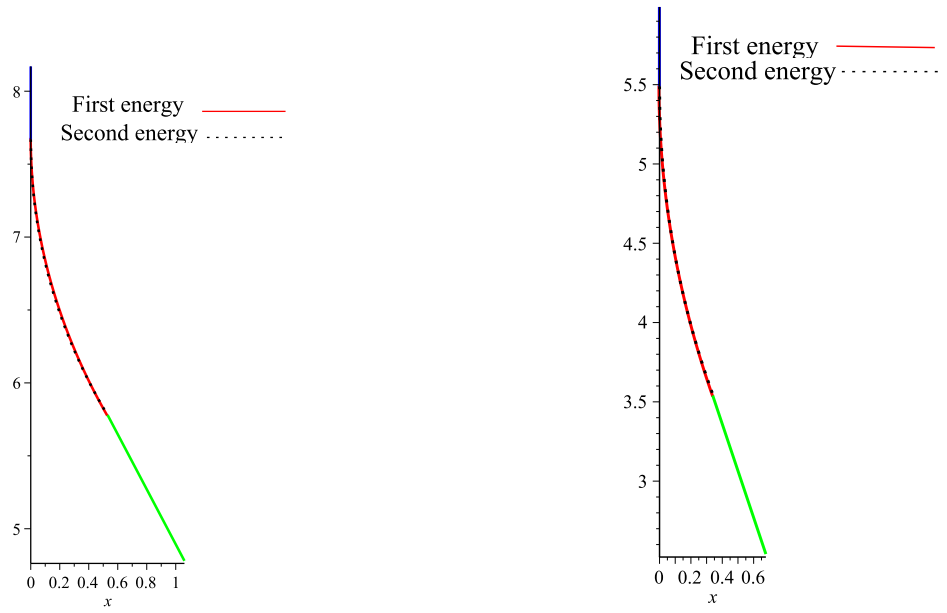

(a) 60° (b) 38.9°

Figure 4.5: The joining based on first and second energies for nanocones angles 60° and 38.9°

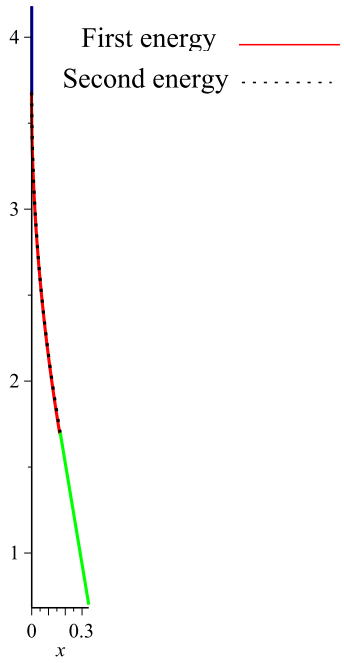

Figure 4.6: The joining based on first and second energies for nanocones angle 19.2°.

4.3.2 Modelling the joining between two carbon nanocones

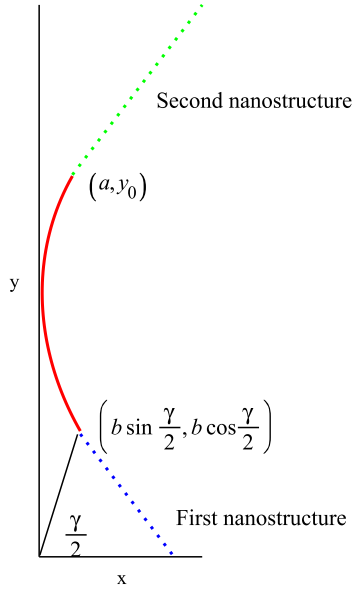

Figure 4.7: Model I for joining between two carbon nanostructure.

Here we use the two energies to join two carbon nanocones. The first energy is Model I as shown in Figure 4.7 with the boundary conditions at the first carbon nanostructure as follows:

$$y(b\cos\gamma/2) = b\sin\gamma/2,$$

$$\dot{y}(b\cos\gamma/2) = -\cot\gamma/2.$$

The value of $\dot{y}$ ranges from $-\cot\gamma/2$ at $x = b\cos\gamma/2$ to $\cot\gamma/2$ at $x = a$, and therefore the boundary condition at the second carbon nanostructure is $\dot{y}(a) = \infty$. The second energy corresponds to the catenoid of the form

$$x(y) = \cosh\left(\frac{1}{B}(y+c)\right) - d,$$

where B, c and d are constants as shown in Figure 4.8.

Here we match the gradient and join carbon nanocones for five cases based on angles of carbon nanocones as in Table 3.1. Figure 4.9(a) is when $\gamma = 112.9°$ and Figure 4.9(b) is when $\gamma = 83°$. Figure 4.10(a) corresponds the case when $\gamma = 60°$. Figure 4.10(b) is when $\gamma = 38.9°$. Figure 4.11 is when $\gamma = 19°$.

Furthermore, we use numerical integration, Simpson's rule, to calculate the difference between the two energies. For the first angle 112.9° the relative error is 6%, for the angle 83.6° is

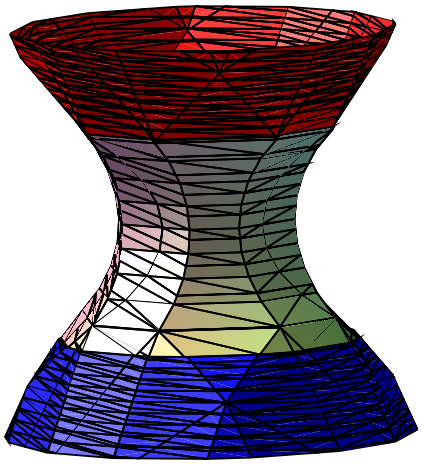

Figure 4.8: Joining two carbon nanocones with piece of catenoid.

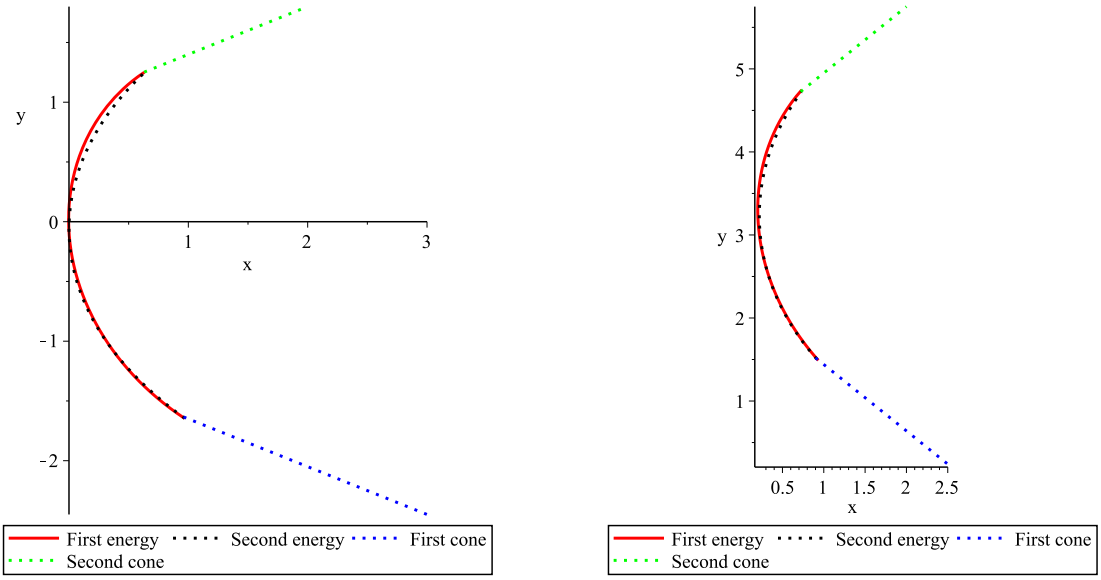

(a) 112.9°

(b) 83.6°

Figure 4.9: The joining based on first and second energies for nanocones with angles 112.9° and 83.6°.

4%, for the angle 60° is 3%, for the angle 38.9° is 14% and for the angle 19.2° is 12%.

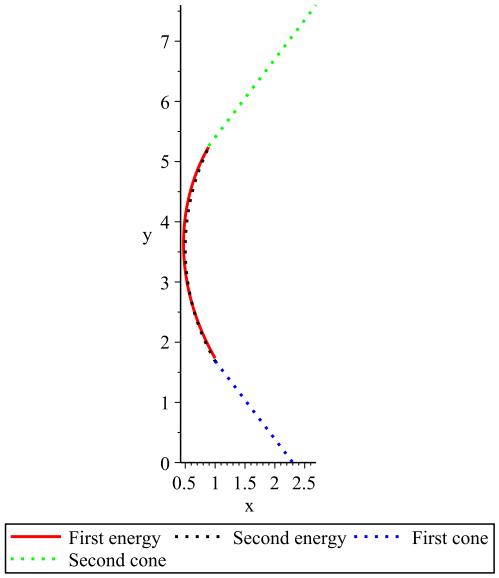

(a) 60°

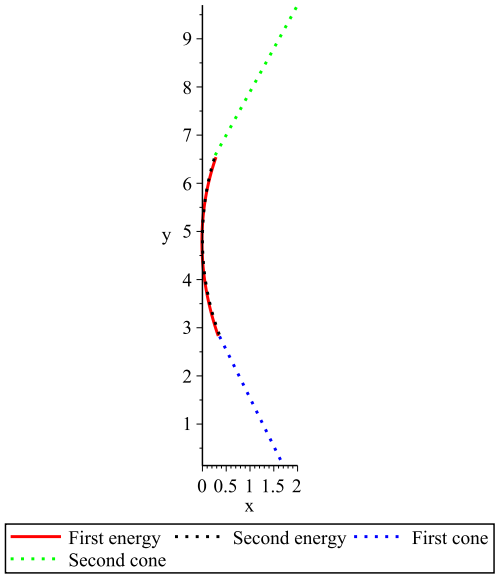

(b) 38.9°

Figure 4.10: The joining based on first and second energies for nanocones with angles 60° and 38.9°

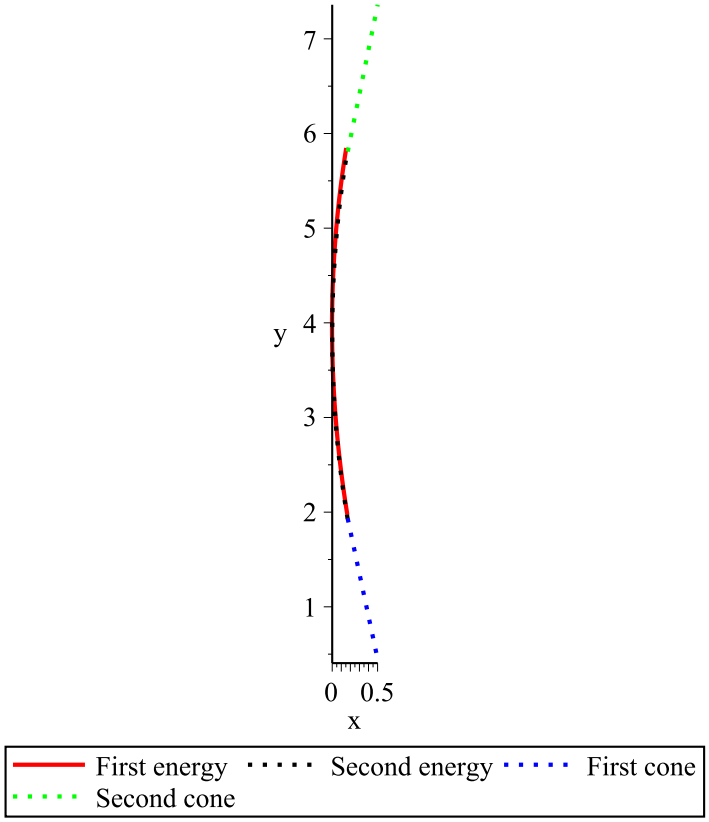

Figure 4.11: The joining based on first and second energies for nanocones with angle 19.2°.

4.3.2.1 Modelling the joining between large carbon nanocone and narrow carbon nanocone

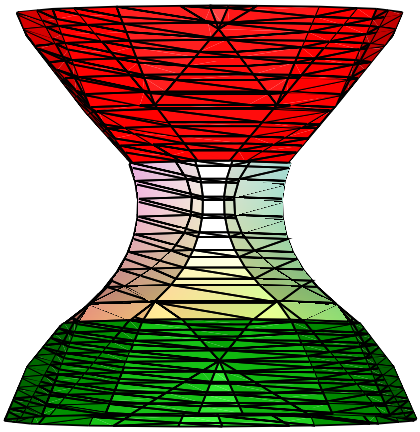

Figure 4.12: Joining of large carbon nanocone and narrow carbon nanocone with piece of catenoid.

In this case the first and second energies are the same as in joining two carbon nanocones. The second energy of this case is shown in Figure 4.12. In particular, in Figure 4.13 we join two carbon nanocones where the angle of the first nanocone is 112.9° and the second angle of the nanocone is 60°. Again here we use Simpson's rule to calculate the difference between the two energies, the relative error is 2%.

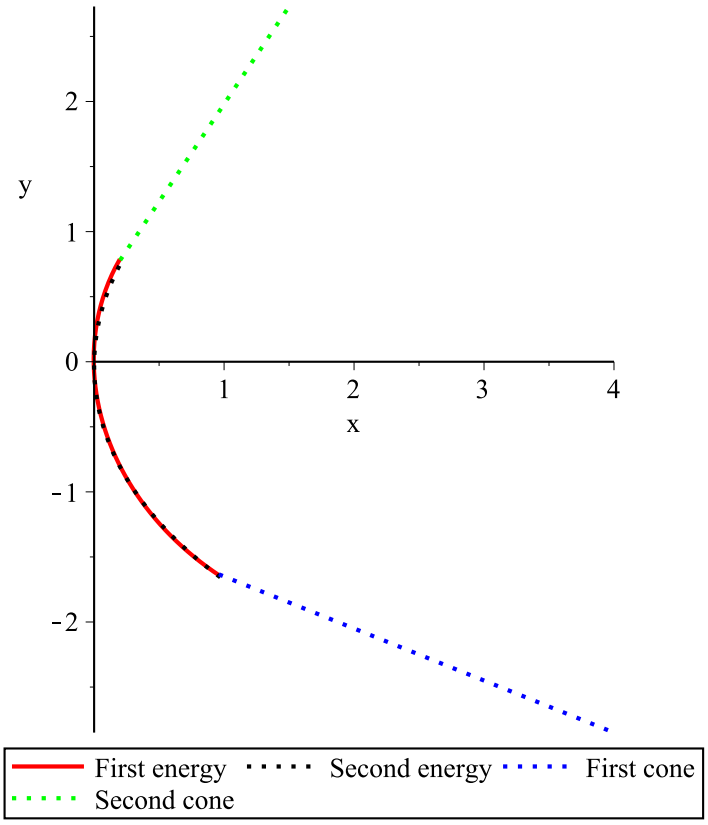

Figure 4.13: The joining based on first and second energies for nanocones with angles 112.9° and 60°.

4.3.2.2 Modelling the joining between two fullerenes

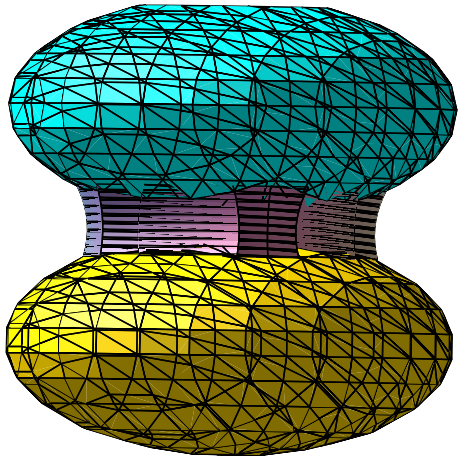

Figure 4.14: Joining two fullerenes with piece of catenoid.

Again in this case the first and second energies are the same as in joining two carbon nanocones. The second energy is shown in Figure 4.14 where in this Figure the scale in the horizontal and vertical directions is not the same. In Figure 4.15 we join two symmetric fullerenes with angle 112.9°. We also join two different fullerenes with angles 60° and 43°. Again here we use Simpson's rule to calculate the difference between the two energies, the relative error for the symmetric case is 9% and the other case is 6%.

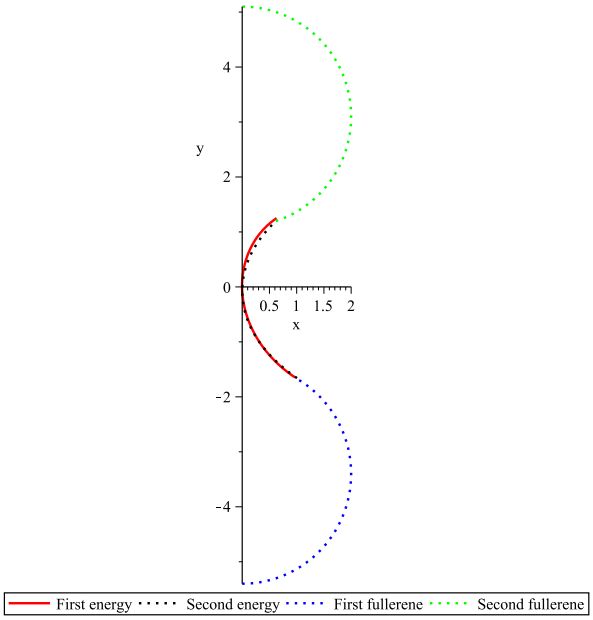

(a) symmetric fullerenes

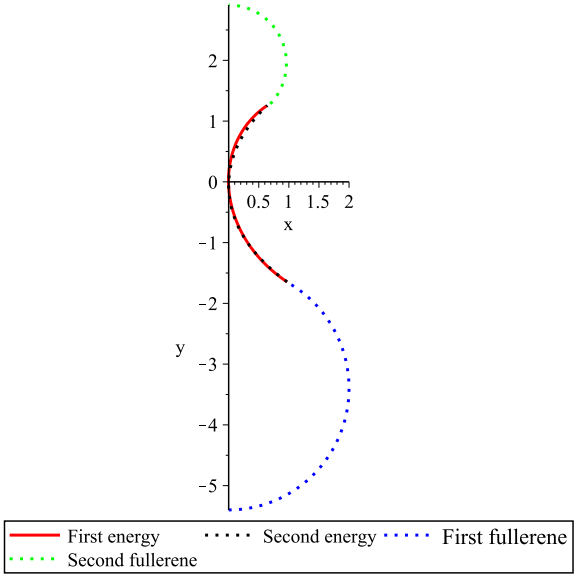

(b) different angles fullerenes

Figure 4.15: The joining based on first and second energies.

4.4 Conclusion

This chapter adopted calculus of variations to investigate and compare two different energies that are used to join different carbon nanostructures; carbon nanocone and carbon nanotube, two symmetric carbon nanocones, narrow carbon nanocones and large carbon nanocone and two fullerenes. Furthermore, the join of carbon nanotubes and carbon nanocones is the best joining case because of the small value of relative error. As a result of this comparison we conclude that both of these energies are suitable for the joining between carbon nanostructures.

However, the rotational curvature does not contribute much in the total energy. Based on the above joining cases we emphasise that using Willmore energy instead of the first energy makes only a little difference. Future work could compare the two different energies in other joining scenarios.

Chapter 5

Summary

The purpose of this thesis is to use applied mathematical techniques to formulate models for nanostructures. In this thesis three main topics were examined:

- Modelling curves on a sphere with an application to nanoantennas.
- Determination of join regions between carbon nanostructures using calculus of variations.
- Comparison of different energies for modelling the joining between different carbon nanostructures.

In Chapter 2 we used calculus of variations and the geometry of space curves to model curves on the sphere. Starting with the general form of the Euler-Lagrange equations for minimizing an energy functional defined for a space curve that depends on its curvature, torsion and their first derivatives, we examined the energy for curves on a sphere that gives rise to solutions for Euler-Lagrange equations. In detail, we studied the solutions for mathematical spherical helix, revolutionary curves on a sphere and other cases. In the case of an energy depending only on the curvature, we obtained solutions for Euler-Lagrange equations based on the revolutionary curves on a sphere with certain forms.

However, mathematical helices are not the solution. In the case of energy depending on the curvature as well as its first derivative, we found solutions for Euler-Lagrange equations for all the different cases of mathematical spherical helix, revolutionary curves on a sphere and other cases. We further studied these cases when the energy depends on its torsion, that only gives a solution for Euler-Lagrange equations for curves on a sphere but not a mathematical helix.

In Chapter 3 we investigated the geometry of joining to combine two different nanostructures, by adopting calculus of variations to minimize the elastic energy, leading to Euler-Lagrange equations which determine the joining curve between two carbon nanostructures. The joining curve depends on the sign of the curvature, Model I refers to positive curvature and Model II refers to both positive and negative curvature. Based on these models we have two different ways to join the nanostructures. As a result, we join various different types of nanostructures including carbon nanocone and fullerene, two carbon nanocones, carbon nanocone and flat sheet of graphene, fullerene and flat sheet of graphene, two parallel sheets of graphene with carbon nanocone and fullerene.

In Chapter 4 we compared two different energies used in determining the region between carbon nanostructures; carbon nanotube and carbon nanocone, narrow carbon nanocone and large carbon nanocone, two symmetric carbon nanocones and two fullerenes. The first energy depends on the axial curvature only whereas the second energy depends on both the axial curvature and the rotational curvature. By analyzing the obtained results for each case we concluded that both of these energies give similar results for joining of carbon nanostructures.

Bibliography

[1] A. Alsuhaibani. Nanoantenna. Technical report, Electrical engineering department in king Fahd university of petroleum and minerals, 2010.

[2] M. Alvin. *Device for conversion of light power to electric power.* US4445050 A, 1984.

[3] R. Ansari and M. Hosseinzadeh. Mechanics of single-walled carbon nanotubes inside open single-walled carbon nanocones. *Journal of Mechanical Science and Technology*, 27(11):3363–3370, 2013.

[4] R. Ansari, A. Momen, S. Rouhi, and S. Ajori. On the variation of single-walled carbon nanocones: molecular mechanics approach versus molecular dynamics simulations. *Shock and Vibration*, 2014(410783):8, 2014.

[5] R. Ansari, H. Rouhi, and A. Nasiri. Vibrational analysis of carbon nanocones under different boundary conditions: An analytical approach. *Mechanics Research Communications*, 56:130–135, 2014.

[6] P. Avouris and C. Dimitrakopoulos. Graphene: synthesis and applications. *Materials Today*, 15(3):86–97, 2012.

[7] A. Balandin, S. Ghosh, W. Bao, I. Calizo, D. Teweldebrhan, F. Miao, and C. Lau. Superior thermal conductivity of single-layer graphene. *Nano Letters*, 8(3):902–907, 2008.

[8] C. Balanis. *Antenna theory: analysis and design constantine.* New York: Wiley, 2nd ed edition, 1997.

[9] C. Balanis. *Antenna theory: Analysis and design.* John Wiley and Sons, third edn edition, 2005.

[10] D. Baowan, B. Cox, and J. Hill. Discrete and continuous approximations for nanobuds. *Fullerenes, Nanotubes and Carbon Nanostructures*, 18(2):160–177, 2010.

[11] D. Baowan, B. Cox, and J. Hill. Modelling the joining of nanocones and nanotubes. *Journal of Mathematical Chemistry*, 49(2):475–488, 2011.

[12] D. Baowan, B. Cox, and J. Hill. Modeling the join curve between two co-axial carbon nanotubes. *Zeitschrift fur angewandte Mathematik und Physik*, 63(2):331–338, 2012.

[13] D. Baowan, B. Cox, and J. Hill. Determination of join regions between carbon nanostructures using variational calculus. *The ANZIAM Journal*, 54, 2013.

[14] D. Baowan, B.J. Cox, and J.M. Hill. A continuous model for the joining of two fullerenes. *Philosophical Magazine*, 88(23):2953–2964, 2008.

[15] M. Barros and A. Ferrandes. A conformal variational approach for helices in nature. *J. Math. Phys*, 50(103529), 2009.

[16] E. Baykasoglu, A. Celebi, E. Icer, and A. Mugan. Vibration and elastic buckling analyses of single walled carbon nanocones. Third south-east european conference on computational mechanicsan ECCOMAS and IACM special interest conference., 2013.

[17] C. Baykasoglu1, A. Celebi, E. Icer, and A. Mugan. Vibration and elastic buckling analysys of single-walled carbon nanocones. In I. Tuncer (eds.) M. Papadrakakis, M. Kojic, editor, *3rd South-East European Conference on Computational Mechanicsan ECCOMAS and IACM Special Interest Conference*. Kos Island, Greece, 12-14 June 2013.

[18] K. Bolotin, K. Sikes, Z. Jiang, M. Klima, G. Fudenberg, J. Hone, P. Kim, and H. Stormer. Ultrahigh electron mobility in suspended graphene. *Solid State Communications*, 146(910):351–355, 2008.

[19] S. Bosi, T. Da, G. Spalluto, and M. Prato. Fullerene derivatives: an attractive tool for biological applications. *European Journal of Medicinal Chemistry*, 38(11-12):913–923, 2003.

[20] P. Byrd and M. Friedman. *Handbook of elliptic integrals for engineers and scientists.* Springer, Berlin, 2nd edition, 1971.

[21] J. Cardoso and A. Safaai-Jazi. Spherical helical antenna with circular polarization over a broad beam. *Electronics Letters*, 29(4):325–326, 1993.

[22] J. Cardoso and A. Safaai-Jazi. Radiation characteristics of a spherical helix antenna. *IEE Proc-Microw. Antennas Propag*, 143(1):7–12, 1996.

[23] L. Carvalho-Santos and R. Dandoloff. Coupling between magnetic field and curvature in heisenberg spins on surfaces with rotational symmetry. *Physics Letters A*, 376(46):3551 – 3554, 2012.

[24] V.L. Carvalho-Santos, F.A. Apolonio, and N.M. Oliveira-Neto. On geometry-dependent vortex stability and topological spin excitations on curved surfaces with cylindrical symmetry. *Physics Letters A*, 377(18):1308 – 1316, 2013.

[25] S. Cedex. Antenna parameters. Technical report, European telecommunications standards institute (ETSI), 2002.

[26] F. Cheng, S. Wang, C. Su, T. Tsai, P. Wu, D. Shieh, J. Chen, P. Hsieh, and C. Yeh. Stabilizer-free poly(lactide-co-glycolide) nanoparticles for multimodal biomedical probes. *Biomaterials*, 29(13):2104–2112, 2008.

[27] Y. Chung, I. Chen, and C. Chen. The surface modification of silver nanoparticles by phosphoryl disulfides for improved biocompatibility and intracellular uptake. *Biomaterials*, 29(12):1807–1816, 2008.

[28] J.R. Clark. Multifilar hemispherical helical antenna. Blacksburg, Virginia, 2003.

[29] B. Cox, D. Baowan, B. Wolfgang, and J. Hill. Relating elasticity and graphene folding conformation. *RSC Adv.*, 5(71):57515–57520, 2015.

[30] B. Cox and J. Hill. A variational approach to the perpendicular joining of nanotubes to plane sheets. *J. Phys. A: Math.Theor.*, 41(125203), 2008.

[31] Y. Dai, H. Jiang, Y. Hu, and C. Li. Hydrothermal synthesis of hollow mn2o3 nanocones as anode material for li-ion batteries. *RSC Adv.*, 3:19778–19781, 2013.

[32] A. Darwish. Fullerenes. *Annu. Rep. Prog. Chem., Sect. A: Inorg. Chem.*, 105:363–381, 2009.

[33] N. Delibozov. Analysis of graphene nanoribbons passivated with gold copper and indium. *International journal of theoretical and applied nanotechnology*, 1(2):41–46, 2013.

[34] C. Deng, J. Chen, X. Chen, C. Xiao, L. Nie, and S. Yao. Direct electrochemistry of glucose oxidase and biosensing for glucose based on boron-doped carbon nanotubes modified electrode. *Biosensors and Bioelectronics*, 23(8):1272–1277, 2008.

[35] V. Dhand, K. Rhee, H. Kim, and D. Jung. A comprehensive review of graphene nanocomposites: Research status and trends. *J. Nanomaterials*, 2013:14, 2013.

[36] Y. Ding, J. Qiu, and W. Qin. A new spherical helical antenna. *IEEE*, pages 292–295, 2005.

[37] D. Dobkin. Chapter 3 - radio basics for {UHF} {RFID}. In Daniel M Dobkin, editor, *The RF in RFID*, pages 51 – 101. Newnes, 2008.

[38] F. D'Souza. Carbon buckyballs to nanotubes. *The Electrochemical Society Interface*, 15(2):27, 2006.

[39] S. Dubey, A. Dwivedi, I. Kim, M. Sillanpaa, Y. Kwon, and C. Lee. Synthesis of graphene carbon sphere hybrid aerogel with silver nanoparticles and its catalytic and adsorption applications. *Chemical Engineering Journal*, 244:160–167, 2014.

[40] A. Galano. Carbon nanotubes: promising agents free radicals. *The royal society of chemistry*, 2:373–380, 2010.

[41] M. Ge and K. Sattler. Observation of fullerene cones. *Chemical Physics Letters*, 220(3-5):192–196, 1994.

[42] I. Ghoreishian. *The Spiro-Helical Antenna*. Blacksburg, Virginia Tech, 1999.

[43] O. Gohardani, M. Chapartegui, and C. Elizetxea. Potential and prospective implementation of carbon nanotubes on next generation aircraft and space vehicles: A review of current and expected applications in aerospace sciences. *Progress in Aerospace Sciences*, 70:42 – 68, 2014.

[44] L. Guang, R. Abdu, and J. Bockris. Investigation of resonance light absorption and rectification by subnanostructures. *Journal of Applied Physics*, 80(1), 1996.

[45] L. Guang, R. Abdu, and J. Bockris. Investigation of resonance light absorption and rectification by subnanostructures. *Journal of Applied Physics*, 80(1):565–568, 1996.

[46] M. Hakimi and P. Alimard. Graphene: Synthesis and applications in biotechnology - a review. *World Applied Programming*, 2(6):377–388, 2012.

[47] Y. Hao, R. Wang, and C. Li. Minimal quasi-bzier surface. *Applied Mathematical Modelling*, 36(12):5751 – 5757, 2012.

[48] L. He and C. Toh. Recent advances in analytical chemistrya material approach. *Analytica Chimica Acta*, 556(1):1–15, 2006.

[49] P. Holister, C. Vas, and T. Harper. Fullerenes. *Cientifica*, 2003.

[50] Y. Hu, K. Liew, X. He, Z. Li, and J. Han. Free transverse vibration of single-walled carbon nanocones. *Carbon*, 50(12):4418–4423, 2012.

[51] Y. Huang and K. Boyle. *Antenna from Theory to Practice*. John Wiley and Sons, 2008.

[52] H. Hui, K. Chan, and E. Yung. The input impedance and the antenna gain of the spherical helical antenna. *IEEE Transactions on Antennas and Propagation*, 49:1235–1237, 2001.

[53] R. Khare and S. Bose. Carbon nanotube based composites-a review. *Journal of Minerals and Materials Characterization and Engineering*, 4(1):31–46, 2005.

[54] D. Kotter, S. Novack, W. Slafer, and P. Pinhero. Solar nantenna electromagnetic collectors. *INL/CON-08-13925. Idaho National Laboratory, Idaho Falls ID*, 2008.

[55] J. Kraus. *Antennas*. McCraw-Hill, 2nd edn edition, 1988.

[56] M. Stankovic L. Velimirovic, G. Radivojevic and D. Kostic. Minimal surfaces for architectural constructions. *Facta universitatis series: Architecture and Civil Engineering*, 6(1):89–96, 2008.

[57] DOE/Idaho National Laboratory. Flexible nanoantenna arrays capture abundant solar energy. ScienceDaily, 12 August 2008.

[58] Y. LH, J. Xinzhe, Y. XY, and Z. Jian J. Surface modeling using partial differential equations: A survey. In *Information Visualisation (IV), 2013 17th International Conference*, pages 474–481. IEEE, 2013.

[59] X. Li, Y. Zhu, W. Cai, M. Borysiak, B. Han, D. Chen, R. Piner, L. Colombo, and R. Ruoff. Transfer of large-area graphene films for high-performance transparent conductive electrodes. *Nano Letters*, 9(12):4359–4363, 2009.

[60] M. Liao. Thermal stability of an axial-compressed open-tip carbon nanocone. *Applied Mechanics and Materials*, 575:227–230, 2014.

[61] K. Liew, J. Wei, and X. He. Carbon nanocones under compression: Buckling and post-buckling behaviors. *Phys. Rev. B*, 75:195435, 2007.

[62] M. Lipschutz. *Schaum's outline of theory and problems of differential geometry*. New York McGraw-Hill, 1969.

[63] K. Lu, G. Zhao, and X. Wang. A brief review of graphene-based material synthesis and its application in environmental pollution management. *Chinese Science Bulletin*, 57(11):1223–1234, 2012.

[64] D. Mackay, M. Janish, U. Sahaym, P. Kotula, K. Jungjohann, C. Carter, and M. Norton. Template-free electrochemical synthesis of tin nanostructures. *Journal of Materials Science*, 49(4):1476–1483, 2014.

[65] R. Majidi and K. Ghafoori. Study of neon adsorption on carbon nanocones using molecular dynamics simulation. *Physica B: Condensed Matter*, 405(8):2144–2148, 2010.

[66] N. Marinkovic. Carbon nanotubes. *Journal of the Serbian Chemical Society*, 73(8-9):891–913, 2008.

[67] J. McCoy. Helices for mathematical modelling of proteins, nuclide acids and polymers. *J. Math. Anal. Appl*, 347:255–265, 2008.

[68] J. McCoy. *Protein structure*, chapter Mathematical modelling of helical protein structure, pages 105–121. Nova Science, 2011.

[69] J. Monterde. Curves with constant curvature ratios. *Bol. Soc. Mat. Mexicana*, 13:177–186, 2007.

[70] S. Morozov, K. Novoselov, M. Katsnelson, F. Schedin, D. Elias, J. Jaszczak, and A. Geim. Giant intrinsic carrier mobilities in graphene and its bilayer. *Phys. Rev. Lett.*, 100:016602, 2008.

[71] K. Novoselov, V. Falko, L. Colombo, P. Gellert, M. Schwab, and K. Kim. A roadmap for graphene. *Nature*, 490(7419):192–200, 2012.

[72] Q. Pan and G. Xu. Construction of minimal subdivision surface with a given boundary. *Computer-Aided Design*, 43(4):374 – 380, 2011.

[73] H. Paul, C. Roman, and H. Tim. Nanotubes. *Cienifica, white paper*, 15, 2003.

[74] M. Rahim, T. Masri, O. Ayop, and H. Majid. Circular polarization array antenna. In *Microwave Conference, 2008. APMC 2008. Asia-Pacific*, pages 1–4, Dec 2008.

[75] B. Robert. Electromagnetic wave energy converter. US3760257 A, 1972.

[76] V. Ruxandra, R. Masoud, M. Morteza, E. Marius, P. Dan, and O. Ioan. Nanostructures: A platform for brain repair and augmentation. *Frontiers in Systems Neuroscience*, 8(91):1662–5137, 2014.

[77] K. Scida, P. Stege, G. Haby, G. Messina, and C. Garcia. Recent applications of carbon-based nanomaterials in analytical chemistry: Critical review. *Analytica Chimica Acta*, 691(1-2):6–17, 2011.

[78] Y. Shao, J. Wang, H. Wu, J. Liu, I. Aksay, and Y. Lin. Graphene based electrochemical sensors and biosensors: A review. *Electroanalysis*, 22(10):1027–1036, 2010.

[79] O. Shenderova, V. Zhirnov, and D. Brenner. Carbon nanostructures. *Critical Reviews in Solid State and Material Sciences*, 27(3-4):227–356, 2002.

[80] C. Slaney. Fullerenes. *Young Scientists Journal*, 2(7):32–34, 2009.

[81] R. Souam. Selected chapters in classical minimal surfaces theory. *Geometries et Dynamiques*, page 69.

[82] J. Stillwell. Numbers and geometry. *Springer New York*, 1998.

[83] M. Stoller, S. Park, Y. Zhu, J. An, and R. Ruoff. Graphene-based ultracapacitors. *Nano Letters*, 8(10):3498–3502, 2008.

[84] C. Talbot. Fullerene and nanotube chemistry: an update. *School Science Review*, 81(295):37–48, 1999.

[85] N. Thamwattana, J. McCoy, and J. Hill. Energy density functions for protein structures. *The Quarterly Journal of Mechanics and Applied Mathematics*, 61(3):431–451, 2008.

[86] T. Tiedje, E. Yablonovitch, G.D. Cody, and B.G. Brooks. Limiting efficiency of silicon solar cells. *Electron Devices, IEEE Transactions on*, 31:711–716, 1984.

[87] Y. Tretyakov and E. Goodilin. Key trends in basic and application-oriented research on nanomaterials. *Russian Chemical Reviews*, 78(9):801–820, 2009.

[88] R. Tristan. Analysis aspects of willmore surfaces. *Inventions mathematicae*, 174(1):1–45, 2008.

[89] Z. Tu and Z. Ou-Yang. Single-walled and multiwalled carbon nanotubes viewed as elastic tubes with the effective young's moduli dependent on layer number. *Phys. Rev. B*, 65:233407, 2002.

[90] E. Ulloa. Fullerenes and their applications in science and technology. *EEE-5425, Introduction to nanotechnology*, 4138296, 2013.

[91] T. Webster, C. Ergun, R. Doremus, R. Siegel, and R. Bizios. Specific proteins mediate enhanced osteoblast adhesion on nanophase ceramics. *Journal of Biomedical Materials Research*, 51(3):475–483, 2000.

[92] E. Weeratumanoon. Helical antennas with truncated spherical geometry. Master thesis, Virginia Tech, 2000.

[93] N. Wohner, P. Lam, and K. Sattler. Energetic stability of graphene nanoflakes and nanocones. *Carbon*, 67(0):721 – 735, 2014.

[94] E. Wolff. *Antenna analysis*. John Wiley and sons, first edition edition, 1966.

[95] B. Yadav and R. Kumar. Structure, properties and applications of fullerenes. *International Journal of Nanotechnology and Applications*, 1:15–24, 2008.

[96] J. Yan, K. Liew, and L. He. A mesh-free computational framework for predicting buckling behaviors of single-walled carbon nanocones under axial compression based on the moving kriging interpolation. *Computer Methods in Applied Mechanics and Engineering*, 247-248(0):103–112, 2012.

[97] J. Yan, K. Liew, and L. He. Buckling and post-buckling of single-wall carbon nanocones upon bending. *Composite Structures*, 106:793–798, 2013.

[98] J. Yan, L. Zhang, K. Liew, and L. He. A higher-order gradient theory for modeling of the vibration behavior of single-wall carbon nanocones. *Applied Mathematical Modelling*, 38(11-12):2946–2960, 2013.

[99] M. Yang, N. Zhang, and Y. Xu. Synthesis of fullerene, carbon nanotube, and graphene tio2 nanocomposite photocatalysts for selective oxidation: A comparative study. *ACS Applied Materials and amp; Interfaces*, 5(3):1156–1164, 2013.

[100] C. Yec and H. Zeng. Synthesis of complex nanomaterials via ostwald ripening. *J. Mater. Chem. A*, 2:4843–4851, 2014.

[101] S. Yu and W. Zheng. Effect of n/b doping on the electronic and field emission properties for carbon nanotubes, carbon nanocones, and graphene nanoribbons. *Nanoscale*, 2(7):1069–1082, 2010.

[102] J. Zang, A. Treibergs, Y. Han, and F. Liu. Geometric constant defining shape transitions of carbon nanotubes under pressure. *Phys. Rev. Lett.*, 92:105501, 2004.

[103] B. Zhang, X. Zheng, H. Li, and J. Lin. Application of carbon-based nanomaterials in sample preparation: A review. *Analytica Chimica Acta*, 784:1–17, 2013.

[104] H. Zhang, D. Xia, B. sun, and J. Li. A novel low-profile spherical helical antenna, j. of electromagn. *Waves and Appl*, 22:1131–1139, 2008.

[105] W. Zhou, T. Arslan, and B. Flynn. A reconfigurable feed network for a dual circularly polarised antenna array. *Personal Indoor and Mobile Radio Communications (PIMRC)*, pages 430–434, 2013.

[106] D. Zill and W. Wright. *Advance engineering mathematics*. Jones and Barlett, fourth edition, 2009.

Appendix A

Euler-Lagrange equations derivations

Firstly we derive the variational quantities which are used to determined Euler-Lagrange equations [85]. The variation of $\mathbf{r}(s)$ is given by

$$\tilde{\mathbf{r}} = \mathbf{r}(s) + \varepsilon_1\psi_1(s)\mathbf{T} + \varepsilon_2\psi_2(s)\mathbf{N} + \varepsilon_3\psi_3(s)\mathbf{B},$$

where ε_i are parameters and $\psi_i(s)$ are arbitrary functions with compact support on $[a, b]$. By using Frênet equations in equation 2.3 and $\dot{\mathbf{r}} = \mathbf{T}$ we get

$$\dot{\tilde{\mathbf{r}}} = [1 + \varepsilon_1\dot{\psi_1} - \varepsilon_2\kappa\psi_2]\mathbf{T} + [\varepsilon_1\kappa\psi_1 + \varepsilon_2\dot{\psi_2} - \varepsilon_3\tau\psi_3]\mathbf{N} + [\varepsilon_2\psi_2\tau + \varepsilon_3\dot{\psi_3}]\mathbf{B}, \tag{A.1}$$

and

$$|\dot{\tilde{\mathbf{r}}}|^2 = [1 + \varepsilon_1\dot{\psi_1} - \varepsilon_2\kappa\psi_2]^2 + [\varepsilon_1\kappa\psi_1 + \varepsilon_2\dot{\psi_2} - \varepsilon_3\tau\psi_3]^2 + [\varepsilon_2\psi_2\tau + \varepsilon_3\dot{\psi_3}]^2. \tag{A.2}$$

From (2.3) and (A.1) we have

$$\begin{aligned}\ddot{\tilde{\mathbf{r}}} = {} & [\varepsilon_1(\ddot{\psi_1} - \psi_1\kappa^2) - \varepsilon_2(2\kappa\dot{\psi_2} + \dot{\kappa}\psi_2) + \varepsilon_3\psi_3\kappa\tau]\mathbf{T} \\ & + [\kappa + \varepsilon_1(2\kappa\dot{\psi_1} + \psi_1\dot{\kappa}) + \varepsilon_2(\ddot{\psi_2} - \psi_2\kappa^2 - \psi_2\tau^2) - \varepsilon_3(2\dot{\psi_3}\tau + \psi_3\dot{\tau})]\mathbf{N} \\ & + [\varepsilon_1\kappa\tau\psi_1 + \varepsilon_2(2\dot{\psi_2}\tau + \psi_2\dot{\tau}) + \varepsilon_3(\ddot{\psi_3} - \tau^2\psi_3)]\mathbf{B},\end{aligned} \tag{A.3}$$

then from (A.1) and (A.3) we have

$$\begin{aligned}\dot{\tilde{\mathbf{r}}} \times \ddot{\tilde{\mathbf{r}}} = {} & [-\kappa(\varepsilon_2\psi_2\tau + \varepsilon_3\dot{\psi_3}) + o(\varepsilon_i^2)]\mathbf{T} \\ & - [\varepsilon_1\kappa\tau\psi_1 + \varepsilon_2(2\dot{\psi_2}\tau + \psi_2\dot{\tau}) + \varepsilon_3(\ddot{\psi_3} - \tau^2\psi_3) + o(\varepsilon_i^2)]\mathbf{N} \\ & + [\kappa + \varepsilon_1(3\kappa\dot{\psi_1} + \psi_1\dot{\kappa}) + \varepsilon_2(\ddot{\psi_2} - 2\kappa^2\psi_2 - \tau^2\psi_2) - \varepsilon_3(2\tau\dot{\psi_3} + \dot{\tau}\psi_3) + o(\varepsilon_i^2)]\mathbf{B}.\end{aligned}$$

Therefore

$$
\begin{aligned}
|\dot{\tilde{\mathbf{r}}} \times \ddot{\tilde{\mathbf{r}}}|^2 &= [-\kappa(\varepsilon_2\psi_2\tau + \varepsilon_3\dot{\psi_3}) + o(\varepsilon_i^2)]^2 \\
&- [\varepsilon_1\kappa\tau\psi_1 + \varepsilon_2(2\dot{\psi_2}\tau + \psi_2\dot{\tau}) + \varepsilon_3(\ddot{\psi_3} - \tau^2\psi_3) + o(\varepsilon_i^2)]^2 \\
&+ [\kappa + \varepsilon_1(3\kappa\dot{\psi_1} + \psi_1\dot{\kappa}) + \varepsilon_2(\ddot{\psi_2} - 2\kappa^2\psi_2 - \tau^2\psi_2) - \varepsilon_3(2\tau\dot{\psi_3} + \dot{\tau}\psi_3) + o(\varepsilon_i^2)]^2,
\end{aligned}
\tag{A.4}
$$

so from (A.2) and (A.4) we have the following relations

$$
\begin{aligned}
\frac{\partial|\dot{\tilde{\mathbf{r}}}|^2}{\partial\varepsilon_1}|_{\bar{\varepsilon}=0} &= 2\dot{\psi_1}, \\
\frac{\partial|\dot{\tilde{\mathbf{r}}}|^2}{\partial\varepsilon_2}|_{\bar{\varepsilon}=0} &= -2\kappa\psi_2, \\
\frac{\partial|\dot{\tilde{\mathbf{r}}}|^2}{\partial\varepsilon_3}|_{\bar{\varepsilon}=0} &= 0,
\end{aligned}
$$

and

$$
\begin{aligned}
\frac{\partial|\dot{\tilde{\mathbf{r}}} \times \ddot{\tilde{\mathbf{r}}}|^2}{\partial\varepsilon_1}|_{\bar{\varepsilon}=0} &= 2\kappa(3\kappa\dot{\psi_1} + \psi_1\dot{\kappa}) \\
\frac{\partial|\dot{\tilde{\mathbf{r}}} \times \ddot{\tilde{\mathbf{r}}}|^2}{\partial\varepsilon_2}|_{\bar{\varepsilon}=0} &= 2\kappa(\ddot{\psi_2} - 2\kappa^2\psi_2 - \tau^2\psi_2) \\
\frac{\partial|\dot{\tilde{\mathbf{r}}} \times \ddot{\tilde{\mathbf{r}}}|^2}{\partial\varepsilon_3}|_{\bar{\varepsilon}=0} &= -2\kappa(2\tau\dot{\psi_3} + \psi_3\dot{\tau}),
\end{aligned}
$$

where $\tilde{\varepsilon} = 0$ means $\varepsilon_1 = \varepsilon_2 = \varepsilon_3 = 0$. Further from $|\dot{\tilde{\mathbf{r}}}|^2|_{\bar{\varepsilon}=0} = 1, |\dot{\tilde{\mathbf{r}}} \times \ddot{\tilde{\mathbf{r}}}|^2|_{\bar{\varepsilon}=0} = \kappa^2$ and

$$
\frac{\partial|\dot{\tilde{\mathbf{r}}}|}{\partial\varepsilon_i} = \frac{1}{2|\dot{\tilde{\mathbf{r}}}|}\frac{\partial|\dot{\tilde{\mathbf{r}}}|^2}{\partial\varepsilon_i},
$$

we have that

$$
\begin{aligned}
\frac{\partial|\dot{\tilde{\mathbf{r}}}|}{\partial\varepsilon_1}|_{\bar{\varepsilon}=0} &= \dot{\psi_1}, & \frac{\partial|\dot{\tilde{\mathbf{r}}} \times \ddot{\tilde{\mathbf{r}}}|}{\partial\varepsilon_1}|_{\bar{\varepsilon}=0} &= 3\kappa\dot{\psi_1} + \psi_1\dot{\kappa} \\
\frac{\partial|\dot{\tilde{\mathbf{r}}}|}{\partial\varepsilon_2}|_{\bar{\varepsilon}=0} &= -\kappa\psi_2, & \frac{\partial|\dot{\tilde{\mathbf{r}}} \times \ddot{\tilde{\mathbf{r}}}|}{\partial\varepsilon_2}|_{\bar{\varepsilon}=0} &= \ddot{\psi_2} - 2\kappa^2\psi_2 - \tau^2\psi_2 \\
\frac{\partial|\dot{\tilde{\mathbf{r}}}|}{\partial\varepsilon_3}|_{\bar{\varepsilon}=0} &= 0, & \frac{\partial|\dot{\tilde{\mathbf{r}}} \times \ddot{\tilde{\mathbf{r}}}|}{\partial\varepsilon_3}|_{\bar{\varepsilon}=0} &= -2\tau\dot{\psi_3} - \psi_3\dot{\tau}.
\end{aligned}
\tag{A.5}
$$

Next we calculate

$$\dddot{\mathbf{r}} = [-\kappa^2 + \varepsilon_1(-3\kappa^2\dot{\psi}_1 - 3\kappa\dot{\kappa}\psi_1 + \dddot{\psi}_1) - \varepsilon_2(3\kappa\ddot{\psi}_2 + 3\dot{\kappa}\dot{\psi}_2 + \ddot{\kappa}\psi_2 - \kappa^3\psi_2 - \tau^2\kappa\psi_2)$$
$$+ \varepsilon_3(\dot{\kappa}\tau\psi_3 + 2\kappa\dot{\tau}\psi_3 + 3\kappa\tau\dot{\psi}_3)]\mathbf{T} + [\dot{\kappa} + \varepsilon_1(3\kappa\ddot{\psi}_1 + 3\dot{\kappa}\dot{\psi}_1 - \psi_1\kappa^3 - \psi_1\kappa\tau^2 + \ddot{\kappa}\psi_1)$$
$$+ \varepsilon_2(\dddot{\psi}_2 - 3\tau^2\dot{\psi}_2 - 3\kappa^2\dot{\psi}_2 - 3\kappa\dot{\kappa}\psi_2 - 3\tau\dot{\tau}\psi_2)$$
$$+ \varepsilon_3(-3\tau\ddot{\psi}_3 - 3\dot{\tau}\dot{\psi}_3 + \kappa^2\tau\psi_3 + \tau^3\psi_3 - \ddot{\tau}\psi_3)]\mathbf{N}$$
$$+ [\kappa\tau + \varepsilon_1(3\kappa\tau\dot{\psi}_1 + 2\dot{\kappa}\tau\psi_1 + \kappa\tau\dot{\psi}_1) + \varepsilon_2(3\ddot{\psi}_2\tau - \tau\kappa^2\psi_2 - \tau^3\psi_2 + 3\dot{\tau}\dot{\psi}_2 + \ddot{\tau}\psi_2)$$
$$+ \varepsilon_3(\dddot{\psi}_3 - 3\tau^2\dot{\psi}_3 - 3\tau\dot{\tau}\psi_3)]\mathbf{B}. \tag{A.6}$$

Now by using (A.1),(A.3) and (A.6) we can calculate $\det(\dot{\tilde{\mathbf{r}}}, \ddot{\tilde{\mathbf{r}}}, \dddot{\tilde{\mathbf{r}}})$ which given by

$$\det(\dot{\tilde{\mathbf{r}}}, \ddot{\tilde{\mathbf{r}}}, \dddot{\tilde{\mathbf{r}}}) = \begin{vmatrix} M_{11} & M_{12} & M_{13} \\ M_{21} & M_{22} & M_{23} \\ M_{31} & M_{32} & M_{33} \end{vmatrix}$$

where $M_{ij}(i, j = 1, 2, 3)$ denote the coefficients of vectors $\mathbf{T}, \mathbf{N}, \mathbf{B}$ in $\dot{\tilde{\mathbf{r}}}, \ddot{\tilde{\mathbf{r}}}, \dddot{\tilde{\mathbf{r}}}$. We obtain that

$$\det(\dot{\tilde{\mathbf{r}}}, \ddot{\tilde{\mathbf{r}}}, \dddot{\tilde{\mathbf{r}}}) = [1 + \varepsilon_1\dot{\psi}_1 - \varepsilon_2\kappa\psi_2]M_1 - [\varepsilon_1\kappa\psi_1 + \varepsilon_2\dot{\psi}_2 - \varepsilon_3\tau\psi_3]M_2$$
$$+[\varepsilon_2\psi_2\tau + \varepsilon_3\dot{\psi}_3]M_3$$

where $M_1 = M_{22}M_{33} - M_{23}M_{32}, M_2 = M_{21}M_{33} - M_{23}M_{31}$ and $M_3 = M_{21}M_{32} - M_{22}M_{31}$. Then we have that

$$\frac{\partial \det(\dot{\tilde{\mathbf{r}}}, \ddot{\tilde{\mathbf{r}}}, \dddot{\tilde{\mathbf{r}}})}{\partial\varepsilon_1}|_{\bar{\varepsilon}=0} = \frac{\partial M_1}{\partial\varepsilon_1}|_{\bar{\varepsilon}=0} + \dot{\psi}_1 M_1|_{\bar{\varepsilon}=0} - \kappa\psi_1 M_2|_{\bar{\varepsilon}=0}$$
$$\frac{\partial \det(\dot{\tilde{\mathbf{r}}}, \ddot{\tilde{\mathbf{r}}}, \dddot{\tilde{\mathbf{r}}})}{\partial\varepsilon_2}|_{\bar{\varepsilon}=0} = \frac{\partial M_1}{\partial\varepsilon_2}|_{\bar{\varepsilon}=0} - \kappa\psi_2 M_1|_{\bar{\varepsilon}=0} - \dot{\psi}_2 M_2|_{\bar{\varepsilon}=0+\psi_2\tau M_3|_{\bar{\varepsilon}=0}}$$
$$\frac{\partial \det(\dot{\tilde{\mathbf{r}}}, \ddot{\tilde{\mathbf{r}}}, \dddot{\tilde{\mathbf{r}}})}{\partial\varepsilon_3}|_{\bar{\varepsilon}=0} = \frac{\partial M_1}{\partial\varepsilon_3}|_{\bar{\varepsilon}=0} + \tau\psi_3 M_2|_{\bar{\varepsilon}=0} + \dot{\psi}_3 M_3|_{\bar{\varepsilon}=0},$$

so, as a result from (A.1), (A.3) and (A.6) we have that

$$\frac{\partial \det(\dot{\tilde{\mathbf{r}}}, \ddot{\tilde{\mathbf{r}}}, \dddot{\tilde{\mathbf{r}}})}{\partial\varepsilon_1}|_{\bar{\varepsilon}=0} = 6\kappa^2\tau\dot{\psi}_1 + (2\tau\kappa\dot{\kappa} + \kappa^2\dot{\tau})\psi_1,$$
$$\frac{\partial \det(\dot{\tilde{\mathbf{r}}}, \ddot{\tilde{\mathbf{r}}}, \dddot{\tilde{\mathbf{r}}})}{\partial\varepsilon_2}|_{\bar{\varepsilon}=0} = 4\kappa\tau\ddot{\psi}_2 + (3\kappa\dot{\tau} - 2\tau\dot{\kappa})\dot{\psi}_2 + (\kappa\ddot{\tau} - 2\kappa^3\tau - 2\kappa\tau^3 - \dot{\kappa}\dot{\tau})\psi_2,$$
$$\frac{\partial \det(\dot{\tilde{\mathbf{r}}}, \ddot{\tilde{\mathbf{r}}}, \dddot{\tilde{\mathbf{r}}})}{\partial\varepsilon_3}|_{\bar{\varepsilon}=0} = \kappa\dddot{\psi}_3 - \dot{\kappa}\ddot{\psi}_3 + (\kappa^3 - 5\kappa\tau^2)\dot{\psi}_3 + (\dot{\kappa}\tau^2 - 4\kappa\tau\dot{\tau})\psi_3. \tag{A.7}$$

By noting that $\dot{\tilde{\mathbf{r}}}|_{\bar{\varepsilon}=0} = \mathbf{T}, \ddot{\tilde{\mathbf{r}}}|_{\bar{\varepsilon}=0} = \kappa\mathbf{N}$ and $\dddot{\tilde{\mathbf{r}}}|_{\bar{\varepsilon}=0} = -\kappa^2\mathbf{T} + \dot{\kappa}\mathbf{N} + \kappa\tau\mathbf{B}$ we have $\det(\dot{\tilde{\mathbf{r}}}, \ddot{\tilde{\mathbf{r}}}\dddot{\tilde{\mathbf{r}}})|_{\bar{\varepsilon}=0} = \kappa^2\tau$.

Now we consider the more general case where the energy depends on the curvature, the torsion and their derivatives. The first derivative conditions become

$$\frac{\partial}{\partial\varepsilon_i}\int f(\kappa,\tau,\dot\kappa,\dot\tau)|\dot{\tilde{\mathbf{r}}}|ds|_{\bar\varepsilon=0}=0,(i=1,2,3).$$

This can be expanded as

$$\begin{aligned}&\int\frac{\partial f}{\partial\kappa}\frac{\partial\kappa}{\partial\varepsilon_i}|\dot{\tilde{\mathbf{r}}}|_{\bar\varepsilon=0}ds+\int\frac{\partial f}{\partial\tau}\frac{\partial\tau}{\partial\varepsilon_i}|\dot{\tilde{\mathbf{r}}}|_{\bar\varepsilon=0}ds+\int\frac{\partial f}{\partial\dot\kappa}\frac{\partial\dot\kappa}{\partial\varepsilon_i}|\dot{\tilde{\mathbf{r}}}|_{\bar\varepsilon=0}ds+\\&\int\frac{\partial f}{\partial\dot\tau}\frac{\partial\dot\tau}{\partial\varepsilon_i}|\dot{\tilde{\mathbf{r}}}|_{\bar\varepsilon=0}ds+\int f\frac{\partial|\dot{\tilde{\mathbf{r}}}|}{\partial\varepsilon_i}|_{\bar\varepsilon=0}ds=0.\end{aligned}\tag{A.8}$$

By using (2.1) and (2.2) to find the curvature κ and the torsion τ, we have that

$$\begin{aligned}\frac{\partial\kappa}{\partial\varepsilon_i}&=\frac{1}{|\dot{\tilde{\mathbf{r}}}|^6}\left[|\dot{\tilde{\mathbf{r}}}|^3\frac{\partial|\dot{\tilde{\mathbf{r}}}\times\ddot{\tilde{\mathbf{r}}}|}{\partial\varepsilon_i}-3|\dot{\tilde{\mathbf{r}}}|^2|\dot{\tilde{\mathbf{r}}}\times\ddot{\tilde{\mathbf{r}}}|\frac{\partial|\dot{\tilde{\mathbf{r}}}|}{\partial\varepsilon_i}\right]\\\frac{\partial\tau}{\partial\varepsilon_i}&=\frac{1}{|\dot{\tilde{\mathbf{r}}}\times\ddot{\tilde{\mathbf{r}}}|^4}\left[|\dot{\tilde{\mathbf{r}}}\times\ddot{\tilde{\mathbf{r}}}|^2\frac{\det(\dot{\tilde{\mathbf{r}}},\ddot{\tilde{\mathbf{r}}},\dddot{\tilde{\mathbf{r}}})}{\partial\varepsilon_i}-2|\dot{\tilde{\mathbf{r}}}\times\ddot{\tilde{\mathbf{r}}}|\det(\dot{\tilde{\mathbf{r}}},\ddot{\tilde{\mathbf{r}}},\dddot{\tilde{\mathbf{r}}})\frac{\partial|\dot{\tilde{r}}\times\ddot{\tilde{r}}|}{\partial\varepsilon_i}\right],\end{aligned}$$

where $|\dot{\tilde{\mathbf{r}}}|^2|_{\bar\varepsilon=0}=1,|\dot{\tilde{\mathbf{r}}}\times\ddot{\tilde{\mathbf{r}}}|^2|_{\bar\varepsilon=0}=\kappa^2$ and $\det(\dot{\tilde{\mathbf{r}}},\ddot{\tilde{\mathbf{r}}},\dddot{\tilde{\mathbf{r}}})|_{\bar\varepsilon=0}=\kappa^2\tau$, so

$$\begin{aligned}\frac{\partial\kappa}{\partial\varepsilon_i}|_{\bar\varepsilon=0}&=\frac{\partial|\dot{\tilde{\mathbf{r}}}\times\ddot{\tilde{\mathbf{r}}}|}{\partial\varepsilon_i}|_{\bar\varepsilon=0}-3\kappa\frac{\partial|\dot{\tilde{\mathbf{r}}}|}{\partial\varepsilon_i}|_{\bar\varepsilon=0},\\\frac{\partial\tau}{\partial\varepsilon_i}|_{\bar\varepsilon=0}&=\frac{1}{\kappa^2}\frac{\partial\det(\dot{\tilde{\mathbf{r}}},\ddot{\tilde{\mathbf{r}}},\dddot{\tilde{\mathbf{r}}})}{\partial\varepsilon_i}|_{\bar\varepsilon=0}-\frac{2\tau}{\kappa}\frac{\partial|\dot{\tilde{\mathbf{r}}}\times\ddot{\tilde{\mathbf{r}}}|}{\partial\varepsilon_i}|_{\bar\varepsilon=0}.\end{aligned}\tag{A.9}$$

From (A.5), (A.7) and (A.9) we have that

$$\begin{aligned}&\frac{\partial\kappa}{\partial\varepsilon_1}|_{\bar\varepsilon=0}=\dot\kappa\psi_1, &&\frac{\partial\kappa}{\partial\varepsilon_2}|_{\bar\varepsilon=0}=\ddot\psi_2+(\kappa^2-\tau^2)\psi_2,\\&\frac{\partial\kappa}{\partial\varepsilon_3}|_{\bar\varepsilon=0}=-2\tau\dot\psi_3-\dot\tau\psi_3,\end{aligned}\tag{A.10}$$

and

$$\begin{aligned}&\frac{\partial\tau}{\partial\varepsilon_1}|_{\bar\varepsilon=0}=\dot\tau\psi_1,\\&\frac{\partial\tau}{\partial\varepsilon_2}|_{\bar\varepsilon=0}=\frac{2\tau}{\kappa}\ddot\psi_2+(\frac{3\dot\tau}{\kappa}-\frac{2\tau\dot\kappa}{\kappa^2})\dot\psi_2+(2\kappa\tau+\frac{\ddot\tau}{\kappa}-\frac{\dot\kappa\dot\tau}{\kappa^2})\psi_2,\\&\frac{\partial\tau}{\partial\varepsilon_3}|_{\bar\varepsilon=0}=\frac{1}{\kappa}\dddot\psi_3-\frac{\dot\kappa}{\kappa^2}\ddot\psi_3+(\kappa-\frac{\tau^2}{\kappa})\dot\psi_3+(\frac{-2\tau\dot\tau}{\kappa}+\frac{\dot\kappa\tau^2}{\kappa^2})\psi_3.\end{aligned}\tag{A.11}$$

By noting that

$$\dot\kappa=\frac{d\kappa}{ds}\frac{ds}{d\tilde s},\quad\dot\tau=\frac{d\tau}{ds}\frac{ds}{d\tilde s},$$

where $\frac{d}{d\tilde{s}}$ is the intrinsic derivative of the varied curve, and $\tilde{s}$ is the arc length of the varied curve which related to s by $\tilde{s} = \int |\dot{\tilde{\mathbf{r}}}(s)|ds, and\ \frac{ds}{d\tilde{s}} = \frac{1}{|\dot{\tilde{\mathbf{r}}}(s)|}$ we have that

$$\frac{\partial\dot{\kappa}}{\partial\varepsilon_i} = \frac{d\kappa}{ds}\frac{\partial}{\partial\varepsilon_i}\left(\frac{1}{|\dot{\tilde{\mathbf{r}}}|}\right) + \frac{1}{|\dot{\tilde{\mathbf{r}}}|}\frac{\partial}{\partial\varepsilon_i}\left(\frac{d\kappa}{ds}\right) = -\frac{1}{|\dot{\tilde{\mathbf{r}}}|^2}\frac{\partial|\dot{\tilde{\mathbf{r}}}|}{\partial\varepsilon_i}\frac{d\kappa}{ds} + \frac{1}{|\dot{\tilde{\mathbf{r}}}|}\frac{\partial}{\partial\varepsilon_i}\left(\frac{d\kappa}{ds}\right)$$
$$\frac{\partial\dot{\tau}}{\partial\varepsilon_i} = \frac{d\tau}{ds}\frac{\partial}{\partial\varepsilon_i}\left(\frac{1}{|\dot{\tilde{\mathbf{r}}}|}\right) + \frac{1}{|\dot{\tilde{\mathbf{r}}}|}\frac{\partial}{\partial\varepsilon_i}\left(\frac{d\tau}{ds}\right) = -\frac{1}{|\dot{\tilde{\mathbf{r}}}|^2}\frac{\partial|\dot{\tilde{\mathbf{r}}}|}{\partial\varepsilon_i}\frac{d\tau}{ds} + \frac{1}{|\dot{\tilde{\mathbf{r}}}|}\frac{\partial}{\partial\varepsilon_i}\left(\frac{d\tau}{ds}\right),$$

and

$$\frac{\partial\dot{\kappa}}{\partial\varepsilon_i}|_{\bar{\varepsilon}=0} = -\dot{\kappa}\frac{\partial|\dot{\tilde{\mathbf{r}}}|}{\partial\varepsilon_i}|_{\bar{\varepsilon}=0} + \frac{\partial\dot{\kappa}}{\partial\varepsilon_i}|_{\bar{\varepsilon}=0}$$
$$\frac{\partial\dot{\tau}}{\partial\varepsilon_i}|_{\bar{\varepsilon}=0} = -\dot{\tau}\frac{\partial|\dot{\tilde{\mathbf{r}}}|}{\partial\varepsilon_i}|_{\bar{\varepsilon}=0} + \frac{\partial\dot{\tau}}{\partial\varepsilon_i}|_{\bar{\varepsilon}=0}. \tag{A.12}$$

Also, by noting that

$$\frac{\partial\dot{\kappa}}{\partial\varepsilon_i}|_{\bar{\varepsilon}=0} = \frac{d}{ds}\left(\frac{\partial\kappa}{\partial\varepsilon_i}|_{\bar{\varepsilon}=0}\right)$$
$$\frac{\partial\dot{\tau}}{\partial\varepsilon_i}|_{\bar{\varepsilon}=0} = \frac{d}{ds}\left(\frac{\partial\tau}{\partial\varepsilon_i}|_{\bar{\varepsilon}=0}\right), \tag{A.13}$$

here, from (A.8), (A.10), (A.11), (A.12) and (A.13), the variation $\frac{\partial}{\partial\varepsilon_1}\int f(\kappa,\tau,\dot{\kappa},\dot{\tau})|\dot{\tilde{\mathbf{r}}}|ds|_{\bar{\varepsilon}=0} = 0$ in the tangential direction which gives that

$$\int\frac{\partial f}{\partial\kappa}\dot{\kappa}\psi_1 ds + \int\frac{\partial f}{\partial\tau}\dot{\tau}\psi_1 ds + \int\frac{\partial f}{\partial\dot{\kappa}}\ddot{\kappa}\psi_1 ds + \int\frac{\partial f}{\partial\dot{\tau}}\ddot{\tau}\psi_1 ds + \int f\dot{\psi}_1 ds = 0. \tag{A.14}$$

By integrating by parts the last integral in (A.14) and assume $f\psi_1 = 0$ at the boundary, we note the variation in the tangential direction is identically satisfied. By using (A.8), (A.10), (A.11), (A.12) and (A.13), the variation $\frac{\partial}{\partial\varepsilon_2}\int f(\kappa,\tau,\dot{\kappa},\dot{\tau})|\dot{\tilde{\mathbf{r}}}|ds|_{\bar{\varepsilon}=0} = 0$ in the normal direction is

$$\begin{aligned}
&\int\frac{\partial f}{\partial\kappa}\Big[\ddot{\psi}_2 + (\kappa^2-\tau^2)\psi_2\Big]ds\\
&+\int\frac{\partial f}{\partial\tau}\Big[\frac{2\tau}{\kappa}\ddot{\psi}_2 + (\frac{3\dot{\tau}}{\kappa} - \frac{2\dot{\kappa}\tau}{\kappa^2})\dot{\psi}_2 + (2\kappa\tau + \frac{\ddot{\tau}}{\kappa} - \frac{\dot{\kappa}\dot{\tau}}{\kappa^2})\psi_2\Big]ds\\
&+\int\frac{\partial f}{\partial\dot{\kappa}}\Big[\dddot{\psi}_2 + (\kappa^2-\tau^2)\dot{\psi}_2 + (3\kappa\dot{\kappa} - 2\tau\dot{\tau})\psi_2\Big]ds\\
&+\int\frac{\partial f}{\partial\dot{\tau}}\Big[\frac{2\tau}{\kappa}\dddot{\psi}_2 + (\frac{5\dot{\tau}}{\kappa} - \frac{4\tau\dot{\kappa}}{\kappa^2})\ddot{\psi}_2 + (2\kappa\tau + \frac{4\ddot{\tau}}{\kappa} - \frac{6\dot{\kappa}\dot{\tau}}{\kappa^2} - \frac{2\tau\ddot{\kappa}}{\kappa^2} + \frac{4\tau\dot{\kappa}^2}{\kappa^3})\dot{\psi}_2\\
&(2\dot{\kappa}\tau + 3\dot{\tau}\kappa + \frac{\dddot{\tau}}{\kappa} - \frac{2\dot{\kappa}\ddot{\tau}}{\kappa^2} - \frac{\ddot{\kappa}\dot{\tau}}{\kappa^2} + \frac{2\dot{\tau}\dot{\kappa}^2}{\kappa^3})\psi_2\Big]ds - \int f\kappa\psi_2 ds = 0.
\end{aligned}$$

This may be written as

$$
\begin{aligned}
&\int \dddot{\psi}_2\Big[\frac{\partial f}{\partial \dot{\kappa}} + \frac{2\tau}{\kappa}\frac{\partial f}{\partial \dot{\tau}}\Big]ds \\
&+ \int \ddot{\psi}_2\Big[\frac{\partial f}{\partial \kappa} + \frac{2\tau}{\kappa}\frac{\partial f}{\partial \tau} + (\frac{5\dot{\tau}}{\kappa} - \frac{4\tau\dot{\kappa}}{\kappa^2})\frac{\partial f}{\partial \dot{\tau}}\Big]ds \\
&+ \int \dot{\psi}_2\Big[(\frac{3\dot{\tau}}{\kappa} - \frac{2\dot{\kappa}\tau}{\kappa^2})\frac{\partial f}{\partial \tau} + (\kappa^2 - \tau^2)\frac{\partial f}{\partial \dot{\kappa}} \\
&+ (2\kappa\tau + \frac{4\ddot{\tau}}{\kappa} - \frac{6\dot{\kappa}\dot{\tau}}{\kappa^2} - \frac{2\tau\ddot{\kappa}}{\kappa^2} + \frac{4\tau\dot{\kappa}^2}{\kappa^3})\frac{\partial f}{\partial \dot{\tau}}\Big]ds \\
&+ \int \psi_2\Big[(\kappa^2 - \tau^2)\frac{\partial f}{\partial \kappa} + (2\kappa\tau + \frac{\ddot{\tau}}{\kappa} - \frac{\dot{\kappa}\dot{\tau}}{\kappa^2})\frac{\partial f}{\partial \tau} + (3\kappa\dot{\kappa} - 2\tau\dot{\tau})\frac{\partial f}{\partial \dot{\kappa}} \\
&+ (2\dot{\kappa}\tau + 3\dot{\tau}\kappa + \frac{\dddot{\tau}}{\kappa} - \frac{2\dot{\kappa}\ddot{\tau}}{\kappa^2} - \frac{\ddot{\kappa}\dot{\tau}}{\kappa^2} + \frac{2\dot{\tau}\dot{\kappa}^2}{\kappa^3})\frac{\partial f}{\partial \dot{\tau}} - \kappa f\Big]ds = 0.
\end{aligned}
$$

Integrating by parts the terms involving $\dot{\psi}_2, \ddot{\psi}_2$ and $\dddot{\psi}_2$,

$$
\begin{aligned}
&\int \Big[\frac{d^2}{ds^2}\left(\frac{\partial f}{\partial \kappa} + \frac{2\tau}{\kappa}\frac{\partial f}{\partial \tau}\right) + \frac{d}{ds}\left(\frac{2\dot{\kappa}\tau}{\kappa^2}\frac{\partial f}{\partial \tau} - \frac{3\dot{\tau}}{\kappa}\frac{\partial f}{\partial \tau}\right) + [\kappa^2 - \tau^2]\frac{\partial f}{\partial \kappa} \\
&[2\kappa\tau + \frac{\ddot{\tau}}{\kappa} - \frac{\dot{\kappa}\dot{\tau}}{\kappa^2}]\frac{\partial f}{\partial \tau} + [3\kappa\dot{\kappa} - 2\tau\dot{\tau}]\frac{\partial f}{\partial \dot{\kappa}} - \frac{d}{ds}\left([\kappa^2 - \tau^2]\frac{\partial f}{\partial \dot{\kappa}}\right) \\
&- \frac{d^3}{ds^3}\left(\frac{\partial f}{\partial \dot{\kappa}}\right) + [2\dot{\kappa}\tau + 3\dot{\tau}\kappa + \frac{\dddot{\tau}}{\kappa} - \frac{2\dot{\kappa}\ddot{\tau}}{\kappa^2} - \frac{\ddot{\kappa}\dot{\tau}}{\kappa^2} + \frac{2\dot{\tau}\dot{\kappa}^2}{\kappa^3}]\frac{\partial f}{\partial \dot{\tau}} \\
&- \frac{d}{ds}\left([2\kappa\tau + \frac{4\ddot{\tau}}{\kappa} - \frac{6\dot{\kappa}\dot{\tau}}{\kappa^2} - \frac{2\tau\ddot{\kappa}}{\kappa^2} + \frac{4\tau\dot{\kappa}^2}{\kappa^3}]\frac{\partial f}{\partial \dot{\tau}}\right) + \frac{d^2}{ds^2}\left([\frac{5\dot{\tau}}{\kappa} - \frac{4\tau\dot{\kappa}}{\kappa^2}]\frac{\partial f}{\partial \dot{\tau}}\right) \\
&- \frac{d^3}{ds^3}\left(\frac{2\tau}{\kappa}\frac{\partial f}{\partial \dot{\tau}}\right) - \kappa f\Big]\psi_2 ds = 0,
\end{aligned}
\tag{A.15}
$$

then applying fundamental theorem of calculus of variations, so equation (A.15) holds for arbitrary ψ_2 if

$$
\begin{aligned}
&\frac{d^2}{ds^2}\left(\frac{\partial f}{\partial \kappa} + \frac{2\tau}{\kappa}\frac{\partial f}{\partial \tau}\right) + \frac{d}{ds}\left(\frac{2\dot{\kappa}\tau}{\kappa^2}\frac{\partial f}{\partial \tau} - \frac{3\dot{\tau}}{\kappa}\frac{\partial f}{\partial \tau}\right) + \left[\kappa^2 - \tau^2\right]\frac{\partial f}{\partial \kappa} \\
&\left[2\kappa\tau + \frac{\ddot{\tau}}{\kappa} - \frac{\dot{\kappa}\dot{\tau}}{\kappa^2}\right]\frac{\partial f}{\partial \tau} + [3\kappa\dot{\kappa} - 2\tau\dot{\tau}]\frac{\partial f}{\partial \dot{\kappa}} - \frac{d}{ds}\left(\left[\kappa^2 - \tau^2\right]\frac{\partial f}{\partial \dot{\kappa}}\right) \\
&- \frac{d^3}{ds^3}\left(\frac{\partial f}{\partial \dot{\kappa}}\right) + \left[2\dot{\kappa}\tau + 3\dot{\tau}\kappa + \frac{\dddot{\tau}}{\kappa} - \frac{2\dot{\kappa}\ddot{\tau}}{\kappa^2} - \frac{\ddot{\kappa}\dot{\tau}}{\kappa^2} + \frac{2\dot{\tau}\dot{\kappa}^2}{\kappa^3}\right]\frac{\partial f}{\partial \dot{\tau}} \\
&- \frac{d}{ds}\left(\left[2\kappa\tau + \frac{4\ddot{\tau}}{\kappa} - \frac{6\dot{\kappa}\dot{\tau}}{\kappa^2} - \frac{2\tau\ddot{\kappa}}{\kappa^2} + \frac{4\tau\dot{\kappa}^2}{\kappa^3}\right]\frac{\partial f}{\partial \dot{\tau}}\right) + \frac{d^2}{ds^2}\left(\left[\frac{5\dot{\tau}}{\kappa} - \frac{4\tau\dot{\kappa}}{\kappa^2}\right]\frac{\partial f}{\partial \dot{\tau}}\right) \\
&- \frac{d^3}{ds^3}\left(\frac{2\tau}{\kappa}\frac{\partial f}{\partial \dot{\tau}}\right) - \kappa f = 0.
\end{aligned}
\tag{A.16}
$$

By simplify (A.16) we obtain the first equation of the Euler-Lagrange equations

$$\frac{d^2}{ds^2}\left[\frac{\partial f}{\partial \kappa}-\frac{d}{ds}(\frac{\partial f}{\partial \dot{\kappa}})\right]+\frac{2\tau}{\kappa}\frac{d^2}{ds^2}\left[\frac{\partial f}{\partial \tau}-\frac{d}{ds}(\frac{\partial f}{\partial \dot{\tau}})\right]$$
$$+(\frac{\dot{\tau}}{\kappa}-\frac{2\dot{\kappa}\tau}{\kappa^2})\frac{d}{ds}\left[\frac{\partial f}{\partial \tau}-\frac{d}{ds}(\frac{\partial f}{\partial \dot{\tau}})\right]+(\kappa^2-\tau^2)\left[\frac{\partial f}{\partial \kappa}-\frac{d}{ds}(\frac{\partial f}{\partial \dot{\kappa}})\right]$$
$$+2\kappa\tau\left[\frac{\partial f}{\partial \tau}-\frac{d}{ds}(\frac{\partial f}{\partial \dot{\tau}})\right]+\kappa\left[\dot{\kappa}\frac{\partial f}{\partial \dot{\kappa}}+\dot{\tau}\frac{\partial f}{\partial \dot{\tau}}-f\right]=0. \tag{A.17}$$

After that, by finding the variation in the binormal direction $(\frac{\partial}{\partial \bar{\varepsilon}_3})\int f(\kappa,\tau,\dot{\kappa},\dot{\tau})|\dot{\hat{\mathbf{r}}}|ds|_{\bar{\varepsilon}=0}=0$, by using (A.8), (A.10), (A.11), (A.12) and (A.13) gives that

$$-\int\frac{\partial f}{\partial \kappa}\Big[2\tau\dot{\psi}_3+\dot{\tau}\psi_3\Big]ds+\int\frac{\partial f}{\partial \tau}\Big[\frac{1}{\kappa}\dddot{\psi}_3-\frac{\dot{\kappa}}{\kappa^2}\ddot{\psi}_3+(\kappa-\frac{\tau^2}{\kappa})\dot{\psi}_3+(\frac{\dot{\kappa}\tau^2}{\kappa^2}-\frac{2\tau\dot{\tau}}{\kappa})\psi_3\Big]ds$$
$$-\int\frac{\partial f}{\partial \dot{\kappa}}\Big[2\tau\ddot{\psi}_3+3\dot{\tau}\dot{\psi}_3+\ddot{\tau}\psi_3\Big]ds$$
$$+\int\frac{\partial f}{\partial \dot{\tau}}\Big[\frac{1}{\kappa}\ddddot{\psi}_3-\frac{2\dot{\kappa}}{\kappa^2}\dddot{\psi}_3+(\kappa-\frac{\tau^2}{\kappa}-\frac{\ddot{\kappa}}{\kappa^2}+\frac{2\dot{\kappa}^2}{\kappa^3})\ddot{\psi}_3+(\dot{\kappa}-\frac{4\tau\dot{\tau}}{\kappa}+\frac{4\dot{\kappa}\tau^2}{\kappa^2})\dot{\psi}_3$$
$$+(-\frac{2\dot{\tau}^2}{\kappa}-\frac{2\tau\ddot{\tau}}{\kappa}+\frac{4\tau\dot{\tau}\dot{\kappa}}{\kappa^2}+\frac{\ddot{\kappa}\tau^2}{\kappa^2}-\frac{2\tau^2\dot{\kappa}^2}{\kappa^3})\psi_3\Big]ds=0,$$

which is

$$\int\ddddot{\psi}_3\Big[\frac{1}{\kappa}\frac{\partial f}{\partial \dot{\tau}}\Big]ds$$
$$+\int\dddot{\psi}_3\Big[\frac{1}{\kappa}\frac{\partial f}{\partial \tau}-\frac{2\dot{\kappa}}{\kappa^2}\frac{\partial f}{\partial \dot{\tau}}\Big]ds$$
$$+\int\ddot{\psi}_3\Big[-\frac{\dot{\kappa}}{\kappa^2}\frac{\partial f}{\partial \tau}-2\tau\frac{\partial f}{\partial \dot{\kappa}}+(\kappa-\frac{\tau^2}{\kappa}-\frac{\ddot{\kappa}}{\kappa^2}+\frac{2\dot{\kappa}^2}{\kappa^3})\frac{\partial f}{\partial \dot{\tau}}\Big]ds$$
$$+\int\dot{\psi}_3\Big[-2\tau\frac{\partial f}{\partial \kappa}+(\kappa-\frac{\tau^2}{\kappa})\frac{\partial f}{\partial \tau}-3\dot{\tau}\frac{\partial f}{\partial \dot{\kappa}}+(\dot{\kappa}-\frac{4\tau\dot{\tau}}{\kappa}+\frac{4\dot{\kappa}\tau^2}{\kappa^2})\frac{\partial f}{\partial \dot{\tau}}\Big]ds$$
$$+\int\psi_3\Big[-\dot{\tau}\frac{\partial f}{\partial \kappa}+(\frac{\dot{\kappa}\tau^2}{\kappa^2}-\frac{2\tau\dot{\tau}}{\kappa})\frac{\partial f}{\partial \tau}$$
$$-\ddot{\tau}\frac{\partial f}{\partial \dot{\kappa}}+(-\frac{2\dot{\tau}^2}{\kappa}-\frac{2\tau\ddot{\tau}}{\kappa}+\frac{4\tau\dot{\tau}\dot{\kappa}}{\kappa^2}+\frac{\ddot{\kappa}\tau^2}{\kappa^2}-\frac{2\tau^2\dot{\kappa}^2}{\kappa^3})\frac{\partial f}{\partial \dot{\tau}}\Big]ds=0,$$

then by integrating by parts the terms involving $\dot{\psi}_3,\ddot{\psi}_3,\dddot{\psi}_3$ and $\ddddot{\psi}_3$ obtain that:

$$\int\Big[-\frac{d^3}{ds^3}\Big(\frac{1}{\kappa}\frac{\partial f}{\partial \tau}\Big)-\frac{d^2}{ds^2}\Big(\frac{\dot{\kappa}}{\kappa^2}\frac{\partial f}{\partial \tau}\Big)+\frac{d}{ds}\Big(2\tau\frac{\partial f}{\partial \kappa}+\frac{\tau^2}{\kappa}\frac{\partial f}{\partial \tau}-\kappa\frac{\partial f}{\partial \tau}-\kappa\frac{\partial f}{\partial \tau}\Big)$$
$$-\dot{\tau}\frac{\partial f}{\partial \kappa}+[\frac{\dot{\kappa}\tau^2}{\kappa^2}-\frac{2\tau\dot{\tau}}{\kappa}]\frac{\partial f}{\partial \tau}-\ddot{\tau}\frac{\partial f}{\partial \dot{\kappa}}+\frac{d}{ds}\Big(3\dot{\tau}\frac{\partial f}{\partial \dot{\kappa}}\Big)-\frac{d^2}{ds^2}\Big(2\tau\frac{\partial f}{\partial \dot{\kappa}}\Big)$$
$$+[-\frac{2\dot{\tau}^2}{\kappa}-\frac{2\tau\ddot{\tau}}{\kappa}+\frac{4\tau\dot{\tau}\dot{\kappa}}{\kappa^2}+\frac{\ddot{\kappa}\tau^2}{\kappa^2}-\frac{2\tau^2\dot{\kappa}^2}{\kappa^3}]\frac{\partial f}{\partial \dot{\tau}}-\frac{d}{ds}\Big([\dot{\kappa}-\frac{4\tau\dot{\tau}}{\kappa}+\frac{2\dot{\kappa}\tau^2}{\kappa^2}]\frac{\partial f}{\partial \dot{\tau}}\Big)$$
$$+\frac{d^2}{ds^2}\Big([\kappa-\frac{\tau^2}{\kappa}-\frac{\ddot{\kappa}}{\kappa^2}+\frac{2\dot{\kappa}^2}{\kappa^3}]\frac{\partial f}{\partial \dot{\tau}}\Big)-\frac{d^3}{ds^3}\Big(-\frac{2\dot{\kappa}}{\kappa^2}\frac{\partial f}{\partial \dot{\tau}}\Big)+\frac{d^4}{ds^4}\Big(\frac{1}{\kappa}\frac{\partial f}{\partial \dot{\tau}}\Big)\Big]\psi_3ds=0, \tag{A.18}$$

applying fundamental theorem of calculus of variations, so equation (A.18) holds for arbitrary

ψ_3 if

$$
\begin{aligned}
&-\frac{d^3}{ds^3}\left(\frac{1}{\kappa}\frac{\partial f}{\partial \tau}\right)-\frac{d^2}{ds^2}\left(\frac{\dot{\kappa}}{\kappa^2}\frac{\partial f}{\partial \tau}\right)+\frac{d}{ds}\left(2\tau\frac{\partial f}{\partial \kappa}+\frac{\tau^2}{\kappa}\frac{\partial f}{\partial \tau}-\kappa\frac{\partial f}{\partial \tau}-\kappa\frac{\partial f}{\partial \tau}\right)\\
&-\dot{\tau}\frac{\partial f}{\partial \kappa}+\left[\frac{\dot{\kappa}\tau^2}{\kappa^2}-\frac{2\tau\dot{\tau}}{\kappa}\right]\frac{\partial f}{\partial \tau}-\ddot{\tau}\frac{\partial f}{\partial \dot{\kappa}}+\frac{d}{ds}\left(3\dot{\tau}\frac{\partial f}{\partial \dot{\kappa}}\right)-\frac{d^2}{ds^2}\left(2\tau\frac{\partial f}{\partial \dot{\kappa}}\right)\\
&+\left[-\frac{2\dot{\tau}^2}{\kappa}-\frac{2\tau\ddot{\tau}}{\kappa}+\frac{4\tau\dot{\tau}\dot{\kappa}}{\kappa^2}+\frac{\ddot{\kappa}\tau^2}{\kappa^2}-\frac{2\tau^2\dot{\kappa}^2}{\kappa^3}\right]\frac{\partial f}{\partial \dot{\tau}}-\frac{d}{ds}\left(\left[\dot{\kappa}-\frac{4\tau\dot{\tau}}{\kappa}+\frac{2\dot{\kappa}\tau^2}{\kappa^2}\right]\frac{\partial f}{\partial \dot{\tau}}\right)\\
&+\frac{d^2}{ds^2}\left(\left[\kappa-\frac{\tau^2}{\kappa}-\frac{\ddot{\kappa}}{\kappa^2}+\frac{2\dot{\kappa}^2}{\kappa^3}\right]\frac{\partial f}{\partial \dot{\tau}}\right)-\frac{d^3}{ds^3}\left(-\frac{2\dot{\kappa}}{\kappa^2}\frac{\partial f}{\partial \dot{\tau}}\right)+\frac{d^4}{ds^4}\left(\frac{1}{\kappa}\frac{\partial f}{\partial \dot{\tau}}\right)=0. \qquad \text{(A.19)}
\end{aligned}
$$

Simplifying equation (A.19) we obtain the second Euler-Lagrange equation as

$$
\begin{aligned}
&-\frac{1}{\kappa}\frac{d^3}{ds^3}\left[\frac{\partial f}{\partial \tau}-\frac{d}{ds}(\frac{\partial f}{\partial \dot{\tau}})\right]+\frac{2\dot{\kappa}}{\kappa^2}\frac{d^2}{ds^2}\left[\frac{\partial f}{\partial \tau}-\frac{d}{ds}(\frac{\partial f}{\partial \dot{\tau}})\right]\\
&+2\tau\frac{d}{ds}\left[\frac{\partial f}{\partial \kappa}-\frac{d}{ds}(\frac{\partial f}{\partial \dot{\kappa}})\right]+(\frac{\tau^2}{\kappa}+\frac{\ddot{\kappa}}{\kappa^2}-\frac{2\dot{\kappa}^2}{\kappa^3}-\kappa)\frac{d}{ds}\left[\frac{\partial f}{\partial \tau}-\frac{d}{ds}(\frac{\partial f}{\partial \dot{\tau}})\right]\\
&\dot{\tau}\left[\frac{\partial f}{\partial \kappa}-\frac{d}{ds}(\frac{\partial f}{\partial \dot{\kappa}})\right]-\dot{\kappa}\left[\frac{\partial f}{\partial \tau}-\frac{d}{ds}(\frac{\partial f}{\partial \dot{\tau}})\right]=0. \qquad \text{(A.20)}
\end{aligned}
$$

Appendix B

Numerical integration in Matlab

```
function [t,y] = RK4_sys(f, tspan, y0, h)

 % Rung-Kutta fourth order method file (RK4_sys.m)

%solve a system of ODEs using 4th-order RK method

%input: column vector t and row vector y

%return: column vector of values for y'

a = tspan(1); b=tspan(2); n=(b-a)/h;

t = (a+h : h : b)';

k1 = feval(f, a, y0)';

k2 = feval(f, a + h/2, y0 + k1/2*h)';

k3 = feval(f, a + h/2, y0 + k2/2*h)';

k4 = feval(f, a + h, y0+k3*h)';

y(1,:) = y0 + (k1+2*k2+2*k3+k4)/6*h;

for i=1 : n-1

 k1 = feval(f, t(i),     y(i,:))';

k2 = feval(f, t(i)+ h/2, y(i,:) + k1/2*h)';

 k3 = feval(f, t(i)+ h/2, y(i,:) + k2/2*h)';

k4 = feval(f, t(i)+ h  ,  y(i,:)+ k3*h)';

y(i+1,:) = y(i,:) + (k1+2*k2+2*k3+k4)/6*h;

end

t = [a; t]; y = [y0;y]; out = [t y];
```

```
disp('     t           y1              y2              y3  ...');

fprintf('%8.3f  %15.10f  %15.10f \n',out')

function f = example6(t,y) % the three first order ODEs file (example6.m)

% dy1/dt = f1  = y2

% dy2/dt = f2 = y3

% dy3/dt = f3  =

% (1/4*t^3*y1^2*(t^2-1)^3)

%let y(1) = y1, y(2) = y2, y(3)=y3

% tspan = [2 3]

% initial conditions y0 = [2, 2, 2]

f1 = y(2);

f2 = y(3);

f3 = -1/(4*t^3*y(1)^2*(t^2-1)^3)*((2*y(1)*t^3*y(3)*y(2)-t^3*y(2)^3-4*t^5*y(2))

*(t^2-1)^3-(2*t^2*y(1)^2*y(3)-t^2*y(1)*y(2)^2)*(t^2-1)^2)-9*t*y(1)^2*y(2)*(2*t^2-1)

*(t^2-1)+3*y(1)^3*(2*t^2*(8*t^2-7)+5)+4*t^4*y(1)

*((t^2-1)^2*(2*t^2-1));

f = [f1, f2, f3]';

[t,y]=RK4_sys('example6', [2 3], [2, 2, 2], 0.001 );

k=t

p=y(:,1)

p1=1./p

plot(k,p1) % relation curve between k and 1/p

z1=cumtrapz(k,p1)

plot(k,z1) % trapezoidal rule curve

cftool % for curve fitting

Data, x data= k, y data=z1, create data set

s(k)=ak^b+c, c>0, a=-3.802, b=-4.182, c=0.213 % for power function
```

```
s(k)=-Ae^bk+c, A=14.32, b=-2.159, c=0.1958 % for exponential function.

%%%%%%%%%%%%%%%%%%%%%%%%%%%%%%%%%%%%%%%%%%%%%%%%%%%%%%%%%%%%%%%%%%%%%%%%%%%%%%%%%%%%%%%%%%%%%%%%%%%%%%%%%%%%%%%%%%%%%%%%%%%%
```

Appendix C

Derivation for μ_0 and μ_3

Analytical derivations for μ_0 and μ_3 which are the critical values of the parameter μ in chapter 3 are discussed in this appendix. Considering the usual Legendre incomplete elliptic integral of the first kind $F(\phi, k)$, as in Byrd and Friedman [20], for the value of ϕ when $\phi \in (\phi_s, \phi_0)$, we have

$$F(\phi_s, k) - F(\phi_0, k) = \int_{\phi_0}^{\phi_s} \frac{d\phi}{\sqrt{1 - k^2 \sin^2 \phi}},$$

where $\phi_s = \sin^{-1}(1/\sqrt{2}k)$ and $\phi_0 = \sin^{-1}([1 - \sin(\gamma/2)]/2k^2)^{\frac{1}{2}}$, γ is the cone angle. By making the substitution $k \sin \phi = \sin \lambda$ we obtain that

$$F(\phi_s, k) - F(\phi_0, k) = \int_{\pi/4-\gamma/4}^{\pi/4} \frac{d\lambda}{\sqrt{k^2 - \sin^2 \lambda}}, \tag{C.1}$$

applying the same considerations for the incomplete elliptic integral of the second kind $E(\phi, k)$ for $\phi \in (\phi_s, \phi_0)$, we obtain

$$E(\phi_s, k) - E(\phi_0, k) = \int_{\pi/4-\gamma/4}^{\pi/4} \frac{\cos^2 \lambda}{\sqrt{k^2 - \sin^2 \lambda}} d\lambda. \tag{C.2}$$

Then substituting (C.1) and (C.2) into (3.18) we have

$$\begin{aligned} \mu = &\Big(2 \int_{\pi/4-\gamma/4}^{\pi/4} \frac{\cos^2 \lambda}{\sqrt{k^2 - \sin^2 \lambda}} d\lambda - \int_{\pi/4-\gamma/4}^{\pi/4} \frac{d\lambda}{\sqrt{k^2 - \sin^2 \lambda}}\Big) \\ &\times \Big(\int_{\pi/4-\gamma/4}^{\pi/4} \frac{d\lambda}{\sqrt{k^2 - \sin^2 \lambda}}\Big). \end{aligned} \tag{C.3}$$

For μ_0 which is the asymptotic value as k tends to zero, using $\cos 2\theta = 2\cos^2 \theta - 1 = 1 - 2\sin^2 \theta$, (C.3) μ_0 becomes

$$\mu_0 = 1 - 2 \int_{\omega}^{\pi/4} \sin \lambda d\lambda \Big(\int_{\omega}^{\pi/4} \frac{d\lambda}{\sin \lambda}\Big)^{-1}, \tag{C.4}$$

where $\omega = (\pi - \gamma)/4$. By evaluating equation (C.4) we have

$$\mu_0 = 1 + \frac{\sqrt{2}(1 - \sqrt{2}\cos\omega)}{\ln[(\sqrt{2}-1)/\tan(\omega/2)]}.$$

For μ_3, when k tends to ∞, from (C.3) we obtain

$$\mu_3 = \Big(2\int_{\omega}^{\pi/4} \cos^2\lambda d\lambda - \int_{\omega}^{\pi/4} d\lambda\Big)\Big(\int_{\omega}^{\pi/4} d\lambda\Big),$$

giving rise to

$$\mu_3 = \frac{2[1 - \cos(\gamma/2)]}{\gamma}.$$

Appendix D

Maple codes for joining profiles

D.1 Joining nanocones and fullerene

For this code we acknowledge the advise of the authors in [13].

D.1.1 Model I

```
> y1:= (r,alpha,B,phi,ell) -> 2*beta1(alpha,B,ell)*(cos(phic(alpha,B))
-cos(phi))/sqrt(B)+r*cot(alpha/2);
> x1:= (r,alpha,B,phi,ell) -> r + beta1(alpha,B,ell)*(
2*(EllipticE(sin(phi),1/sqrt(B))-EllipticE(sin(phic(alpha,B)),1/sqrt(B)) ) -
(EllipticF(sin(phi),1/sqrt(B))-EllipticF(sin(phic(alpha,B)),1/sqrt(B))) );
> model1:=(r,alpha,B,ell)->[x1(r,alpha,B,phi,ell),y1(r,alpha,B,phi,ell),
phi=phic(alpha,B)..phit(B)];
> model1i:=(r,alpha,B,ell)->[Re(x1(r,alpha,B,I*phi,ell)),
Re(y1(r,alpha,B,I*phi,ell)),phi=evalf(-I*phic(alpha,B))..evalf(-I*phit(B))];
> plot([model1i(10*tan(112.9*Pi*(1/360)), 1.9705, -4, 3.2),
model1i(10*tan(83.6*Pi*(1/360)), 1.4591, -4, 3.2),
model1i(10*tan(60*Pi*(1/360)), 1.0472, -4, 3.2),
model1i(10*tan(38.9*Pi*(1/360)), .6789, -4, 3.2),
model1i(10*tan(19.2*Pi*(1/360)), .3351, -4, 3),
[15.08*t, 10*t, t = 0 .. 1],[8.938*t, 10*t, t = 0 .. 1],
[5.775*t, 10*t, t = 0 .. 1], [3.533*t, 10*t, t = 0 .. 1]
[1.691*t, 10*t, t = 0 .. 1], [16.6*cos(t),12.66+16.6*sin(t),
```

```
t = 0 .. (1/2)*Pi],[10.1*cos(t), 12.81+10.1*sin(t)
, t = 0 .. (1/2)*Pi], [6.6*cos(t),12.91+6.6*sin(t), t = 0 .. (1/2)*Pi],
[4.1*cos(t), 12.97+4.1*sin(t), t = 0 .. (1/2)*Pi],
 [1.9*cos(t),12.99+1.9*sin(t), t = 0 .. (1/2)*Pi]],
scaling = constrained, thickness = 2);
```

D.1.2 Model II

```
> restart;
> with(plots):
> phic := (alpha,B)-> arcsin(sqrt(B*(1-sin(alpha/2))/2));
> #phit := B -> 0;
> phit := B -> arcsin(sqrt(B/2));
> beta1 := (alpha,B,ell) -> ell/(EllipticF(sin(phit(B)),1/sqrt(B))
-EllipticF(sin(phic(alpha,B)),1/sqrt(B)));
> beta2 := (alpha,B,ell) -> ell/(2*EllipticK(1/sqrt(B))
-EllipticF(sin(phit(B)),1/sqrt(B))
-EllipticF(sin(phic(alpha,B)),1/sqrt(B)));
> y21:= (r,alpha,B,phi,ell) -> 2*beta2(alpha,B,ell)*(cos(phic(alpha,B))
-cos(phi))/sqrt(B)+r*cot(alpha/2);
> x21:= (r,alpha,B,phi,ell) -> r + beta2(alpha,B,ell)*
( 2*(EllipticE(sin(phi),1/sqrt(B))-EllipticE(sin(phic(alpha,B)),1/sqrt(B)) )
-(EllipticF(sin(phi),1/sqrt(B))-EllipticF(sin(phic(alpha,B)),1/sqrt(B))) );
> y2:= (r,alpha,B,phi,ell) -> 2*beta2(alpha,B,ell)*(cos(phic(alpha,B))
+cos(phi))/sqrt(B) + r*cot(alpha/2);
> x2:= (r,alpha,B,phi,ell) -> r + beta2(alpha,B,ell)*(2*(2*EllipticE(1/sqrt(B))
-EllipticE(sin(phi),1/sqrt(B))-EllipticE(sin(phic(alpha,B)),1/sqrt(B)))-
(2*EllipticK(1/sqrt(B))-EllipticF(sin(phi),1/sqrt(B))
-EllipticF(sin(phic(alpha,B)),1/sqrt(B))) );
```

```
> model12:=(r,alpha,B,ell)->[x21(r,alpha,B,phi,ell),y21(r,alpha,B,phi,ell),
phi=phic(alpha,B)..Pi/2];
> model22:=(r,alpha,B,ell)->[x2(r,alpha,B,phi,ell),y2(r,alpha,B,phi,ell),
phi=Pi/2..phit(B)];
> Pm2:= (r,alpha,B,ell) -> [model12(r,alpha,B,ell),model22(r,alpha,B,ell)];
> plot([op(Pm2(3*cot(112.9*Pi/360),112.9*Pi/180,1.8,1)),
op(Pm2(3*cot(112.9*Pi/360),112.9*Pi/180,1.8,2))],scaling=constrained);
> plot([op(Pm2(10*tan(112.9*Pi*(1/360)), 1.9705, 1.7, 3)),
op(Pm2(10*tan(83.6*Pi*(1/360)), 83.6*Pi*(1/180),
1.814060252, 3)), op(Pm2(10*tan(60*Pi*(1/360)), 60*Pi*(1/180), 1.814060252, 3)),
op(Pm2(10*tan(38.9*Pi*(1/360)),38.9*Pi*(1/180), 1.814060252, 3)),
op(Pm2(10*tan(19.2*Pi*(1/360)), 19.2*Pi*(1/180), 1.814060252, 3)),
[15.08*t,10*t, t= 0 .. 1],
[8.938*t, 10*t, t = 0 .. 1], [5.775*t, 10*t, t = 0 .. 1],
[3.533*t, 10*t, t = 0 .. 1],[1.691*t,10*t, t = 0 .. 1],
[15.4*cos(t), 12.66+15.4*sin(t), t = 0 .. (1/2)*Pi],
 [9.2*cos(t), 12.81+9.2*sin(t), t = 0 ..(1/2)*Pi],
[5.9*cos(t), 12.91+5.9*sin(t), t = 0 .. (1/2)*Pi],
[3.53*cos(t), 12.97+3.53*sin(t), t = 0 ..(1/2)*Pi],
[1.6*cos(t), 12.99+1.6*sin(t), t = 0 .. (1/2)*Pi]],
scaling = constrained, thickness = 2);
```

D.2 Codes for joining two nanocones

```
> restart;

> mu1:=(a,b,gamma,l)->(a-b*sin(gamma/2))/l;

> sinphi0:=(gamma1,k)->sqrt((1-sin(gamma1/2))/2)/k;

> sinphi1:=(gamma2,k)->sqrt((1-sin(gamma2/2))/2)/k;

> MyE:=(s1,s2,k)->EllipticE(s1,k)-EllipticE(s2,k);

> MyF:=(s1,s2,k)->EllipticF(s1,k)-EllipticF(s2,k);

> mu:=(gamma1,gamma2,k)->2*MyE(sinphi1(gamma2,k),sinphi0(gamma1,k),k)

/MyF(sinphi1(gamma2,k),sinphi0(gamma1,k),k) -1;

> plot(mu(1.97,-1.97,1/sqrt(B)),B=-50..50);

> Re(evalf(mu(.3351,-.3351,1/sqrt(-4))));

> evalf(Im(2/MyF(sinphi0(.3351,1/sqrt(-4)),sinphi1(-.3351,1/sqrt(-4)),

1/sqrt(-4))));

> x:=(beta,k,s0,sinphi,b,gamma1)->beta*(2*MyE(sinphi,s0,k)

-MyF(sinphi,s0,k))+b*sin(gamma1/2);

> y:=(beta,k,s0,sinphi,b,gamma2)->2*beta*k*(cos(arcsin(s0))

-cos(arcsin(sinphi)))+b*cos(gamma2/2);

> plot(x(-2.8746*I,1/sqrt(-4),sinphi0(1.9705,1/sqrt(-4)),sinphi*I,18.09,1.9705),

sinphi=Im(sinphi0(1.9705,1/sqrt(-4)))..Im(sinphi1(-1.9705,1/sqrt(-4))));

>plot(y(-2.8746*I,1/sqrt(-4),sinphi0(1.9705,1/sqrt(-4)),sinphi*I,18.09,1.9705),

sinphi=Im(sinphi0(1.9705,1/sqrt(-4)))..Im(sinphi1(-1.9705,1/sqrt(-4))));

> plot([[x(-2.8746*I, 1/sqrt(-4), sinphi0(1.9705, 1/sqrt(-4)),

I*sinphi, 18.09, 1.9705),y(-2.8746*I, 1/sqrt(-4), sinphi0(1.9705, 1/sqrt(-4)),

 I*sinphi, 18.09, 1.9705),sinphi = Im(sinphi0(1.9705, 1/sqrt(-4)))

 .. Im(sinphi1(-1.9705, 1/sqrt(-4)))],[x(-4.115*I, 1/sqrt(-4),

 sinphi0(1.4591, 1/sqrt(-4)), I*sinphi, 13.41, 1.4591),

y(-4.115*I, 1/sqrt(-4), sinphi0(1.4591, 1/sqrt(-4)),
```

```
I*sinphi, 13.41, 1.4591), sinphi = Im(sinphi0(1.4591, 1/sqrt(-4)))
 .. Im(sinphi1(-1.9705, 1/sqrt(-4)))],[x(-5.994*I, 1/sqrt(-4),
sinphi0(1.0472, 1/sqrt(-4)), I*sinphi, 11.55, 1.0472),
y(-5.994*I, 1/sqrt(-4), sinphi0(1.0472, 1/sqrt(-4)),
 I*sinphi, 11.55, 1.0472),sinphi = Im(sinphi0(1.0472, 1/sqrt(-4)))
 .. Im(sinphi1(-1.0472, 1/sqrt(-4)))],[x(-9.597*I, 1/sqrt(-4),
 sinphi0(.6789, 1/sqrt(-4)), I*sinphi, 10.61, .6789),
y(-9.597*I, 1/sqrt(-4), sinphi0(.6789, 1/sqrt(-4)),
I*sinphi, 10.61, .6789), sinphi = Im(sinphi0(.6789, 1/sqrt(-4)))
.. Im(sinphi1(-.6789, 1/sqrt(-4)))],
[x(-20.08*I, 1/sqrt(-4), sinphi0(.3351, 1/sqrt(-4)),
I*sinphi, 10.14, .3351),y(-20.08*I, 1/sqrt(-4),
 sinphi0(.3351, 1/sqrt(-4)), I*sinphi, 10.14, .3351),
sinphi = Im(sinphi0(.3351, 1/sqrt(-4))) ..
Im(sinphi1(-.3351, 1/sqrt(-4)))],
[15.08*t, 10*t, t = 0 .. 1], [8.938*t, 10*t, t = 0 .. 1],
 [5.775*t, 10*t, t = 0 .. 1],[3.533*t, 10*t, t = 0 .. 1],
 [1.691*t, 10*t, t = 0 .. 1],[1.691*t, 10*t, t = 0 .. 1]
,[16.5-t, 11.8+t, t = 1 .. 16.4], [10.1-t, 12.3+t, t = 1 .. 10],
[6.85-t, 12.5+t, t = 1 .. 6.85], [4.57-t, 12.7+t, t = 1 .. 4.57],
[2.70-t, 12.8+t, t = 1 .. 2.70]], scaling = constrained, thickness = 2);
```

D.2.1 Code for joining two cones with first cone's angle is 112°

```
> restart;

> with(plots):

> phic := (alpha,B)-> arcsin(sqrt(B*(1-sin(alpha/2))/2));

> #phit := B -> 0;

> phit := B -> arcsin(sqrt(B/2));

> beta1 := (alpha,B,ell) -> ell/(EllipticF(sin(phit(B)),1/sqrt(B))
-EllipticF(sin(phic(alpha,B)),1/sqrt(B)));

> beta2 := (alpha,B,ell) -> ell/(2*EllipticK(1/sqrt(B))
-EllipticF(sin(phit(B)),1/sqrt(B))-EllipticF(sin(phic(alpha,B)),1/sqrt(B)));

> y21:= (r,alpha,B,phi,ell) -> 2*beta2(alpha,B,ell)*(cos(phic(alpha,B))
-cos(phi))/sqrt(B)+r*cot(alpha/2);

> x21:= (r,alpha,B,phi,ell) -> r + beta2(alpha,B,ell)*
(2*(EllipticE(sin(phi),1/sqrt(B))-EllipticE(sin(phic(alpha,B)),1/sqrt(B)))-
(EllipticF(sin(phi),1/sqrt(B))-EllipticF(sin(phic(alpha,B)),1/sqrt(B))) );

> y2:= (r,alpha,B,phi,ell) -> 2*beta2(alpha,B,ell)*(cos(phic(alpha,B))
+cos(phi))/sqrt(B) + r*cot(alpha/2);

> x2:= (r,alpha,B,phi,ell) -> r + beta2(alpha,B,ell)*
(2*(2*EllipticE(1/sqrt(B))-EllipticE(sin(phi),1/sqrt(B))
-EllipticE(sin(phic(alpha,B)),1/sqrt(B)))-(2*EllipticK(1/sqrt(B))-EllipticF(sin(phi)
,1/sqrt(B))-EllipticF(sin(phic(alpha,B)),1/sqrt(B))));

> model12:=(r,alpha,B,ell)->[x21(r,alpha,B,phi,ell),y21(r,alpha,B,phi,ell),
phi=phic(alpha,B)..Pi/2];

> model22:=(r,alpha,B,ell)->[x2(r,alpha,B,phi,ell),y2(r,alpha,B,phi,ell),
phi=Pi/2..Pi/3];

> Pm2:= (r,alpha,B,ell) -> [model12(r,alpha,B,ell),model22(r,alpha,B,ell)];

> plot([op(Pm2(10*tan(112.9*Pi*(1/360)), 1.9705, 1.1, 2)),
```

```
op(Pm2(10*tan(112.9*Pi*(1/360)), 1.9705, 1.0001, 2)),
op(Pm2(10*tan(112.9*Pi*(1/360)), 1.9705, 1.3, 2)), op(Pm2(10*tan(112.9*Pi*(1/360)),
1.9705, 1.5, 2)), op(Pm2(10*tan(112.9*Pi*(1/360)), 1.9705, 1.2, 2)),
 op(Pm2(10*tan(112.9*Pi*(1/360)), 1.9705, 1.001, 2)),
op(Pm2(10*tan(112.9*Pi*(1/360)), 1.9705, 1.01, 2))],
scaling = constrained, thickness = 2);
> p11 := plot([op(Pm2(10*tan(112.9*Pi*(1/360)), 1.9705, 1.0001, 3))]);
> p22 := plot([op(Pm2(10*tan(112.9*Pi*(1/360)), 1.9705, 1.1, 3))]);
> p33 := plot([op(Pm2(10*tan(112.9*Pi*(1/360)), 1.9705, 1.01, 3))]);
> p44 := plot([15.09*t, 10*t, t = 0 .. 1], thickness = 2);
> p01 := plot([13.75-t, 8.7+2*t, t = 1 .. 13.75]);
> p02 := plot([14.09-t, 9.4+2*t, t = 1 .. 14.09]);
> p03 := plot([14.8-t, 10.2+2*t, t = 1 .. 14.8]);
> display([p11, p22, p33, p44, p01, p02, p03], thickness = 2);
```
For the other angles we follow this code with the following change

D.2.2 Code for joining two cones with first cone's angle is 83.6°

```
> plot([op(Pm2(10*tan(83.6*Pi*(1/360)), 1.9705, 1.1, 2)),
op(Pm2(10*tan(83.6*Pi*(1/360)), 1.9705, 1.0001, 2)),
op(Pm2(10*tan(83.6*Pi*(1/360)), 1.9705, 1.3, 2)),
op(Pm2(10*tan(83.6*Pi*(1/360)), 1.9705, 1.5, 2)),
 op(Pm2(10*tan(83.6*Pi*(1/360)), 1.9705, 1.2, 2)),
op(Pm2(10*tan(83.6*Pi*(1/360)), 1.9705, 1.001, 2)),
 op(Pm2(10*tan(83.6*Pi*(1/360)), 1.9705, 1.01, 2))],
 scaling = constrained, thickness = 2);
p11 := plot([op(Pm2(10*tan(83.6*Pi*(1/360)), 1.9705, 1.0001, 3))]):
p22 := plot([op(Pm2(10*tan(83.6*Pi*(1/360)), 1.9705, 1.1, 3))]):
p33 := plot([op(Pm2(10*tan(83.6*Pi*(1/360)), 1.9705, 1.01, 3))]):
p44 := plot([9*t, 6*t, t = 0 .. 1], thickness = 2):
p01 := plot([7.5-t, 4.7+2*t, t = 1 .. 7.5]):
p02 := plot([8-t, 5.3+2*t, t = 1 .. 8]):
p03 := plot([8.8-t, 5.8+2*t, t = 1 .. 8.8]):
display([p11, p22, p33, p44, p01, p02, p03], thickness = 2);
```

D.2.3 Code for joining two cones with first cone's angle is 60°

```
> plot([op(Pm2(10*tan(60*Pi*(1/360)), 1.9705, 1.1, 2)),
op(Pm2(10*tan(60*Pi*(1/360)), 1.9705, 1.0001, 2)),
op(Pm2(10*tan(60*Pi*(1/360)), 1.9705, 1.3, 2)),
op(Pm2(10*tan(60*Pi*(1/360)), 1.9705, 1.5, 2)),
op(Pm2(10*tan(60*Pi*(1/360)), 1.9705, 1.2, 2)),
op(Pm2(10*tan(60*Pi*(1/360)), 1.9705, 1.001, 2)),
op(Pm2(10*tan(60*Pi*(1/360)), 1.9705, 1.01, 2))],
scaling = constrained, thickness = 2);
p11 := plot([op(Pm2(10*tan(60*Pi*(1/360)), 1.9705, 1.0001, 3))]):
```

```
p22 := plot([op(Pm2(10*tan(60*Pi*(1/360)), 1.9705, 1.1, 3))]):

p33 := plot([op(Pm2(10*tan(60*Pi*(1/360)), 1.9705, 1.01, 3))]):

p44 := plot([5.8*t, 3.8*t, t = 0 .. 1], thickness = 2):

p01 := plot([4.35-t, 2.63+2*t, t = 1 .. 4.35]):

p02 := plot([4.89-t, 3.1+2*t, t = 1 .. 4.89]):

p03 := plot([5.55-t, 3.9+2*t, t = 1 .. 5.55]):

display([p11, p22, p33, p44, p01, p02, p03], thickness = 2);
```

D.2.4 Code for joining two cones with first cone's angle is 38.9°

```
plot([op(Pm2(10*tan(38.9*Pi*(1/360)), 1.9705, 1.1, 2)),

op(Pm2(10*tan(38.9*Pi*(1/360)), 1.9705, 1.0001, 2)),

op(Pm2(10*tan(38.9*Pi*(1/360)), 1.9705, 1.3, 2)),

op(Pm2(10*tan(38.9*Pi*(1/360)), 1.9705, 1.5, 2)),

 op(Pm2(10*tan(38.9*Pi*(1/360)), 1.9705, 1.2, 2)),

op(Pm2(10*tan(38.9*Pi*(1/360)), 1.9705, 1.001, 2)),

op(Pm2(10*tan(38.9*Pi*(1/360)), 1.9705, 1.01, 2))],

scaling = constrained, thickness = 2);

p11 := plot([op(Pm2(10*tan(38.9*Pi*(1/360)), 1.9705, 1.0001, 3))]):

p22 := plot([op(Pm2(10*tan(38.9*Pi*(1/360)), 1.9705, 1.1, 3))]):

p33 := plot([op(Pm2(10*tan(38.9*Pi*(1/360)), 1.9705, 1.01, 3))]):

p44 := plot([3.6*t, 2.4*t, t = 0 .. 1], thickness = 2):

p01 := plot([2.15-t, 1.1+2*t, t = 1 .. 2.15]):

p02 := plot([2.6-t, 1.7+2*t, t = 1 .. 2.6]):

p03 := plot([3.3-t, 2.4+2*t, t = 1 .. 3.3]):

> display([p11, p22, p33, p44, p01, p02, p03], thickness = 2);
```

D.2.5 Code for joining two cones with first cone's angle is 19.2°

```
plot([op(Pm2(10*tan(19.2*Pi*(1/360)), 1.9705, 1.1, 2)),

op(Pm2(10*tan(19.2*Pi*(1/360)), 1.9705, 1.0001, 2)),
```

```
op(Pm2(10*tan(19.2*Pi*(1/360)), 1.9705, 1.3, 2)),
 op(Pm2(10*tan(19.2*Pi*(1/360)), 1.9705, 1.5, 2)),
op(Pm2(10*tan(19.2*Pi*(1/360)), 1.9705, 1.2, 2)),
 op(Pm2(10*tan(19.2*Pi*(1/360)), 1.9705, 1.001, 2)),
 op(Pm2(10*tan(19.2*Pi*(1/360)), 1.9705, 1.01, 2))],
 scaling = constrained, thickness = 2);
p11:=plot([op(Pm2(10*tan(19.2*Pi*(1/360)), 1.9705, 1.0001, 2))]);
p22:=plot([op(Pm2(10*tan(19.2*Pi*(1/360)), 1.9705, 1.1, 2))]);
p33:=plot([op(Pm2(10*tan(19.2*Pi*(1/360)), 1.9705, 1.01, 2))]);
p44:=plot([1.7*t, 1.13*t, t = 0 .. 1], thickness = 2);
p01:=plot([1.87-t, .5+2*t, t = 1 .. 1.87]);
p02:=plot([1.4-t, 0.3e-1+2*t, t = 1 .. 1.4]);
p03:=plot([1.09-t, -.35+2*t, t = 1 .. 1.09]);
display([p11, p22, p33, p44, p01, p02, p03], thickness = 2);
```

D.3 Codes for joining nanocones and graphene

D.3.1 Model I

```
> restart;
> with(plots):
> phic := (alpha,B)-> -arcsin(sqrt(B*(1-sin(alpha/2))/2));
> phit := B ->0;
> beta1 := (alpha,B,ell) -> ell/(EllipticF(sin(phit(B)),
1/sqrt(B))-EllipticF(sin(phic(alpha,B)),1/sqrt(B)));
> beta2 := (alpha,B,ell) -> ell/(2*EllipticK(1/sqrt(B))-EllipticF(sin(phit(B)),
1/sqrt(B))-EllipticF(sin(phic(alpha,B)),1/sqrt(B)));
For B<2
> y1:= (r,alpha,B,phi,ell)-> 2*beta1(alpha,B,ell)*(1-cos(phi))/sqrt(B);
```

```
> x1:= (r,alpha,B,phi,ell)-> r + beta1(alpha,B,ell)*(2*(EllipticE(sin(phi)
,1/sqrt(B)))-(EllipticF(sin(phi),1/sqrt(B))));
> model1:=(r,alpha,B,ell)->[x1(r,alpha,B,phi,ell),y1(r,alpha,B,phi,ell),
phi=phic(alpha,B)..phit(B)];
> model1i:=(r,alpha,B,ell)->[Re(x1(r,alpha,B,I*phi,ell)),
Re(y1(r,alpha,B,I*phi,ell)),phi=evalf(-I*phic(alpha,B))..evalf(-I*phit(B))];
> graph := [3*t, 0, t = 1 .. 2];
> cone1 := [1.3-t, 2.75*t, t = .2 .. 1.3];
> cone2 := [1.4-t, 3.75*t, t = .2 .. 1.4];
> cone3 := [1.5-t, 4.5*t, t = .2 .. 1.5];
> cone4 := [1.6-t, 5*t, t = .2 .. 1.6];
> cone5 := [1.7-t, 5.5*t, t = .2 .. 1.7];
p0 := plot([3*t, 0.1e-1, t = 1 .. 2], thickness = 3):
p1 := plot([model1i(3, 112.9*Pi*(1/180), -4, 2), cone1],
scaling = constrained, thickness = 2):
p2 := plot([model1i(3, 83.6*Pi*(1/180), -4, 2), cone2],
scaling = constrained, thickness = 2):
p3 := plot([model1i(3, 60*Pi*(1/180), -4, 2), cone3],
scaling = constrained, thickness = 2):
p4 := plot([model1i(3, 38.9*Pi*(1/180), -4, 2), cone4],
 scaling = constrained, thickness = 2):
p5 := plot([model1i(3, 19.2*Pi*(1/180), -4, 2), cone5],
 scaling = constrained, thickness = 2):
display([p0, p1, p2, p3, p4, p5]);
```

D.3.2 Model II

```
> restart;
> with(plots):
```

```
> phi1 := (psi,B)-> 0;

> phi2 := (psi,B) -> arcsin(sqrt(B*(1-sin(psi/2))/2));

> mu1:= (psi1,psi2,B) -> 2*( (EllipticE(sin(phi2(psi2,B)),
1/sqrt(B))-EllipticE(sin(phi1(psi1,B)),1/sqrt(B)))/
(EllipticF(sin(phi2(psi2,B)),1/sqrt(B))-
EllipticF(sin(phi1(psi1,B)),1/sqrt(B))) )-1;

> mu2:= (psi1,psi2,B) -> 2*( (2*EllipticE(1/sqrt(B))-
EllipticE(sin(phi2(psi2,B)),1/sqrt(B))-EllipticE(sin(phi1(psi1,B))
,1/sqrt(B)))/(2*EllipticK(1/sqrt(B))-EllipticF(sin(phi2(psi2,B))
,1/sqrt(B))-EllipticF(sin(phi1(psi1,B)),1/sqrt(B))) )-1;

beta1:= (psi1,psi2,B,ell) -> ell/(EllipticF(sin(phi2(psi2,B)),
1/sqrt(B))-EllipticF(sin(phi1(psi1,B)),1/sqrt(B)));

> beta2:= (psi1,psi2,B,ell) -> ell/(2*EllipticK(1/sqrt(B))
-EllipticF(sin(phi2(psi2,B)),1/sqrt(B))-EllipticF(sin(phi1(psi1,B)),
1/sqrt(B)));

> y2_1:= (a,psi1,psi2,B,phi,ell) -> 2*beta2(psi1,psi2,B,ell)*(cos(phi1(psi1,B))
-cos(phi))/sqrt(B)+a*sin(psi1);

> x2_1:= (a,psi1,psi2,B,phi,ell) -> a*cos(psi1)-
beta2(psi1,psi2,B,ell)*( 2*(EllipticE(sin(phi),1/sqrt(B))-
EllipticE(sin(phi1(psi1,B)),1/sqrt(B)))-
(EllipticF(sin(phi),1/sqrt(B))-EllipticF(sin(phi1(psi1,B)),1/sqrt(B))));

> y2_2:= (a,psi1,psi2,B,phi,ell) -> 2*beta2(psi1,psi2,B,ell)*(cos(phi1(psi1,B))
+cos(phi))/sqrt(B) + a*sin(psi1);

> x2_2:= (a,psi1,psi2,B,phi,ell)-> a*cos(psi1)-beta2(psi1,psi2,B,ell)*
(2*(2*EllipticE(1/sqrt(B))-EllipticE(sin(phi),1/sqrt(B))
-EllipticE(sin(phi1(psi1,B)),1/sqrt(B)))-(2*EllipticK(1/sqrt(B))
-EllipticF(sin(phi),1/sqrt(B))-EllipticF(sin(phi1(psi1,B)),1/sqrt(B))));
```

```
> model2_1:=(a,psi1,psi2,B,phi,ell)->[x2_1(a,psi1,psi2,B,phi,ell),
y2_1(a,psi1,psi2,B,phi,ell),phi=phi1(psi1,B)..Pi/2];
> model2_2:=(a,psi1,psi2,B,phi,ell)->[x2_2(a,psi1,psi2,B,phi,ell),
y2_2(a,psi1,psi2,B,phi,ell),phi=Pi/2..phi2(psi2,B)];
> Pm2:= (a,psi1,psi2,B,ell) -> [model2_1(a,psi1,psi2,B,phi,ell),
model2_2(a,psi1,psi2,B,phi,ell)];
> endpoint2:= (a,psi1,psi2,B,ell) -> [x2_2(a,psi1,psi2,B,phi2(psi2,B),ell),
y2_2(a,psi1,psi2,B,phi2(psi2,B),ell)];
> b2:=(a,psi1,psi2,B,ell)-> x2_2(a,psi1,psi2,B,phi2(psi2,B),ell)/cos(psi2);
> L2:=(a,psi1,psi2,B,ell)-> y2_2(a,psi1,psi2,B,phi2(psi2,B),ell)
-b2(a,psi1,psi2,B,ell)*sin(psi2);
> cone4:=[6.85-t,1.25+t,t=1..6.85];
> ball21:=[5*t,0.01,t=1..2];
> ball22:= [4.5-t,6.5*t,t=1..3.5];
> cone1:=[7-t,0.2+2*t,t=1..7];
> cone2:=[6.8-t,1.2+t,t=1..6.8];
> cone3:=[6.6-t,1.2+t,t=1..6.6];
> cone5 := [6.93-t, -.7+3*t, t = 1 .. 6.93];
p1 := plot([op(Pm2(5, 0, -112.9, 1.1, 3)), ball21, cone1],
 scaling = constrained, thickness = 2, colour = blue);
p2 := plot([op(Pm2(5, 0, -83.6, 1.1, 3)), ball21],
scaling = constrained, thickness = 1, colour = green);
p3 := plot([op(Pm2(5, 0, -60, 1.1, 3))],
scaling = constrained, thickness = 1, colour = red);
p4 := plot([op(Pm2(5, 0, 38.9, 1.1, 3))],
scaling = constrained, thickness = 1, colour = black);
p5 := plot([op(Pm2(5, 0, -19.2, 1.1, 3))],
```

```
scaling = constrained, thickness = 1, colour = purple);

p6 := plot([7-t, .2+2*t, t = 1 .. 7], thickness = 2, colour = blue);

p7 := plot([6.8-t, 1.2+t, t = 1 .. 6.8], thickness = 1, colour = green);

p8 := plot([6.6-t, 1.2+t, t = 1 .. 6.6], thickness = 2, colour = red);

p9 := plot([6.85-t, 1.25+t, t = 1 .. 6.85], thickness = 1, colour = black);

p10 := plot([6.93-t, -.7+3*t, t = 1 .. 6.93], thickness = 2, colour = purple);

p11 := plot([5*t, 0.1e-1, t = 1 .. 2], thickness = 3);

display([p1, p2, p3, p4, p5, p6, p7, p8, p9, p10, p11]);
```

D.4 Codes for joining fullerene and graphene

D.4.1 Model I

```
> y1:= (a,psi1,psi2,B,phi,ell) -> 2*beta1(psi1,psi2,B,ell)*(cos(phi1(psi1,B))
-cos(phi))/sqrt(B)+a*sin(psi1);

> x1:= (a,psi1,psi2,B,phi,ell) -> a*cos(psi1)-beta1(psi1,psi2,B,ell)*
(2*(EllipticE(sin(phi),1/sqrt(B))-EllipticE(sin(phi1(psi1,B)),1/sqrt(B)))-
(EllipticF(sin(phi),1/sqrt(B))-EllipticF(sin(phi1(psi1,B)),1/sqrt(B))));

> model1:=(a,psi1,psi2,B,ell)->[x1(a,psi1,psi2,B,phi,ell),y1(a,psi1,psi2,
B,phi,ell),phi=phi1(psi1,B)..phi2(psi2,B)];

> model1i:=(a,psi1,psi2,B,ell)->[Re(x1(a,psi1,psi2,B,I*phi,ell)),
Re(y1(a,psi1,psi2,B,I*phi,ell)),phi=evalf(-I*phi1(psi1,B))
..evalf(-I*phi2(psi2,B))];

> endpoint:= (a,psi1,psi2,B,ell)->[x1(a,psi1,psi2,B,phi2(psi2,B),ell),
y1(a,psi1,psi2,B,phi2(psi2,B),ell)];

> b:= (a,psi1,psi2,B,ell) -> x1(a,psi1,psi2,B,phi2(psi2,B),ell)/cos(psi2);

> L:= (a,psi1,psi2,B,ell) -> y1(a,psi1,psi2,B,phi2(psi2,B),ell)
-b(a,psi1,psi2,B,ell)*sin(psi2);

> ball1:= [5*t,0.01,t=1..2];

> ball2:= (a,psi1,psi2,B,ell)-> [b(a,psi1,psi2,B,ell)*cos(x),
```

```
L(a,psi1,psi2,B,ell)+b(a,psi1,psi2,B,ell)*sin(x),x=Pi/2..psi2];

> plot([model1(5,0,-Pi/6,1,3),ball1,ball2(5,0,-Pi/6,1,3)],

scaling=constrained,thickness=2);

> ball:=[5*t,0.001,t=1..2];

> plot([model1i(5,0,-Pi/6,-1,3),ball,ball2(5,0,-Pi/6,-1,3)],

scaling=constrained,thickness=2);
```

D.4.2 Model II

```
> y2_1:= (a,psi1,psi2,B,phi,ell) -> 2*beta2(psi1,psi2,B,ell)

*(cos(phi1(psi1,B))-cos(phi))/sqrt(B)+a*sin(psi1);

> x2_1:= (a,psi1,psi2,B,phi,ell) -> a*cos(psi1)-beta2(psi1,psi2,B,ell)

*(2*(EllipticE(sin(phi),1/sqrt(B))-EllipticE(sin(phi1(psi1,B)),1/sqrt(B)))-

(EllipticF(sin(phi),1/sqrt(B))-EllipticF(sin(phi1(psi1,B)),1/sqrt(B))));

> y2_2:= (a,psi1,psi2,B,phi,ell) -> 2*beta2(psi1,psi2,B,ell)

*(cos(phi1(psi1,B))+cos(phi))/sqrt(B) + a*sin(psi1);

> x2_2:= (a,psi1,psi2,B,phi,ell) -> a*cos(psi1)-beta2(psi1,psi2,B,ell)

*(2*(2*EllipticE(1/sqrt(B))-EllipticE(sin(phi),1/sqrt(B))

-EllipticE(sin(phi1(psi1,B)),1/sqrt(B)))-(2*EllipticK(1/sqrt(B))-EllipticF(sin(phi)

,1/sqrt(B))-EllipticF(sin(phi1(psi1,B)),1/sqrt(B))));

> model2_1:=(a,psi1,psi2,B,phi,ell)->[x2_1(a,psi1,psi2,B,phi,ell)

,y2_1(a,psi1,psi2,B,phi,ell),phi=phi1(psi1,B)..Pi/2];

> model2_2:=(a,psi1,psi2,B,phi,ell)->[x2_2(a,psi1,psi2,B,phi,ell),

y2_2(a,psi1,psi2,B,phi,ell),phi=Pi/2..phi2(psi2,B)];

> Pm2:= (a,psi1,psi2,B,ell) -> [model2_1(a,psi1,psi2,B,phi,ell),

model2_2(a,psi1,psi2,B,phi,ell)];

> endpoint2:= (a,psi1,psi2,B,ell) ->[x2_2(a,psi1,psi2,B,phi2(psi2,B),ell),

y2_2(a,psi1,psi2,B,phi2(psi2,B),ell)];

> b2:= (a,psi1,psi2,B,ell) -> x2_2(a,psi1,psi2,B,phi2(psi2,B),ell)/cos(psi2);
```

```
> L2:= (a,psi1,psi2,B,ell) -> y2_2(a,psi1,psi2,B,phi2(psi2,B),ell)
-b2(a,psi1,psi2,B,ell)*sin(psi2);
> ball2_1:=[5*t,0.01,t=1..2];
> ball2_2:= (a,psi1,psi2,B,ell) -> [b2(a,psi1,psi2,B,ell)*cos(x),
L2(a,psi1,psi2,B,ell)+b2(a,psi1,psi2,B,ell)*sin(x),x=Pi/2..psi2];
> plot([op(Pm2(5,0,-Pi/6,1.1,3)),ball2_1,ball2_2(5,0,-Pi/6,1.1,3)],
scaling=constrained,thickness=2);
```

D.5 Joining between two parallel sheets of graphene with nanocone

```
> restart;
> with(plots):
> phi1 := (psi,B)-> 0;
> phi2 := (psi,B) -> arcsin(sqrt(B*(1-sin(psi/2))/2));
> mu1:= (psi1,psi2,B) -> 2*( (EllipticE(sin(phi2(psi2,B)),1/sqrt(B))
-EllipticE(sin(phi1(psi1,B)),1/sqrt(B)))/ (EllipticF(sin(phi2(psi2,B)),
1/sqrt(B))-EllipticF(sin(phi1(psi1,B)),1/sqrt(B))) )-1;
> mu2:= (psi1,psi2,B) -> 2*( (2*EllipticE(1/sqrt(B))-EllipticE(sin(phi2(psi2,B)),
1/sqrt(B))-EllipticE(sin(phi1(psi1,B)),1/sqrt(B)))/(2*EllipticK(1/sqrt(B))
-EllipticF(sin(phi2(psi2,B)),1/sqrt(B))-EllipticF(sin(phi1(psi1,B)),1/sqrt(B))))-1;
> beta1:= (psi1,psi2,B,ell) -> ell/(EllipticF(sin(phi2(psi2,B)),
1/sqrt(B))-EllipticF(sin(phi1(psi1,B)),1/sqrt(B)));
> beta2:= (psi1,psi2,B,ell) -> ell/(2*EllipticK(1/sqrt(B))-EllipticF(sin(phi2(psi2,B)),
1/sqrt(B))-EllipticF(sin(phi1(psi1,B)),1/sqrt(B)));
> y2_1:= (a,psi1,psi2,B,phi,ell) -> 2*beta2(psi1,psi2,B,ell)
*(cos(phi1(psi1,B))-cos(phi))/sqrt(B)+a*sin(psi1);
> x2_1:= (a,psi1,psi2,B,phi,ell) -> a*cos(psi1) - beta2(psi1,psi2,B,ell)
*( 2*(EllipticE(sin(phi),1/sqrt(B))-EllipticE(sin(phi1(psi1,B)),1/sqrt(B)))-
(EllipticF(sin(phi),1/sqrt(B))-EllipticF(sin(phi1(psi1,B)),1/sqrt(B))));
```

```
> y2_2:= (a,psi1,psi2,B,phi,ell) -> 2*beta2(psi1,psi2,B,ell)*(cos(phi1(psi1,B))
+cos(phi))/sqrt(B) + a*sin(psi1);
> x2_2:= (a,psi1,psi2,B,phi,ell) -> a*cos(psi1)-beta2(psi1,psi2,B,ell)
*( 2*(2*EllipticE(1/sqrt(B))-EllipticE(sin(phi),1/sqrt(B))
-EllipticE(sin(phi1(psi1,B)),1/sqrt(B)))-(2*EllipticK(1/sqrt(B))
-EllipticF(sin(phi),1/sqrt(B))-EllipticF(sin(phi1(psi1,B)),1/sqrt(B))));
> model2_1:=(a,psi1,psi2,B,phi,ell)->[x2_1(a,psi1,psi2,B,phi,ell),
y2_1(a,psi1,psi2,B,phi,ell),phi=Pi/18..Pi/2];
> model2_2:=(a,psi1,psi2,B,phi,ell)->[x2_2(a,psi1,psi2,B,phi,ell),
y2_2(a,psi1,psi2,B,phi,ell),phi=Pi/2..Pi/2.4];
> Pm2:= (a,psi1,psi2,B,ell) -> [model2_1(a,psi1,psi2,B,phi,ell),
model2_2(a,psi1,psi2,B,phi,ell)];
> endpoint2:= (a,psi1,psi2,B,ell) -> [x2_2(a,psi1,psi2,B,phi2(psi2,B),ell),
y2_2(a,psi1,psi2,B,phi2(psi2,B),ell)];
> b2:= (a,psi1,psi2,B,ell) -> x2_2(a,psi1,psi2,B,phi2(psi2,B),ell)/cos(psi2);
> L2:= (a,psi1,psi2,B,ell) -> y2_2(a,psi1,psi2,B,phi2(psi2,B),ell)
-b2(a,psi1,psi2,B,ell)*sin(psi2);
> model2_11:=(a,psi1,psi2,B,phi,ell)->[x2_1(a,psi1,psi2,B,phi,ell),
y2_1(a,psi1,psi2,B,phi,ell),phi=Pi/90..Pi/2];
> model2_21:=(a,psi1,psi2,B,phi,ell)->[x2_2(a,psi1,psi2,B,phi,ell),
y2_2(a,psi1,psi2,B,phi,ell),phi=Pi/2..Pi/2.11];
> Pm21:= (a,psi1,psi2,B,ell) -> [model2_11(a,psi1,psi2,B,phi,ell),
model2_21(a,psi1,psi2,B,phi,ell)];
> mu1:=(a,b,gamma,l)->(a-b*sin(gamma/2))/l;
> sinphi0:=(gamma,k)->sqrt((1-sin(gamma/2))/2)/k;
> sinphi1:=k->0;
> MyE:=(s1,s2,k)->EllipticE(s1,k)-EllipticE(s2,k);
```

```
> MyF:=(s1,s2,k)->EllipticF(s1,k)-EllipticF(s2,k);

> mu:=(gamma,k)->2*MyE(sinphi1(k),sinphi0(gamma,k),k)/MyF(sinphi1(k)

,sinphi0(gamma,k),k) -1;

Re(evalf(mu(.3351,1/sqrt(-4))));

evalf(Im(2/MyF(sinphi0(.3351,1/sqrt(-4)),sinphi1(1/sqrt(-4)),1/sqrt(-4))));

> x:=(beta,k,s0,sinphi,b,gamma)->beta*(2*MyE(sinphi,s0,k)-MyF(sinphi,s0,k))

+b*sin(gamma/2);

> y:=(beta,k,s0,sinphi,b,gamma)->2*beta*k*(cos(arcsin(s0))-cos(arcsin(sinphi)))

+b*cos(gamma/2);

> with(plottools) with(plots);

> p1:=plot([op(Pm21(1, (1/3)*Pi, -112.9, 1.1, 3))],

scaling = constrained, thickness = 2):

> p2 := plot([[x(4.115*I, 1/sqrt(-4), sinphi0(1.4591, 1/sqrt(-4)),

I*sinphi, 13.41, 1.4591), y(4.115*I, 1/sqrt(-4), sinphi0(1.4591, 1/sqrt(-4)),

I*sinphi, 13.41, 1.4591), sinphi = Im(sinphi0(1.4591, 1/sqrt(-4)))

.. Im(sinphi1(1/sqrt(-4)))]], scaling = constrained, thickness = 2);

> p3 := display(line([.94, 2.28], [8.95, 10.04], color = black, thickness = 2));

> p4 := display(line([.47, .85], [14, .85], color = blue, thickness = 2));

> p5 := display(line([11.62, 11.19], [15, 11.19], color = blue, thickness = 2));

> display([p1, p2, p3, p4, p5]);
```

D.6 Joining between two parallel sheets of graphene with fullerene

```
> restart;

> with(plots):

> phi1 := (psi,B)-> 0;

> phi2 := (psi,B) -> arcsin(sqrt(B*(1-sin(psi/2))/2));

> mu1:= (psi1,psi2,B) -> 2*( (EllipticE(sin(phi2(psi2,B)),1/sqrt(B))-

EllipticE(sin(phi1(psi1,B)),1/sqrt(B))) / (EllipticF(sin(phi2(psi2,B)),1/sqrt(B))-
```

```
EllipticF(sin(phi1(psi1,B)),1/sqrt(B))) )-1;
> mu2:= (psi1,psi2,B) -> 2*( (2*EllipticE(1/sqrt(B))-EllipticE(sin(phi2(psi2,B)),
1/sqrt(B))-EllipticE(sin(phi1(psi1,B)),1/sqrt(B)))/(2*EllipticK(1/sqrt(B))-
EllipticF(sin(phi2(psi2,B)),1/sqrt(B))-EllipticF(sin(phi1(psi1,B)),1/sqrt(B))))-1;
> beta1:= (psi1,psi2,B,ell) -> ell/(EllipticF(sin(phi2(psi2,B)),1/sqrt(B))-
EllipticF(sin(phi1(psi1,B)),1/sqrt(B)));
> beta2:= (psi1,psi2,B,ell) -> ell/(2*EllipticK(1/sqrt(B))-
EllipticF(sin(phi2(psi2,B)),
1/sqrt(B))-EllipticF(sin(phi1(psi1,B)),1/sqrt(B)));
> y2_1:= (a,psi1,psi2,B,phi,ell) -> 2*beta2(psi1,psi2,B,ell)
*(cos(phi1(psi1,B))-cos(phi))/sqrt(B)+a*sin(psi1);
> x2_1:= (a,psi1,psi2,B,phi,ell) -> a*cos(psi1) - beta2(psi1,psi2,B,ell)
*( 2*(EllipticE(sin(phi),1/sqrt(B))-EllipticE(sin(phi1(psi1,B)),1/sqrt(B)))
- (EllipticF(sin(phi),1/sqrt(B))-EllipticF(sin(phi1(psi1,B)),1/sqrt(B))));
> y2_2:= (a,psi1,psi2,B,phi,ell) -> 2*beta2(psi1,psi2,B,ell)*(cos(phi1(psi1,B))+
cos(phi))/sqrt(B) + a*sin(psi1);
> x2_2:= (a,psi1,psi2,B,phi,ell) -> a*cos(psi1) - beta2(psi1,psi2,B,ell)
*( 2*(2*EllipticE(1/sqrt(B))-EllipticE(sin(phi),1/sqrt(B))-EllipticE(sin(phi1(psi1,B))
,1/sqrt(B))) - (2*EllipticK(1/sqrt(B))-EllipticF(sin(phi),1/sqrt(B))
-EllipticF(sin(phi1(psi1,B)),1/sqrt(B))));
> model2_1:=(a,psi1,psi2,B,phi,ell)->[x2_1(a,psi1,psi2,B,phi,ell),
y2_1(a,psi1,psi2,B,phi,ell),phi=Pi/18..Pi/2];
> model2_2:=(a,psi1,psi2,B,phi,ell)->[x2_2(a,psi1,psi2,B,phi,ell),
y2_2(a,psi1,psi2,B,phi,ell),phi=Pi/2..Pi/2];
> Pm2:= (a,psi1,psi2,B,ell) -> [model2_1(a,psi1,psi2,B,phi,ell),
model2_2(a,psi1,psi2,B,phi,ell)];
> endpoint2:= (a,psi1,psi2,B,ell) -> [x2_2(a,psi1,psi2,B,phi2(psi2,B),ell),
```

```
y2_2(a,psi1,psi2,B,phi2(psi2,B),ell)];
> b2:= (a,psi1,psi2,B,ell) -> x2_2(a,psi1,psi2,B,phi2(psi2,B),ell)/cos(psi2)
> L2:= (a,psi1,psi2,B,ell) -> y2_2(a,psi1,psi2,B,phi2(psi2,B),ell)
-b2(a,psi1,psi2,B,ell)*sin(psi2);
> mu1:=(a,b,gamma,l)->(a-b*sin(gamma/2))/l;
> sinphi0:=(gamma,k)->sqrt((1-sin(gamma/2))/2)/k;
> sinphi1:=k->0;
> MyE:=(s1,s2,k)->EllipticE(s1,k)-EllipticE(s2,k);
> MyF:=(s1,s2,k)->EllipticF(s1,k)-EllipticF(s2,k);
> mu:=(gamma,k)->2*MyE(sinphi1(k),sinphi0(gamma,k),k)/
MyF(sinphi1(k),sinphi0(gamma,k),k) -1;
> Re(evalf(mu(.3351,1/sqrt(-4))));
> evalf(Im(2/MyF(sinphi0(.3351,1/sqrt(-4)),sinphi1(1/sqrt(-4)),1/sqrt(-4))));
> x:=(beta,k,s0,sinphi,b,gamma)->beta*(2*MyE(sinphi,s0,k)-MyF(sinphi,s0,k))+
b*sin(gamma/2);
> y:=(beta,k,s0,sinphi,b,gamma)->2*beta*k*(cos(arcsin(s0))-
cos(arcsin(sinphi)))+b*cos(gamma/2);
> with(plottools);
> with(plots);
> p1:=plot([[x(5.994*I, 1/sqrt(-4), sinphi0(1.0472, 1/sqrt(-4)),
I*sinphi, 11.55, 1.0472), y(5.994*I, 1/sqrt(-4), sinphi0(1.0472, 1/sqrt(-4)),
I*sinphi, 11.55, 1.0472), sinphi = Im(sinphi0(1.0472, 1/sqrt(-4)))
.. Im(sinphi1(1/sqrt(-4)))]], scaling = constrained):
> p2 := plot([op(Pm2(5, (1/3)*Pi, -112.9, 1.1, 3))],
scaling = constrained, thickness = 2):
> p3 := display(line([15, 4.31], [2.45, 4.31],
color = blue, thickness = 2)):
```

```
> p4 := display(line([10.3, 12.47], [15, 12.47],

color = blue, thickness = 2)):

> c1 := circle([-3.76, 13.2], 10, color = blue);

> display([p1, p2, p3, p4, c1]);
```

Appendix E

Codes for the comparison between the two energies in chapter 4

E.1 Numerical integration Maple

```
restrat;

with(plots):

sinphi0:=(gamma,k)->sqrt((1-sin(gamma/2))/2)/k;

sinphi1:=k->1/(sqrt(2)*k);

MyE:=(s1,s2,k)->EllipticE(s1,k)-EllipticE(s2,k);

MyF:=(s1,s2,k)->EllipticF(s1,k)-EllipticF(s2,k);

x:=(beta,k,s0,sinphi,b,gamma)->-beta*(2*MyE(sinphi,s0,k)-MyF(sinphi,s0,k))

+b*cos(gamma/2);

y:=(beta,k,s0,sinphi,b,gamma)->2*beta*k*(cos(arcsin(s0))-cos(arcsin(sinphi)))

+b*sin(gamma/2); a1:=evalf(x(-2.8746*I,1/sqrt(-4),sinphi0(Pi/1.59,1/sqrt(-4)),

sinphi*I,1.77,Pi/1.59));

a2:=evalf(y(-2.8746*I,1/sqrt(-4),sinphi0(Pi/1.59,1/sqrt(-4)),

sinphi*I,18.09,Pi/1.59));

h:=abs(a1-a2);

c1:=Student[Calculus1][ApproximateInt](h, Im(sinphi0(Pi/(1.59),

1/sqrt(-4))) .. Im(sinphi1(1/sqrt(-4))), 'partition' = 100,

'method' = trapezoid, 'partitiontype' = normal, 'output' = 'plot');

c2:= Student[Calculus1][ApproximateInt](a1, Im(sinphi0(Pi/(1.59),
```

```
1/sqrt(-4))) .. Im(sinphi1(1/sqrt(-4))), 'partition' = 100,

'method' = trapezoid, 'partitiontype' = normal, 'output' = 'plot');

c3:=c1/c2 *100;
```

E.2 Codes for various configurations

E.2.1 Catenoid with cone and tube

```
restart;

with(plots);

p1 := implicitplot3d({x^2+y^2 = sqrt(x^2+y^2)/(1.141)}, x = -Pi .. Pi,

 y = -Pi .. Pi,z = 0 .. 4, color = green);

p2 := implicitplot3d({x^2+y^2 = -z}, x = -Pi .. Pi,

  y = -Pi .. Pi,z = -4 .. -1.63, color = blue);

p3 := implicitplot3d({x^2+y^2 = cosh((z+0.6e-1)/(1.22))-.36}, x = -Pi .. Pi,

y = -Pi .. Pi, z = -1.63 .. 0);

display([p2, p1, p3]);
```

E.2.2 Catenoid with two cones

```
with(plots):

p1:=implicitplot3d({x^2+y^2=z},x =-Pi..Pi,y =-Pi..Pi,z =1.24..2.5,color=red);

p2:=implicitplot3d({x^2+y^2=-z},x =-Pi..Pi,y =-Pi..Pi,z =-2.9..-1.63,color = blue);

p3:=implicitplot3d({x^2+y^2 =cosh((z+0.6e-1)/(1.22))-.36},x =-Pi..Pi,y =-Pi..Pi,

z =-1.63..1.24);

display([p2, p1, p3]);
```

E.2.3 Catenoid with large and narrow cones

```
with(plots);

p1:=implicitplot3d({x^2+y^2=z},x=-Pi..Pi,y=-Pi..Pi,z=.5..2.5,color=red);

p2:=implicitplot3d({x^2+y^2=-z},x=-Pi..Pi,y=-Pi..Pi,z=-2.9..-1.63,color=blue);

p3:=implicitplot3d({x^2+y^2=cosh((z+0.6e-1)/(1.1))-.59},x=-Pi..Pi,y=-Pi..Pi,
```

```
z=-1.63...5);

display([p2, p1, p3]);
```

E.2.4 Catenoid with two fullerens

```
with(plots); p1:=implicitplot3d({x^2+y^2+(z+1)^2=1},x=-1..1,y= -1 .. 1,

z = -2 .. 0, color = red);

p2:=implicitplot3d({x^2+y^2+(z-1.1)^2=1}, x = -1 .. 1, y = -1 .. 1,

z = 0 .. 2, color = blue);

p3:=implicitplot3d({x^2+y^2=cosh(z+0.1e-1)-.5}, x = -Pi .. Pi, y = -Pi .. Pi,

z = -.23 .. .4);

display([p1, p2, p3]);
```